AFRL-AFOSR-UK-TR-2017-0003

Method for Predicting Hypergolic Mixture Flammability Limits

Laurent Catoire
Ecole Nat Sup De Techniques Avancees

02/01/2017
Final Report

Air Force Research Laboratory
AF Office Of Scientific Research (AFOSR)/ IOE
Arlington, Virginia 22203
Air Force Materiel Command

REPORT DOCUMENTATION PAGE

Form Approved
OMB No. 0704-0188

1. REPORT DATE *(DD-MM-YYYY)*	2. REPORT TYPE	3. DATES COVERED *(From - To)*
02-02-2017	Final	25 Mar 2013 to 30 Sep 2016

4. TITLE AND SUBTITLE
Method for Predicting Hypergolic Mixture Flammability Limits

5a. CONTRACT NUMBER

5b. GRANT NUMBER
FA8655-13-1-3035

5c. PROGRAM ELEMENT NUMBER
61102F

6. AUTHOR(S)
Laurent Catoire

5d. PROJECT NUMBER

5e. TASK NUMBER

5f. WORK UNIT NUMBER

7. PERFORMING ORGANIZATION NAME(S) AND ADDRESS(ES)
Ecole Nat Sup De Techniques Avancees
828, Boulevard Des Marechaux
PALAISEAU, 91120 FR

8. PERFORMING ORGANIZATION REPORT NUMBER

9. SPONSORING/MONITORING AGENCY NAME(S) AND ADDRESS(ES)
EOARD
Unit 4515
APO AE 09421-4515

10. SPONSOR/MONITOR'S ACRONYM(S)
AFRL/AFOSR IOE

11. SPONSOR/MONITOR'S REPORT NUMBER(S)
AFRL-AFOSR-UK-TR-2017-0003

12. DISTRIBUTION/AVAILABILITY STATEMENT
A DISTRIBUTION UNLIMITED: PB Public Release

13. SUPPLEMENTARY NOTES

14. ABSTRACT
This report is in support of the Integrated High Payoff Rocket Propulsion Technology(IHPRPT)Demonstration Program, which provides a technology roadmap for demonstrating significant enhancements in mission capabilities, cost efficiencies, and operability for various future propulsion needs. The scope of this project is to demonstrate that it is feasible to numerically construct diagrams of flammability limits for energetic ionic liquid (IL) fuel/oxidizer combinations, which will significantly aid AFRL/RQRP in its ability to identify hypergolic propellants and predict their ignition delay times, prior to carrying out any synthetic or empirical screening activities. The execution of the proposed modeling and simulation (M&S) study early in the life-cycle of the IL propellant development program provides a mitigation strategy to reduce the risk of failure for the insertion of IL fuel technology into the small satellite market as AFRL/RQRP continues to meet IHPRPT goals. This report is divided into three parts. The first is devoted to the proposal of a thermodynamic method able to discuss a priori the hypergolic abilities of a fuel/oxidant system and its flammability limits. This method is shown to be valid for non ionic liquid/oxidant systems and is then extended to ionic liquid/oxidant systems. It is somehow difficult to prove that this method is accurate in terms of limits just because there is a lack in experimental data for ionic liquid/oxidant systems. The second is devoted to a fundamental understanding of what happens in the liquid phase, in the gas phase, at the liquid/liquid interface and at the gas/liquid interface during hypergolic ignition and the interactions of all these phases.

15. SUBJECT TERMS
EOARD, rocket propulsion, combustion chemistry, energetic ionic liquids, flammability limits, fuel/oxidizer combinations, hypergolics

16. SECURITY CLASSIFICATION OF:			17. LIMITATION OF ABSTRACT	18. NUMBER OF PAGES	19a. NAME OF RESPONSIBLE PERSON
a. REPORT	b. ABSTRACT	c. THIS PAGE			MILLER, KENT
Unclassified	Unclassified	Unclassified	SAR	152	19b. TELEPHONE NUMBER *(Include area code)* 011-44-1895-616022

Standard Form 298 (Rev. 8/98)
Prescribed by ANSI Std. Z39.18

CONTRACT FA8655-13-1-3035 EOARD

Final report (due December 31st, 2016)

METHOD FOR PREDICTING HYPERGOLIC MIXTURE FLAMMABILITY LIMITS

Supervisor
Dr. Laurent CATOIRE University Professor, ENSTA ParisTech, Head of Chemical Engineering Lab(UCP)


This report is in support of the Integrated High Payoff Rocket Propulsion Technology (IHPRPT) Demonstration Program, which provides a technology roadmap for demonstrating significant enhancements in mission capabilities, cost efficiencies, and operability for various

future propulsion needs. The scope of this project is to demonstrate that it is feasible to numerically construct diagrams of flammability limits for energetic ionic liquid (IL) fuel/oxidizer combinations, which will significantly aid AFRL/RQRP in its ability to identify hypergolic propellants and predict their ignition delay times, prior to carrying out any synthetic or empirical screening activities. The execution of the proposed modeling and simulation (M&S) study early in the life-cycle of the IL propellant development program provides a mitigation strategy to reduce the risk of failure for the insertion of IL fuel technology into the small satellite market as AFRL/RQRP continues to meet IHPRPT goals.

This report is divided into three parts. The first is devoted to the proposal of a thermodynamic method able to discuss *a priori* the hypergolic abilities of a fuel/oxidant system and its flammability limits. This method is shown to be valid for non ionic liquid/oxidant systems and is then extended to ionic liquid/oxidant systems. It is somehow difficult to prove that this method is accurate in terms of limits just because there is a lack in experimental data for ionic liquid/oxidant systems.

The second is devoted to a fundamental understanding of what happens in the liquid phase, in the gas phase, at the liquid/liquid interface and at the gas/liquid interface during hypergolic ignition and the interactions of all these phases. The ignition happens in the gas-phase but products formed here and there (in the liquid phase or at the liquid/gas interface) and then released in the gas-phase can play a role in the ignition process.

The third one is an attempt to propose a strategy devoted to the building of detailed chemical kinetic models in the liquid phase to try to understand what are the species formed and presumably present in the gas phase.

Part one:

METHOD FOR PREDICTING HYPERGOLIC MIXTURE FLAMMABILITY LIMITS

Table of Contents

List of Figures

List of Tables

Introduction

This report is in support of the Integrated High Payoff Rocket Propulsion Technology (IHPRPT) Demonstration Program, which provides a technology roadmap for demonstrating significant enhancements in mission capabilities, cost efficiencies, and operability for various future propulsion needs. The scope of this project is to demonstrate that it is feasible to numerically construct diagrams of flammability limits for energetic ionic liquid (IL) fuel/oxidizer combinations, which will significantly aid AFRL/RQRP in its ability to identify hypergolic propellants and predict their ignition delay times, prior to carrying out any synthetic or empirical screening activities. The execution of the proposed modeling and simulation (M&S) study early in the life-cycle of the IL propellant development program provides a mitigation strategy to reduce the risk of failure for the insertion of IL fuel technology into the small satellite market as AFRL/RQRP continues to meet IHPRPT goals.

Globally in the last few decades, pioneering fuel research has been carried out in order to replace existing fuels for various economic and ecologic reasons. This development has not just been limited to auto fuels but has included all types of combustion fuels, including space fuels. One of the most utilized bipropellant combinations for satellite propulsion and interplanetary missions, monomethylhydrazine (MMH)/nitrogen tetroxide (NTO), falls under this scope. The mixture is very energetic and presents some practical advantages in space propulsion; however, its components at the same time possess drawbacks. MMH and NTO are toxic and carcinogenic compounds and MMH vapors are flammable. One of the alternatives proposed to replace MMH are ionic liquid fuels.

Ionic liquids exhibit physico-chemical properties (of low vapor pressure, good thermal stability, etc.) that make them suitable for replacing MMH while also maintaining their hypergolicity with propellant oxidizers (such as nitric acid and NTO). Due to the large number of ionic liquids (10^{18}) possible, and the impossibility for scientists to test them all, it is necessary to determine a simple physico-chemical criterion (like the adiabatic flame temperature) to predict mixture flammability limits to model hypergolic conditions, as well as to understand the chemical risks associated during the handling of IL propellants.

The part of this study is divided into three sections. In the first section, a bibliographic search is presented and a determination of the flame temperature criterion is also discussed. In the second section, the thermodynamic data for these ionic liquids and the methods used to obtain the data is discussed. The computed results obtained for ionic liquid + oxidant mixtures are reported in the third section of the report.

1 State of the art

In most cases, liquids or gases once mixed do not react violently at room temperature. However, some combinations are known to react rapidly and under appropriate mixing ratios can lead to violent explosions. Monomethylhydrazine and nitrogen tetroxide (MMH & NTO) is one such combination and is the preferred choice for creating propulsive thrust in numerous spacecraft applications. These low temperature (at 298 K or below) self- or auto-ignitions are often referred to as hypergolic ignitions. In addition to the MMH & NTO combination, MMH, hydrazine and unsymmetrical dimethyl hydrazine have also been used with nitric acid. It is crucial to be able to predict, *a priori,* the auto-ignition behavior that may arise from the mixing of two or more liquids, either for the development of new chemical rocket propulsion technologies or for the purpose of mitigating the chemical risks associated in the transportation and management of rocket fuels. An extensive search in the open literature has shown that there are no computational methods currently available to address these needs. The objective of this research is to present a procedure to predict mixture flammability limits to model hypergolic conditions, as well as to understand the chemical risks associated when handling hypergolic propellants.

1.1 Ionic Liquids

Since the beginning of the early 2000s, ionic liquids have emerged as important classes of compounds for many chemical applications, especially as industrial solvents. Smiglak and co-workers have recently reviewed these applications and determined that >8,000 studies have been published on ionic liquids [Smiglak M. et al., 2007].

1.1.1 Definition

Salts are compounds formed by the association of ions. Ionic liquids are salts with melting points equal to or below 100°C. Room temperature ionic liquids (RTILs) are liquid salts at ambient temperatures (20 - 25°C). The first RTIL, ethylammonium nitrate, was described in 1914 by Walden and has a melting point equal to 12°C [Pucheault M, 2010].

Ionic liquids are synthesized by the reaction of a base with a strong acid. Ionic liquids consist of negative and positive ions. It is generally accepted that the anion (negative ion) is more important in controlling the physical properties of the ionic liquid and that the nature of the cation (positive ion) affects the stability and reactivity of the ionic liquid. Therefore, it is possible to adjust IL physico-chemical properties by making changes in their component ion structures to suit requirements when designing energetic materials. Approximately 10^{18} different ionic liquids are possible. The number of known ionic liquids has expanded exponentially over the past two decades and it is certain that new classes will be developed in the forthcoming years. Therefore, it is not practical to study experimentally all of these ionic liquids. Hence, a few theoretical tools have been developed for some of the properties and new ones have to be developed to predict remaining physico-chemical properties so as to

allow for an efficient approach to screen and design energetic ionic liquids [Catoire L. et al., 2008] .

Basic scientific data concerning ionic liquids, such as their physico-chemical properties, their thermal stability, etc., are reported here. The ionic liquids considered are not all energetic ionic liquids (EILs), but trends observed with non-energetic ionic liquids may also be of interest to EILs.

1.1.2 Properties

Smiglak et al. have reported the performance requirements for EILs (see Table 1) [Smiglak M. et al., 2007].

Physical properties	
Melting Point	Less than – 40°C
Density	> 1.4 $g.cm^{-3}$
Viscosity	As low as possible
Surface tension	< 1.10^{-3} $N.cm^{-1}$
Thermal Stability	
TGA (75°C, isothermal)	< 1% loss of material over 24hr
TGA (rate 10°C/min)	> 120°C for T_{decomp}
Thermodynamic Properties	
Heat of Formation	As positive as possible
Heat of Combustion	> 6 $kcal.g^{-1}$
Toxicology	
LD_{50}	> 0.5 $g.kg^{-1}$
AMES	Negative

Legend: TGA: Thermogravimetric analysis; LD_{50}: Median Lethal Dose; AMES: The Ames test is a widely employed method that uses bacteria to test whether a given chemical can cause cancer.

Table 1: Performance requirements for EILs [Smiglak et al., 2007]

Energetic ionic liquids of interest are salts that have melting points that fall well below room temperature (-40 °C). Since it is impossible to measure the melting points for the large number of ILs and EILs, numerical methods have to be derived and validated (with little data available). Several attempts have been made [Catoire et al., 2008] but all of them suffer from several weaknesses. The most unexpected result reported by Catoire et al. concerns the fact that for some of the ionic liquids studied, the melting and the freezing points are different.

This is due to the fact that ionic liquids tend to super-cool [Van Valkenburg et al., 2005]. Another interesting feature, potentially of importance for propulsion applications, is that these authors report that some ionic liquids solidified at room temperature after several months.

Another interesting feature of ionic liquids is that they are generally denser than organic liquids. For propulsion applications this is of great interest. Smiglak et al. report that a density above 1.4 gcm^{-3} is required for EILs. One other important fact reported is that ionic liquids are generally not pure and that water is a very common contaminant, which can decrease the density of the ionic liquid [Van Valkenburg et al., 2005]. Fredlake and co-workers have measured the density of some imidazolium-based ionic liquids [Fredlake et al., 2004]. A decrease in the density has been observed with an increase in temperature, as expected for molecular liquids. Other general trends for these imidazolium-based ionic liquids are: the density falls off as the alkyl-substituted chain length of the cation increases and the density rises with increasing molecular weight of the anion. Other relevant physio-chemical data has been reported by Catoire and co-workers [Catoire et al., 2008, Interim report].

1.1.3 Interest in Ionic Liquids

Concerning propulsion applications, EILs have several advantages compared to existing hypergolic fuels such as hydrazine (N_2H_4) and its methylated derivatives MMH (monomethylhydrazine, CH_3NHNH_2) and UDMH (unsymmetrical dimethyl hydrazine, $(CH_3)_2NNH_2$). These 'traditional' fuels are toxic (short-term effects) and carcinogenic (long-term effects) at very short exposures, which can be very problematic since they have relatively high vapor pressures. Moreover, their flashpoints are quite low and this can be a source of chemical risk (explosion) during handling and storage. On the contrary, ionic liquids are thermally stable and have a negligible vapor pressure, high density and large liquidous range. Physico-chemical properties are available only for relatively few compounds, even for such basic properties as density and melting point. Performance requirements for EILs in terms of melting point, surface tension, density, viscosity, etc., are given in Table 1, [Smiglak et al., 2007].

1.1.4 Chemical nature of vapor above ionic liquids

Different experimental studies have been carried out in the last few years, [Catoire et al., 2008 and Catoire et al., 2009], to determine the enthalpy of formation of ILs. Enthalpy of formation is not only required in the liquid phase but also in the gas phase above the ionic liquid since ignition occurs in the gas phase. It is experimentally far from being obvious to perform constant-volume combustion calorimetry with the gas phase above an ionic liquid. First, the vapor pressure of an ionic liquid is generally negligible at room temperature. Second, once the ionic liquid is heated, the vapor pressure above the liquid increases but an analysis has to be performed to determine whether or not the vapor above the liquid is representative of the ionic liquid. In other words, the gas phase can be composed of gases resulting from the thermal decomposition of the ionic liquid. For computations, this is not necessarily a problem but in that case one can hardly define an unambiguous enthalpy of

formation of the vapor above the liquid. One has to know beforehand the chemical nature of the gas phase above the ionic liquid [Catoire et al., 2008 and Catoire et al., 2009].

The chemical nature of the vapor above an ionic liquid is difficult to determine experimentally. It is, however, important to know how the vapor pressure forms above an ionic liquid. Four possibilities exist. At equilibrium above the liquid phase, ion pairs can exist, or separated ions can exist, or neutral pairs can exist, or finally separated neutrals can exist. Experimental findings and theoretical calculations are reported in the literature on this issue. It appears that ionic liquids have to be divided into two classes: protic ionic liquids and aprotic ionic liquids.

The data reported below has been taken from our previous reports [Catoire et al., 2008 and Catoire et al., 2009].

Protic Ionic Liquids

According to Earle and co-workers, for protic ionic liquids, equilibrium exists between ionic and non-ionic species [Earle et al., 2006]:

$$BH^+ + X^-_{(\ell)} \leftrightarrow B_{(\ell)} + HX_{(\ell)} \leftrightarrow B_{(g)} + HX_{(g)}$$

Where (ℓ) represents the liquid phase and (g) represents the gas phase. Calculations made by Schmidt and co-workers on protic triazolium-based energetic ionic liquids show that the neutral pair is of lower energy than the ionic pair [Schmidt et al, 2005]. Separation of the species in the ion pair requires a significant amount of energy; >50 kJ mol^{-1}. One of the conclusions of this paper is that the ionic pair once formed will transfer one proton to form a neutral pair. This proton transfer is therefore fundamental for the decomposition of the triazolium-based species considered. However, Baranyai and co-worker did not observe the formation of species according to the proton transfer process, and therefore, their mechanism is questionable [Baranyai et al., 2004]. Zorn et al. deduced from their calculations on protic tetrazolium-based ionic liquids that when a cation is paired with an oxygen rich anion, an isolated gas phase ion pair was not generally found to be stable [Zorn et al, 2006]. In fact, a proton transfers barrierlessly from the cation to the anion to form a neutral pair. This result is consistent with the experimental findings of Leal and co-workers, who report that the gas phase above a protic ionic liquid is composed of separated neutral molecules [Leal et al., 2007].

Aprotic Ionic Liquids

Calculations made by Emel'yanenko and co-workers on the gas phase equilibrium:

$$\text{ion pair} \leftrightarrow \text{separated ions}$$

for 1-butyl-3-methylimidazolium dicyanamide indicate that dissociation of the ion pair is marginal [Emel'yanenko et al., 2007]. Experimental and theoretical works reported by Strasser and co-workers suggest that the vapor pressure of an aprotic ionic liquid (1-ethyl-3-methylimidazolium bis(trifluoromethylsulfonyl)imide) is composed of isolated ion pairs

[Strasser. et al., 2007]. The presence of clusters of ion pairs seems to be negligible. This conclusion is supported by another experimental work performed by Leal et al., who find that the gas phase is composed of isolated ion pairs and that no experimental evidence supports the formation of ion clusters [Leal et al., 2007]. For aprotic ionic liquids, the only possible mechanism for volatilization, according to Earle et al., is as ion pairs, isolated or as clusters [Earle et al., 2006]. Armstrong and co-workers performed an analysis of the vapor pressure of 1-ethyl-3-methylimidazolium ethylsulfate by mass spectrometry (MS) [Armstrong et al., 2007]. They deduced from their experiments that the vapor pressure of these ionic liquids consists of ion pairs, although they do not observe directly these ion pairs because the ionized ion pair (formed in the ionization chamber of the mass spectrometer by electron bombardment) is unstable and, therefore, fragmentation occurs in their experiments. One other finding by Armstrong and co-workers is that clusters of ion pairs do not seem to form in the gas phase [Armstrong et al., 2007].

1.2 Hypergolic mixtures with ionic liquids

The aim of the second part of the state of the art section is to document hypergolic IL mixtures. In 2011, Schneider and co-workers reported hydrogen-rich ionic liquids that were hypergolic with hydrogen peroxide [Schneider et al., 2011]. Before this time, no ionic liquids were known to be hypergolic with hydrogen peroxide. The Schneider et al. study considered hydrogen-rich ILs with metal hydride anions. Two different ionic liquids were tested (see Figure 1).

The ionic liquid, listed as **1**, is the trihexyltetradecylphosphonium (THTDP) cation with borohydride (BH_4^-) anion. The second ionic liquid listed as **2** is the THTDP cation with aluminum borohydride ABH ($Al(BH_4)_4^-$) anion. These two ionic liquids were subjected to drop tests to determine their reactivity with common propulsion oxidizers. A drop test consists of dropping the ionic liquid into the oxidant and to measure the time between the contact of the two liquids and the time when ignition is observed. The (THTDP)(BH_4^-) ignites only 3s after dropping onto H_2O_2, while the ignition delay of (THTDP)($Al(BH_4)_4^-$) was quite short (less than 30 ms) for two different H_2O_2 solutions (90 and 98%). This ionic liquid also reacted with N_2O_4 (NTO) and WFNA (white fuming nitric acid). Schneider et al. concluded that a RTIL with a complex ABH anion would be hypergolic with all common propellant oxidizers including H_2O_2 [Schneider et al., 2011].

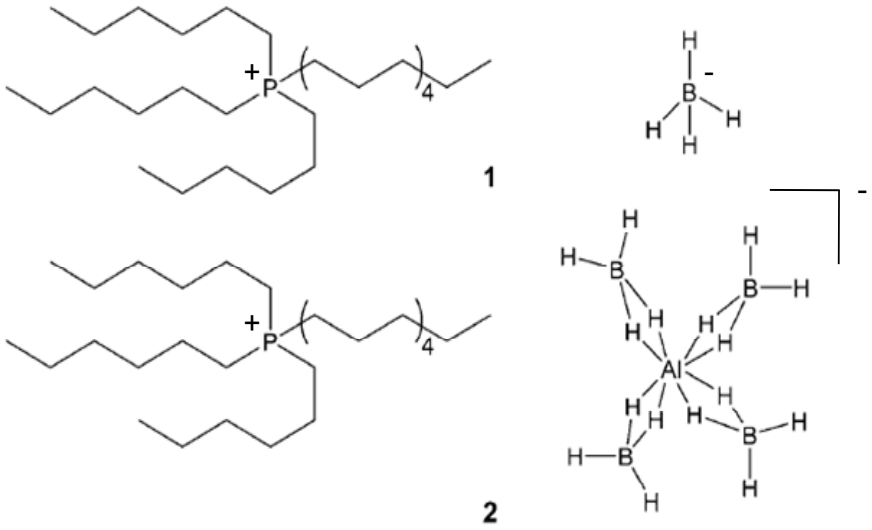

Legend: **1**: Cation: Trihexyltetradecylphosphonium - Anion: Borohydride ; **2**: Cation: Trihexyltetradecylphosphonium - Anion: Tetra(tetrahydroborato)aluminide

Figure 1: Hydrogen-rich ILs with metal hydride anions [Schneider et al., 2011]

In 2011, Zhang and co-workers studied dicyanoborate-based ionic liquids [Zhang et al. 2011a]. Compared to borohydride-based (BH_4^-) and cyanoborate-based ($BH_3(CN)^-$) ionic liquids, these ionic liquids are water-stable and can be synthesized in aqueous media. The ten dicyanoborate-based ionic liquids considered are shown in Figure 2, consisting of five different cations (N,Ndimethylhydrazinium, N-methylimidazolium, pyridinium, N-methylpyrrolidinium, and N-methyltriazolium) with two different substituents (butyl and allyl groups) [Zhang et al. 2011a]. All of these $BH_2(CN)_2^-$-based ionic liquids were found to be hypergolic with WFNA. The characteristics of these ILs are given in the Table 2.

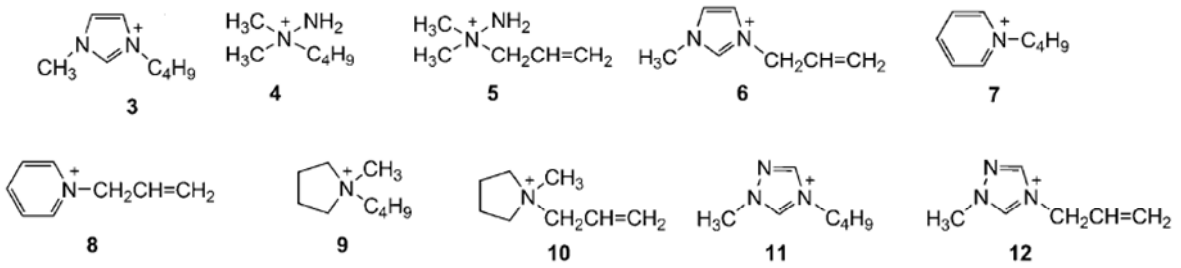

Legend: **3**: 1-methyl-3-butylimidazolium ; **4**: 1-butyl-N,N-dimethylhydrazinium ; **5**: 1-allyl-N,N-dimethylhydrazinium, **6**: 1-methyl-3-allylimidazolium ; **7**: 1-butylpyridinium ; **8**: 1allylpyridinium ; **9**: 1-butyl-N-methylpyrrolidinium ; **10**: 1-allyl-N-methylpyrrolidinium ; **11**: 1-methyl-4-butyl-1,2,4-triazolium ; **12**: 1-methyl-4-allyl-1,2,4-triazolium.

Figure 2: Different cations tested for the dicyanoborate-based ionic liquids studied by Zhang et al. [Zhang et al., 2011a]

In Table 2, it is seen that these ionic liquids have a long liquidous range, between -80°C and >200°C for many of them. Compared to the requirement of density >1.4 g.cm^{-3} for energetic ionic liquids ([Smiglak et al., 2007]), the densities of the dicyanoborate-based materials are lower and vary from 0.91 to 1.03 g.cm^{-3}. The ignition delay times of these ionic liquids are relatively short and vary over a narrow range from 4 to 32 ms. When the dicyanoborate anion of the ILs is replaced by the dicyanamide ($N(CN)_2^-$) anion and by the nitrocyanamide ($N(NO_2)(CN)^-$) anion, the ignition delay (measured in a drop test) of the mixture increase substantially. For example, for the IL with the butyl-dimethylhydrazinium cation (**4**), and with the dicyanoborate anion, the ignition delay is equal to 6 ms, but when the anion is the dicyanamide, the ignition delay is equal to 46, and 228 ms when the anion is the nitrocyanamide (see Table 2) [Zhang et al. 2011a].

With good physico-chemical properties (such as melting point, viscosity, etc.) and ignition delay time as short as 4 ms, dicyanoborate-based ILs appear to be promising substitutes for the replacement of hydrazine and its derivatives in hypergolic propellant systems [Zhang et al. 2011a].

IL	T_m/T_g [°C]	T_d [°C]	ρ [g cm^{-3}]	η [mPa s]	ID [ms]
3[b]	< −80	307	0.96	17.3	28
3 (DCA)					47
3 (NCA)	−90	256	1.13	57	81
4[b]	< −80	222	0.91	39.4	6
4 (DCA)	20	263	1.01	113.9	46
4 (NCA)	9	286	1.11	119.5	228
5[b]	< −80	189	0.93	35.0	4
5 (DCA)		199	1.05	78.6	30
5 (NCA)		208	1.16	84.9	130
6[b]	< −80	266	0.99	12.4	8
6 (DCA)	−85	207		42	43
6 (NCA)	−91	220	1.11	44	46
7[b]	< −80	252	0.96	19.8	18
8[b]	< −80	203	1.00	13.5	6
9[b]	< −80	303	0.92	22.3	26
9 (DCA)					44
10[b]	< −80	259	0.94	16.6	8
11[b]	< −80	220	0.99	29.9	32
12[b]	< −80	217	1.03	21.0	6

[a] T_m/T_g: phase-transition temperature, T_d: decomposition temperature (onset), ρ: Density (25 °C), η: viscosity (25 °C), ID: ignition delay time (WFNA), DCA: corresponding dicyanamide-based ionic liquid, NCA: corresponding nitrocyanamide-based ionic liquid. [b] $^-BH_2(CN)_2$, this work.

Legend: The molecule number corresponds to the one given in the Figure 2

Table 2 : Properties of the dicyanoborate-based ILs and the corresponding dicyanamide- and nitrocyanamide-based ionic liquids [Zhang et al., 2011a]

In 2009, Gao and co-workers studied hypergolic mixtures with 2,2-dialkyltriazanium-based ionic liquids [Gao et al., 2009], which due to the multiple nitrogen-nitrogen bond character of the cation, also had a potential for having a high heat of formation (see Figure 3).

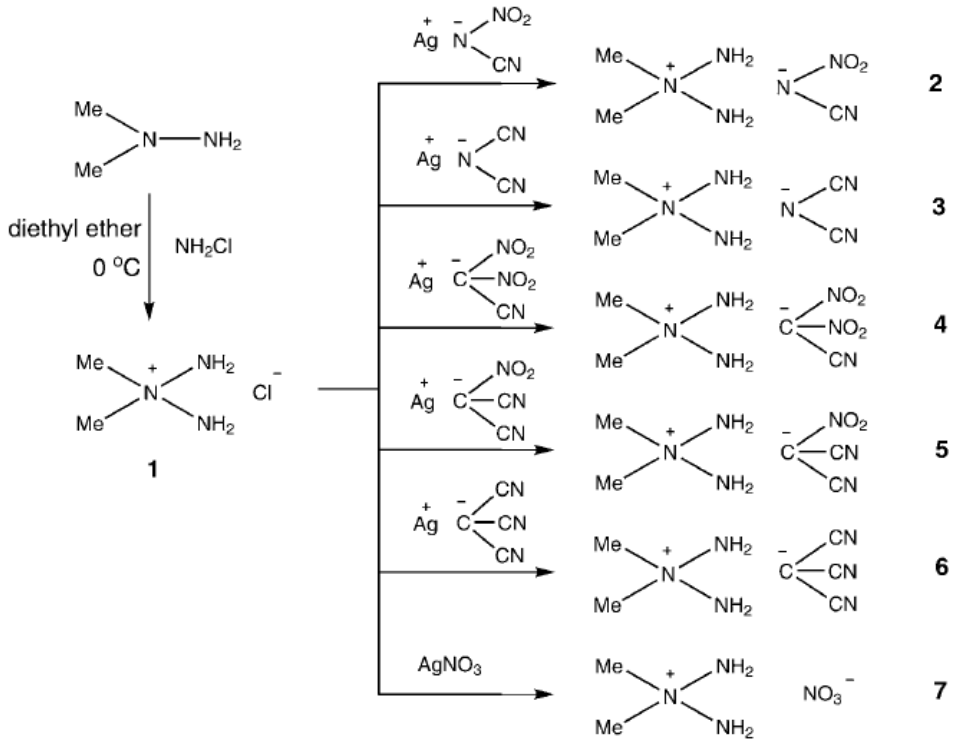

Figure 3: Synthesis of 2,2-dimethyltriazanium salts [Gao et al., 2009]

The physico-chemical properties of the ionic liquids with a 2,2-dimethyltriazanium cation are given in the Table 3. The results show that the ionic liquids # **2**, **3** and **7** are hypergolic with NTO (N_2O_4) or white fuming nitric acid (WFNA = 100% HNO_3), but only the ionic salts # **2** and **7** exhibit very short ignition delay times (less than 10 ms). These ignition delay times were measured via droplet tests. However, the ionic salt # **7** is a solid at ambient temperature (Melting Point = 99.0 °C). The ionic salts # **1** and **7** have densities equal to 1.47 g.cm^{-3}, and meet Smiglak and co-workers' requirements of density >1.4 g.cm^{-3} [Smiglak et al., 2007]. ILs # **2** and **3** have densities of, respectively, 1.26 and 1.15 g.cm^{-3}. Ionic salts # **4**, **5**, and **6** do not exhibit hypergolicity with N_2O_4 or WFNA. This phenomenon was not explained by the authors (see Table 3) [Gao et al., 2009].

Salts	d[a]	T_m[b]	T_d[c]	Ignition delay[d]	
				N_2O_4	WFNA
1	1.47		–	26	nh
2	1.26	−0.19	145.7	8	16
3	1.15	10.7°	134.2	sh	22
4	1.48	–	134.2	nh	nh
5	1.35	47.8	142.5	nh	nh
6	1.20	74.4	153.3	nh	nh
7	1.47	99.0	145.6	10	4

Legend: [a] density (g.cm^{-3}) ; [b] melting point (°C) ; [c] Decomposition temperature (°C) ; [d] in ms ; nh = not hypergolic ; sh = hypergolic when a second drop of fuel was dropped into N_2O_4. The molecule numbers correspond to the ones given in the Figure 3

Table 3: Properties of energetic 2,2-dimethyltriazanium salts [Gao et al., 2009]

In 2010, Zhang and co-workers reported the synthesis of N,N-dimethylhydrazinium-based ionic liquids [Zhang et al., 2010]. The salts were obtained by quaternizing N,N-dimethylhydrazine with alkyl halides followed by metathesis reactions with silver dicyanamide or silver nitrocyanamide (see Figure 4).

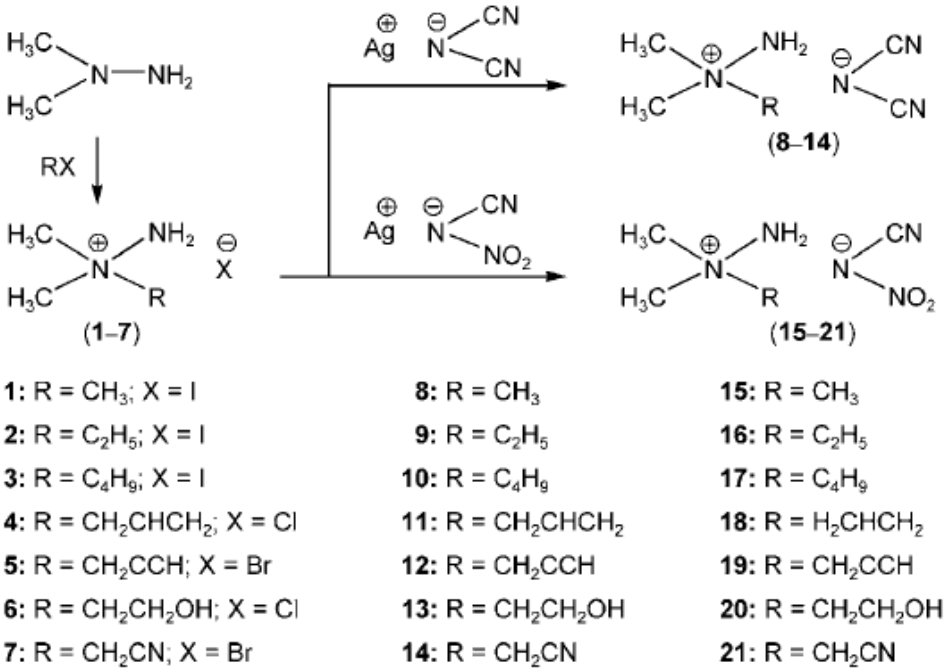

Figure 4: Synthesis of N,N-dimethylhydrazinium ionic liquids [Zhang et al., 2010]

The physico-chemical properties of these salts are given in Table 4. The N,N-dimethylhydrazinium salts are liquids at ambient temperature except for salts # **8**, **9**, **15** and **16**. There is no detectable phase-transition temperature (T_m and T_g) for compound # **11-14** and **18-21** in the temperature range between -25 and 60 °C. The decomposition temperatures of these ILs vary from 144.8 (compound # **14**) to 296.9 °C (compound # **16**), with the nitrocyanamide anion ILs exhibiting greater thermal stability than the dicyanamide analogues [Zhang et al., 2010]. Density and viscosity of the N,N-dimethylhydrazinium ionic liquids vary from 1.01 to 1.28 g.cm^{-3} and 67.5 to 1310 mPa.s, respectively. The nitrocyanamide salts have a higher density and viscosity than the corresponding dicyanamides due to the presence of the nitro (NO_2) group (see Table 4).

All of these ionic liquids show hypergolicity with WFNA. Among these, salts # **9**, **11**, **12** and **13** have ignition delay times below or equal to 40 ms. Presence of the nitrocyanamide anion instead of the dicyanamide anion in the IL results in an increase in the ignition delay

time for a given cation. For nitrocyanamide salts, the shortest ignition delay (ID) time is observed for compound # **15** with an ID equal to 126 ms (see Table 4) [Zhang et al., 2010].

Salts	$T_m(T_g)$[a] [°C]	T_d[b] [°C]	ρ[c] [g cm^{-3}]	η[d] [mPas]	ID[e] [ms]
8	60.5	253.5	1.10	–	58
9	30.9	267.1	1.06	67.5	22
10	20.4	263.3	1.01	113.9	46
11	–	199.2	1.05	78.6	24
12	–	174.3	1.13	228.6	30
13	–	236.0	1.15	161.8	40
14	–	144.8	1.17	1057.0	1286
15	35.2	292.4	1.24	–	126
16	25.4	296.9	1.17	–	198
17	9.0	285.5	1.11	119.5	228
18	–	208.2	1.16	84.9	130
19	–	189.3	1.21	269.8	134
20	–	269.1	1.26	185.9	247
21	–	193.5	1.28	1310.0	1642

Legend: [a] Melting point ; [b] Decomposition temperature ; [c] Density ; [d] Viscosity (25°) ; [e] Ignition delay time with WFNA. The molecule number corresponds to the one given in the Figure 4.

Table 4: Properties of N,N-dimethylhydrazinium ionic liquids [Zhang et al., 2010]

In 2012, Wang and co-workers investigated hypergolicity of boronium-cation based ionic liquids [Wang et al., 2012]. With additional literature data, the authors concluded that molecules with strongly reduced B-H bonds appear to enhance hypergolic ignition. The synthesis scheme for boronium-cation based ILs used by Wang et al. is shown in Figure 5. Due to the short B-H bond, a strong interaction between B and H exists, which leads to a weak reducing potential of hydrogen. This may explain the excellent stability of these ionic liquids in water [Wang et al., 2012].

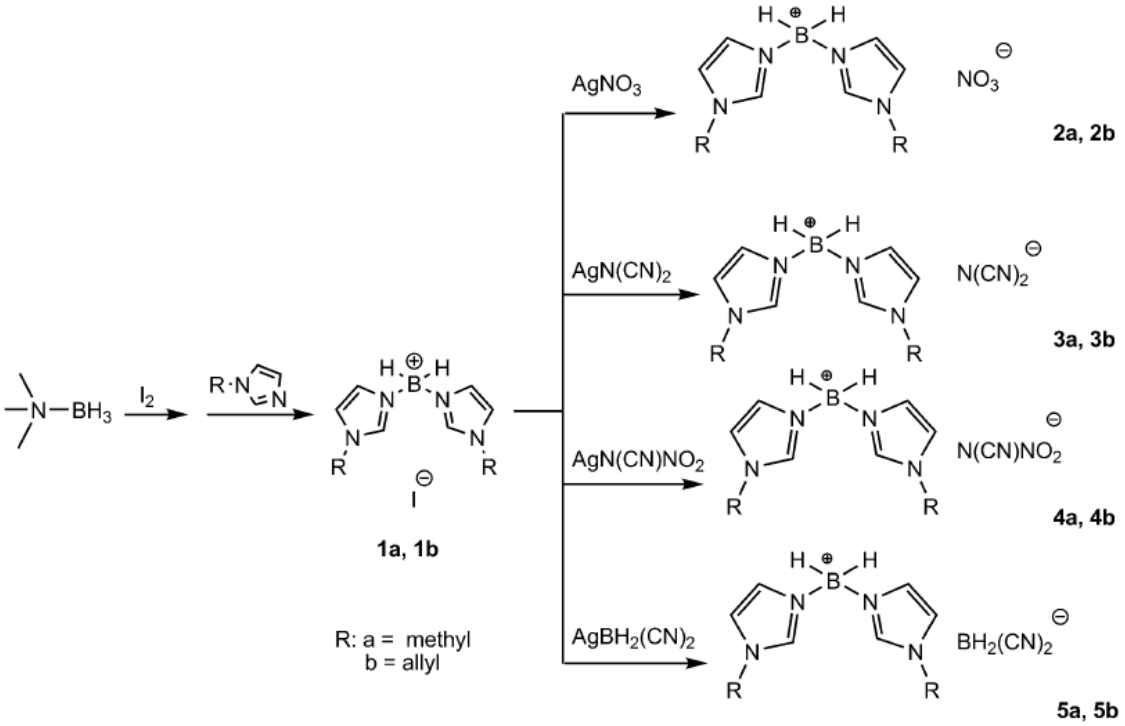

Figure 5: Synthesis of boronium-based ionic liquids [Wang et al., 2012]

The physico-chemical properties of these boronium-based ionic liquids are shown in Table 5. All of these eight compounds have melting points below 100 °C, but only 5 of them are liquids at room temperature (**2b**, **3b**, **4a**, **4b** and **5b**). The decomposition temperatures of these ionic liquids range from 190 to 306 °C, showing that they are thermally stable [Wang et al., 2012].

High density and low viscosity are two important properties of hypergolic ionic liquids. However, high (or low) density is often concomitant with high (or low) viscosity. For example, IL **2b** has the second highest density (1.15 $g.cm^{-3}$) and the highest viscosity (844 mPa.s), on the contrary, IL **5b** possesses the lowest density (1.05 $g.cm^{-3}$) and viscosity (35 mPa.s). Ignition delays of these ILs with WFNA were measured via droplet tests. A characteristic light-green flame due to boron combustion was observed upon ignition. Ionic liquid **5b** has the shortest ignition delay (14 ms) followed by ILs **3b** and **4b** (both 18 ms) and **3a** (26 ms). If we compare, the methyl-substituted series-a and the allyl-substituted series-b, the first one gives longer ignition delay times, suggesting the positive impact of the allyl substituent on the ignition properties of hypergolic mixtures with WFNA. The authors concluded that ionic liquid **5b** is the most promising hypergolic fuel (short ID, low viscosity and liquid over a wide range of temperature) (see Table 5) [Wang et al., 2012].

Salt	T_m [a] [°C]	T_d [b] [°C]	ρ [c] [g cm^{-3}]	ID [d] [ms^{-1}]	I_{sp} [e] [s]	η [f] [mPas]
2a	90	217	1.28	nh	183.1	–
2b	<−80	198	1.15	64	178.2	844
3a	30	196	1.12	26	160.4	43
3b	<−80	190	1.09	18	159.0	69
4a	<−80	227	1.20	34	181.3	60
4b	<−80	236	1.14	18	176.5	103
5a	62	306	1.12	h	164.5	–
5b	<−80	266	1.05	14	162.4	35

Legend: [a] Melting point ; [b] Decomposition temperature ; [c] Density ; [d] Ignition delay time with WFNA ; [e] Specific impulse ; [f] Viscosity (25°) ; nh = not hypergolic ; h = hypergolic. The molecule numbers correspond to the ones given in the Figure 5.

Table 5: Properties of boronium cation-based ionic liquids [Wang et al., 2012]

In 2010, He and co-workers studied hypergolicity of nitrocyanamide anion-based ionic liquids [He et al., 2010]. Synthesis of imidazolium-based salts with the nitrocyanamide anion is shown in Figure 6. These ILs were synthesized by anion exchange between imidazolium-based halides and silver nitrocyanamide in methanol. After filtration, the filtrates were dried to give light-yellow liquids (compounds **1** to **4**) or a light-brown solid (compound **5**).

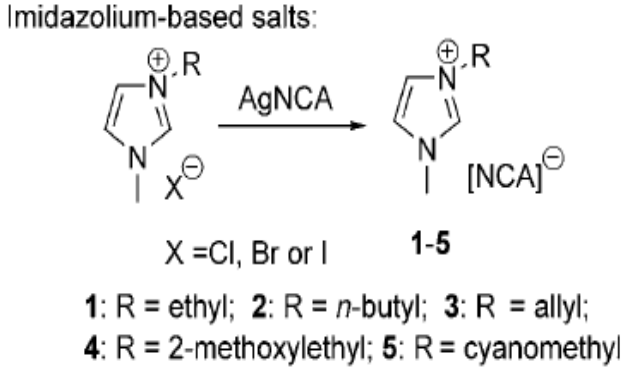

Legend: NCA^- = nitrocyanamide anion $N(CN)(NO_2)^-$

Figure 6: Synthesis of nitrocyanamide anion-based ionic liquids [He et al., 2010]

The physico-chemical properties of these compounds are summarized in Table 6. All of these have melting points below 100 °C but only ILs **1** to **4** are liquids at room temperature. Compound **5** possesses a melting point of 83 °C, which is due to the cyano-methyl group interactions. All of these ionic liquids have high decomposition temperatures (T_d above 200 °C) and low viscosities (η below 60 cP), which are the preferred attributes for any new bipropellant application. Compounds # **1**, **2**, **3** and **4** were screened for hypergolic activity in

drop tests. All were found to be hypergolic with WFNA with values of ignition delay times ranging between 46 (compound **3**) to 81 ms (compound **2**) (see Table 6) [He et al., 2010].

Compound	T_m/T_g[a] (°C)	T_d[b] (°C)	ρ[c] ($g.cm^{-3}$)	η[d] (cP)	ID[e] (ms)
1	-/-73	253	1.18	23	78
2	-/-90	256	1.13	57	81
3	-/-91	220	1.11	44	46
4	-/-83	266	1.21	54	65
5	83/-	203	1.47		

Legend: [a]: Melting point/phase transition temperature ; [b]: Decomposition temperature ; [c]: Density, 25°C ; [d]: Viscosity, 25°C ; [e]: Ignition delay time with WFNA (100% HNO_3). The molecule numbers correspond to the ones given in the Figure 6.

Table 6: Physicochemical properties of nitrocyanamide anion-based ionic liquids [He et al., 2010]

In 2008, Schneider and co-workers studied the hypergolicity of different dicyanamide anion-based ionic liquids [Schneider et al., 2008]. The authors chose these dicyanamide-based ionic liquids because these ionic liquids possess some of the lowest viscosities among known ionic liquids. The imidazolium cation was considered for this study because they generally possess greater stability than their triazolium or tetrazolium analogues. The synthesis of these ILs is shown in Figure 7.

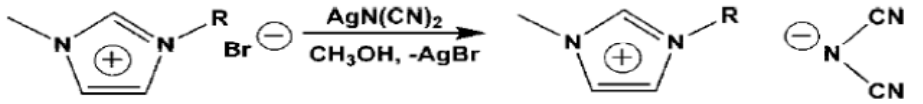

R = -allyl(1), -(3-butenyl)(2), -propargyl(3), -(2-butynyl)(4), -(2-pentynyl)(5)

Cation 6 : 1-methyl-4-amino-1,2,4-triazolium (the formation pathway is identical to the others)

Figure 7: Synthesis of dicyanamide anion-based ionic liquids [Schneider et al., 2008]

Table 7 shows the physico-chemical properties of these dicyanamide-anion based systems. All of these compounds are ionic liquids (melting points below 100 °C), but compounds # **4** and **5** are solids at room temperature. Only ILs **1** and **2** show good thermal stability (T_d above 200 °C) and low viscosity with values equal to 42 and 27 cP, respectively. The ignition delay times of these ILs were measured via droplet tests with WFNA. Compounds # **1**, **3** and **6** were found to be hypergolic with the WFNA. Compounds **4** and **5** were not tested because of their unsuitability as liquid propellants (see Table 7) [Schneider et al., 2008].

Compound	T_g[a] (°C)	T_m[b] (°C)	T_d[c] (°C)	η[d] (cP)	ID[e] (ms)

1	-85		207	42	43
2	-90		210	27	Not measured
3	-61	17	144	110	15
4		49	179		
5		59	184		
6	-66		143	92	31

Legend: [a] Glass transition temperature [b]: Melting point ; [c]: Decomposition temperature ; [d]: Viscosity, 25°C ; [e]: Ignition delay time with WFNA (100% HNO_3). The molecule numbers correspond to the ones given in the Figure 7.

Table 7: Properties of dicyanamide-anion based ionic liquids [Schneider et al., 2008]

In 2011, Zhang and co-workers reviewed all of the recent work on hypergolic mixtures [Zhang et al, 2011b]. Also in this review, they extended the work of Joo and co-workers on azide-containing hypergolic mixtures [Joo et al., 2010].

The azido group is a highly energetic moiety, which can add approximately 280 $kJ.mol^{-1}$ to the energy content of a molecule. 2-azido-N,N-dimethylethylamine (DMAZ) is a reduced-hazard liquid fuel with many of its physical properties comparable to those of monomethylhydrazine (MMH) fuel. Literature data is available suggesting DMAZ is less toxic than MMH. Methylation of DMAZ with iodomethane, with a slight excess of the corresponding silver salts (silver nitrocyanamide and silver dicyanamide) results in ILs **23** to **26**. When hydrazoic acid (HN_3) was reacted with N,Ndimethylisopropylamine or triethylamine, the corresponding, white-solid, ammonium azides (**27** & **28**) were obtained. The latter two compounds were shown to be first examples of hypergolic salts containing an azide anion (see Figure 8) [Zhang et al, 2011b].

(a)

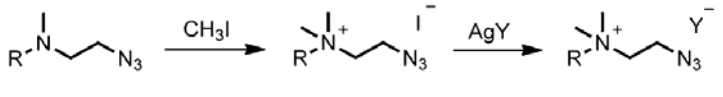

R = CH_3; Y = $N(NO_2)(CN)$ (**23**), $N(CN)_2$ (**24**)
R = $CH_2CH_2N_3$; Y = $N(NO_2)(CN)$ (**25**), $N(CN)_2$ (**26**)

(b)

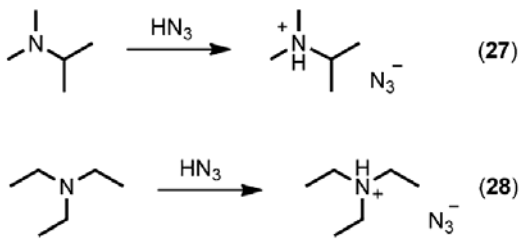

(**27**)

(**28**)

Figure 8: Synthesis of hypergolic ionic liquids (a) with mono- or bis- (azidoethyl)ammonium cations and (b) with azide anion [Zhang et al., 2011b]

Table 8 summarizes the physico-chemical properties of these azide cation (and anion) -based salts. Compounds **23**, **24**, **27** and **28** are ionic liquids (T_m below 100 °C) but only one of them (# **24**) is a liquid at ambient temperature. Compounds **23** to **26** have relatively high decomposition temperatures (T_d above 200°C) and high densities. On the contrary, ILs **27** and **28** have low densities with values around 1 $g.cm^{-3}$. Hypergolicity of these ILs was evaluated via droplet testing with WFNA (**23** to **26**) or N_2O_4 (**27** and **28**). Compounds **27** and **28** are protic liquids and were found to be hypergolic only with N_2O_4 (see Table 8) [Joo et al., 2010 and Zhang et al, 2011b].

Compd	T_m[a] [°C]	T_d[b] [°C]	d[c] [$g\,cm^{-3}$]	ID[e] [ms]	ΔH_f[f] [$kJ\,g^{-1}$]	I_{sp}[g] [s]
23	28	245	1.24	8	1.9	218
24	9	235	1.15	20	2.4	202
25	–	222	1.32	226	3.2	231
26	–	222	1.21	16	3.8	221
27	75	subl.	0.99	hg[h] (N_2O_4)	3.3	249
28	80	subl.	1.01	hg[h] (N_2O_4)	3.2	245

[a] Melting point, DSC, 10°C min^{-1}. [b] Decomposition onset, DSC, 10°C min^{-1}; subl. = sublimes. [c] Density, 25 °C. [d] Viscosity, 25 °C. [e] Ignition delay (WFNA). [f] Enthalpy of formation. [g] Specific impulse, calculated isobarically at 68 atm (Cheetah 5.0). [h] Hypergolic.

Legend: The molecule numbers correspond to the ones given in the Figure 8.

Table 8 : Properties of azide-functionalized ionic liquids [Zhang et al., 2011b]

Table 9 shows all of the systems for which hypergolicity has been observed experimentally. It is, however, worthy to note that no composition has been reported either in the liquid phase or in the gas phase for these cases.

Hypergolic mixtures		
Cation	Anion	Oxidant
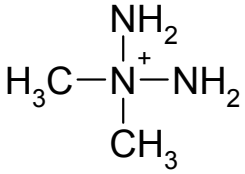	$N(CN)(NO_2)^-$	WFNA and N_2O_4
	NO_3^-	WFNA
	$N(CN)_2^-$	WFNA and N_2O_4
	Cl^-	N_2O_4

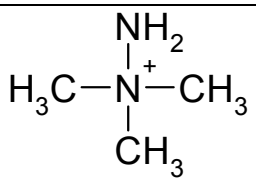	$N(CN)(NO_2)^-$	WFNA
	$N(CN)_2^-$	WFNA
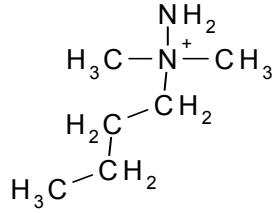	$BH_2(CN)_2^-$	WFNA
	$N(CN)(NO_2)^-$	WFNA
	$N(CN)_2^-$	WFNA
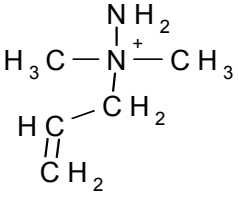	$BH_2(CN)_2^-$	WFNA
	$N(CN)(NO_2)^-$	WFNA
	$N(CN)_2^-$	WFNA
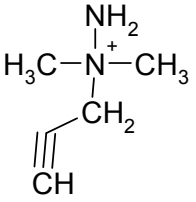	$BH_2(CN)_2^-$	WFNA
	$N(CN)(NO_2)^-$	WFNA
	$N(CN)_2^-$	WFNA
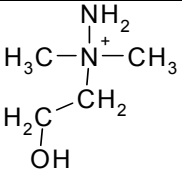	$N(CN)(NO_2)^-$	WFNA
	$N(CN)_2^-$	WFNA
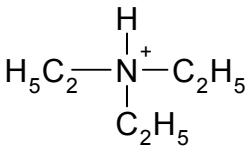	N_3^-	N_2O_4
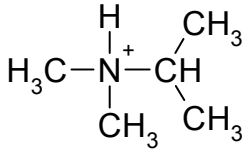	N_3^-	N_2O_4
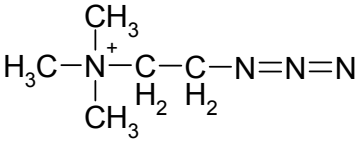	$N(CN)(NO_2)^-$	WFNA
	$N(CN)_2^-$	WFNA
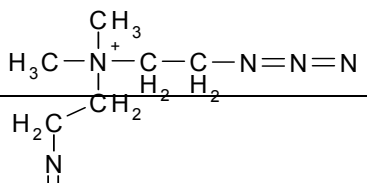	$N(CN)(NO_2)^-$	WFNA
	$N(CN)_2^-$	WFNA

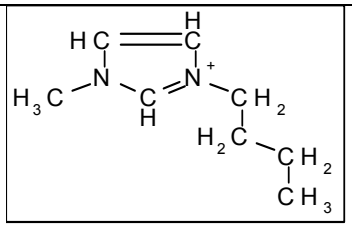	$BH_2(CN)_2^-$	WFNA
	$N(CN)(NO_2)^-$	WFNA
	$N(CN)_2^-$	WFNA
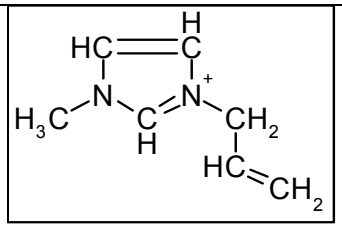	$BH_2(CN)_2^-$	WFNA
	$N(CN)(NO_2)^-$	WFNA
	$N(CN)_2^-$	WFNA
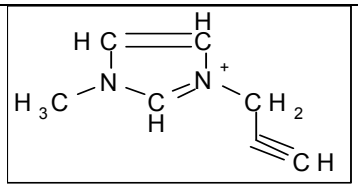	$N(CN)_2^-$	WFNA
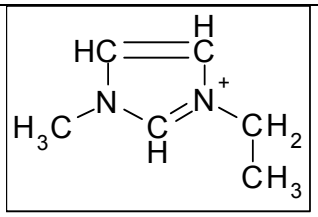	$N(CN)(NO_2)^-$	WFNA
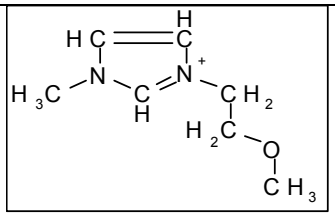	$N(CN)(NO_2)^-$	WFNA
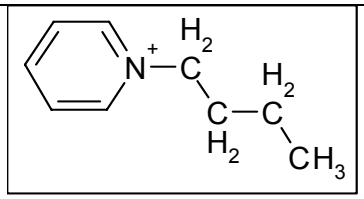	$BH_2(CN)_2^-$	WFNA
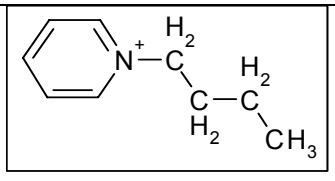	$BH_2(CN)_2^-$	WFNA
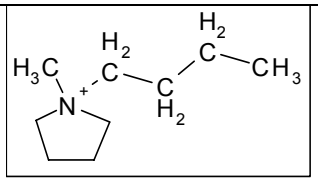	$BH_2(CN)_2^-$	WFNA
	$N(CN)_2^-$	WFNA

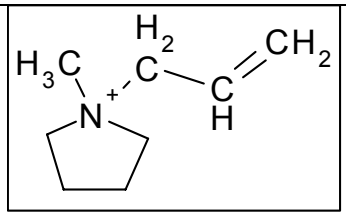	$BH_2(CN)_2^-$	WFNA
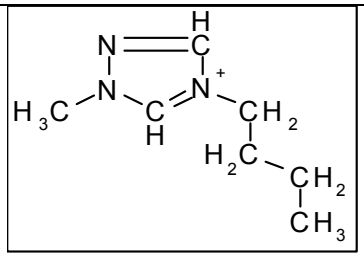	$BH_2(CN)_2^-$	WFNA
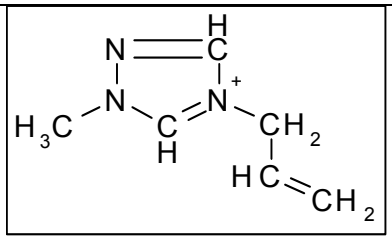	$BH_2(CN)_2^-$	WFNA

Table 9: Summary of all the systems found as hypergolic and presented in this report.

1.3 Flame Temperature Criterion

In this part, the flame temperature criterion considered for the construction of flammability limits diagram is explained. The data reported here are taken from a research proposal by Catoire [Catoire, 2012].

Previous studies on non-hypergolic systems have shown that the adiabatic flame temperature at the LFL and UFL remains approximately constant, and that the reported experimental flammability limits correspond to adiabatic flame temperatures in the 1000-1500 K range for hydrocarbon/air systems. One may therefore assume that flammability diagrams for hypergolic mixtures can also be rationalized with such a simple thermochemical criterion. This assumption has been applied to the monomethylhydrazine (MMH) - nitrogen tetroxide (NTO) system by using available gas phase experimental flammability diagrams at room temperature in which the condition of rapid adiabatic mixing was assumed. High speed videography was used to record the auto-ignition events. An example of igniting and non-igniting zones as a function of total pressure and equivalence ratio at a given mol% of He diluent is given in Figure 9. Additional data is available in the research proposal [Catoire, 2012].

As a proof-of-concept, Catoire and co-workers used their MMH/NTO detailed chemical kinetics model [Catoire et al., 2004] to establish a numerical criterion to predict flammability diagrams for MMH/NTO hypergolic combinations. Calculations were carried out to determine the adiabatic flame temperature at constant volume. For non-igniting mixtures, the calculated flame temperature was below the flame temperature calculated for igniting mixtures (Figures 6 to 8 in ref Catoire, 2012). For a stoichiometric mixture at low

total pressure, in which ignition was observed, the temperature profile reported in Figure 10 exhibits a flame temperature of about 3000 K. Moreover, this point is located right on the ignition limit (pressure of 6 kPa and equivalence ratio of 1.0). This observation and similar others allow for the establishment of a simple numerical criterion to predict ignition events under non-adiabatic conditions, which are more representative of the actual experimental conditions used in the MMH/NTO/He study; i.e., a rapid one-step or two-step temperature profile leading to a flame temperature at least equal to 2900 K. Near the limit, in the non-ignition zone (just below the lines in Figures 1-5 in ref Catoire, 2012), flame temperatures of about 2700-2800 K are computed. However, it is to be noted that for adiabatic experimental conditions, flames are likely to be observed in this zone [Catoire, 2012].

The temperature criterion determined here is dependent on the experimental setup used (i.e., rapid adiabatic mixing), and it is assumed that the threshold for the theoretical flame temperature to estimate flammability limits is much higher for hypergolic mixtures than it is for non-hypergolic mixtures, such as those in hydrocarbon-air systems.

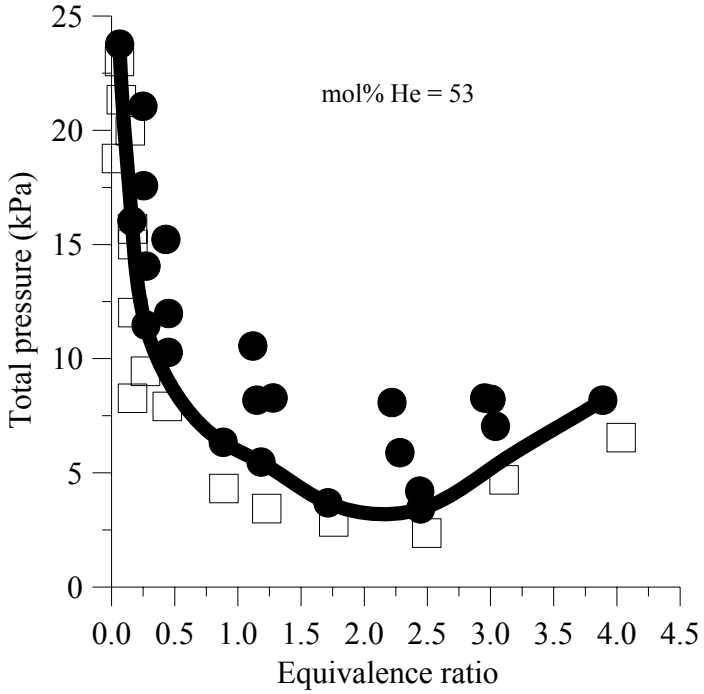

Figure 9: Flammability as a function of total mixture pressure and equivalence ratio obtained by assuming rapid mixing for MMH/NTO/He mixtures. □ : no ignition; ● : ignition

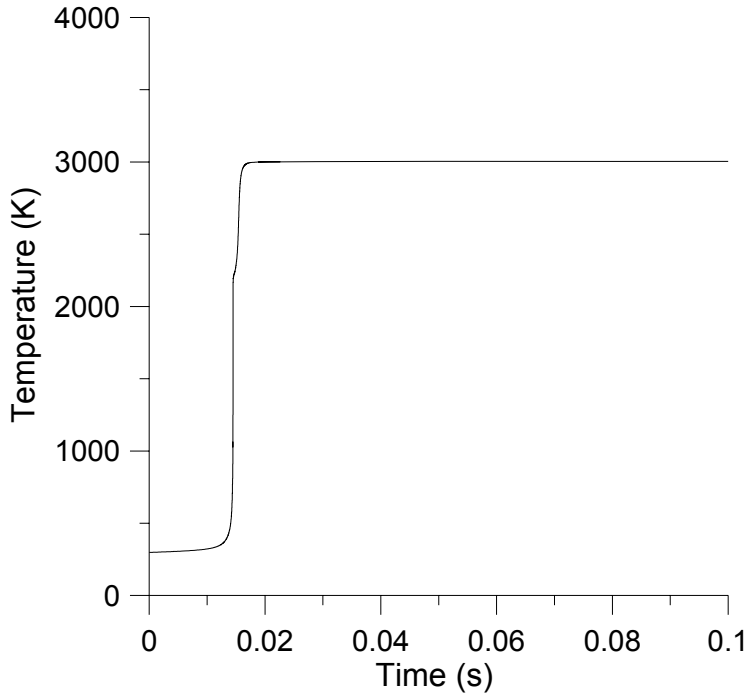

Figure 10: Typical temperature profile computed under adiabatic and constant volume assumptions for an igniting mixture (equivalence ratio 1.0 and low total pressure of 6 kPa).

Figure 11 shows that the use of this numerical criterion is quite consistent with the experimental results. This agreement between experiments and computations is to be expected for this mixture because the criterion was established according to experimental results of Figure 9. Furthermore, the good agreement also observed between experiments and computations for other mixtures (Figure 11 in ref Catoire, 2012) shows that the criterion can be extrapolated to other MMH/NTO mixtures with a high degree of confidence.

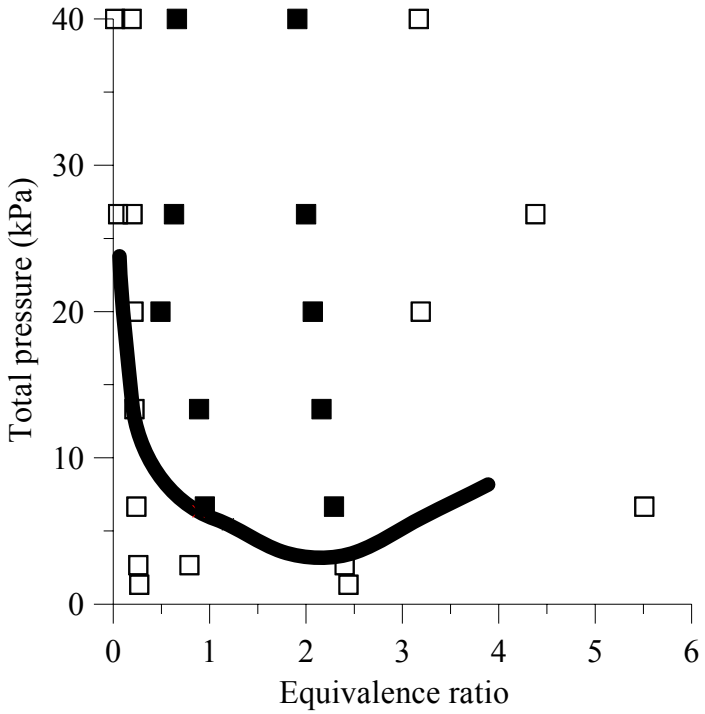

Figure 11: Computed flammability diagram (mol% He = 53). The line is the experimental limit between ignition and non-ignition regions given in Figure 9. □ : no ignition; ■ : ignition

The predictive ability of this thermodynamic method is extended successfully to numerous other non-ionic liquid/oxidant mixtures used for space applications. These results have been published in Combustion and Flame in 2017.

To summarize this part of the report, new hypergolic ionic liquid/oxidant mixtures that have recently been reported in the literature were surveyed. A simple thermodynamic criterion for the adiabatic flame temperature at constant volume is proposed herein to ascertain if a given IL/oxidant mixture will be hypergolic or not.

In the present work, a mixture is considered hypergolic if its adiabatic flame temperature at constant volume is equal or above 2700 K. When this is identified, the flammability limits are then computed as described below.

2 Thermochemistry of ionic liquids

Ionic liquids are important emerging compounds because of their potential applications as energetic propellants. In the last few years, efforts have been made to determine their thermodynamic data, but data are still scarce even for the simplest compounds.

Thermodynamic data, such as standard enthalpy of formation at 298.15 K, standard heat capacities (at constant pressure, $C_p°$ or at constant volume, $C_v°$) over a wide range of temperatures and standard absolute entropies S° over a wide range of temperature are needed for chemical equilibrium modeling studies [Catoire et al., 2009].

2.1 Estimation of thermodynamic data

Ab initio calculations have been shown to be reliable methods for estimating the thermochemistry of many compounds. Three methods for estimation of gas-phase standard enthalpy of formation at 298.15 K have been proposed by Osmont and co-workers [Osmont, 2007 and Osmont et al., 2007] by using quantum chemistry computations at the B3LYP/6-31G(d,p) level. Two of these methods can be applied to ionic liquids . One of these methods is devoted to general organic compounds and the other to energetic materials, in particular nitro and nitrate compounds. The gas-phase standard enthalpy of formation of molecule *j* at 298.15 K can be determined from the following equation [Catoire et al., 2009 and Osmont et al., 2007]:

$$\Delta_f H^0{}_{298.15\,K\,(g)} = 627.51 \times \left(E_j + ZPE_j + thermal\ corrections + \sum_i \alpha_i\, c_i^* \right)$$

where α_i is the number of atoms *i* in molecule *j* and C_i* the atomic correction for atom *i*. E_j and ZPE_j denote, respectively, the absolute electronic energy and zero-point energy, calculated using the GAUSSIAN 03 software package. The units are Hartree molecule^{-1} for E_j, ZPE_j and thermal corrections, and Hartree atom^{-1} for C_i*, whereas $\Delta_f H°_{298.15\ K\ (g)}$ is in kcal mol^{-1}. Four atomic corrections (for C, H, O and N) are considered here for the method established for organic compounds and seven atomic corrections (for C, H, O, N, C_d, O_d, and N_d) are considered for the method established for energetic compounds with one more atomic correction for hypervalent nitrogen (noted N_{hyp}) as encountered in ionic liquids. The values of these coefficients are given for the energetic compounds and the organic compounds, respectively in Table 10 and Table 11.

C_P, C_V and S are calculated from statistical thermodynamic equations once the vibration frequencies and inertia moments have been determined in the Gaussian package [Catoire et al., 2009].

Atom	C_i*
H	0.58188704
C	38.11447874
N	54.76547900
O	75.15682281
N_d	54.75925621
C_d	38.11542265
O_d	75.15439445
N_{hyp}	54.75799267

Table 10: Atomic corrections used in the energetic compounds method [Osmont, 2007 and Osmont et al., 2007]

Atom	C_i*
H	0.582238
C	38.114781
N	54.760090
O	75.150299

Table 11: Atomic corrections used in the organic compounds method [Osmont, 2007 and Osmont et al., 2007]

2.2 Validation of the method

The enthalpy of formation calculations are validated by comparison with literature values. Table 12 compares the experimental enthalpy of formation values with those calculated using both methods for different imidazoles, triazoles and tetrazoles. These compounds are not ionic, but they are structurally quite close to the cations present in the ILs considered here [Catoire et al., 2009].

Table 12 shows, unambiguously, that the method established for energetic compounds performs better than the method established for general organic compounds. The former method has previously been established for nitro and nitrate compounds and therefore should provide reasonably accurate results for the ionic liquids [Catoire et al., 2009].

Compound	Experimental $\Delta_f H°_{298.15\ K\ (g)}$ (kcal.mol^{-1})	Calculated $\Delta_f H°_{298.15\ K\ (g)}$ with the method for organic compounds (kcal.mol^{-1})	Calculated $\Delta_f H°_{298.15\ K\ (g)}$ with the method for energetic compounds (kcal.mol^{-1})
1H-1,2,4-triazole	46.1±0.2 45.05	40.7	43.4
2-ethyl-1H-imidazole	16.3±0.31	13.5	15.6
1H-tetrazole	76.6±0.7	71.7	74.0
1H-imidazole	33.29±0.45 30.6±1.8	29.1	32.3
2-methyl-1H-imidazole	21.5±0.26	18.5	21.1
1H-1,2,3-triazole	59	57	59.7
1H-pyrazole	42.9 43.3	39.2	42.4
Pyrrole	25.9±0.1 34.23	26.4	30.0

Table 12: Comparison between experimental gas-phase standard enthalpy of formation at 298.15 K and calculated gas-phase standard enthalpy of formation at 298.15 K for imidazoles, triazoles and tetrazoles taken from [Catoire et al., 2009].

However, as seen previously for aprotic ionic liquids, the chemical vapor above the IL can be composed of ions. It is therefore important to also validate these methods for cations and anions. Table 13 compares the experimental enthalpy of formation values with those calculated with both methods for different cations and anions. The experimental enthalpies of formation are taken from Mathieu and co-workers [Mathieu et al., 2010] and from Halim and co-workers [Halim et al., 1986].

The results show that for the cations, the method for organic compounds gives better agreement. This result is excepted because the cations considered are not energetic ions. However, for the anions, both methods give values in considerable disagreement with experimental values. Errors of up to 145 % (for OH^-) are seen, which lead us to conclude that the use of the B3LYP/6-31G(d,p) method for the determination of the enthalpy of formation of anions is not reliable (see Table 13).

Compound	Experimental $\Delta_f H°_{298.15\ K\ (g)}$ (kcal.mol^{-1}) [Mathieu et al., 2010 and Halim et al., 1986]	Calculated $\Delta_f H°_{298.15\ K\ (g)}$ with the method for organic compounds (kcal.mol^{-1})	Calculated $\Delta_f H°_{298.15\ K\ (g)}$ with the method for energetic compounds (kcal.mol^{-1})
NH_4^+(s)	155	153.9	146.3
$CH(OH)_2^+$(s)	96	96.1	103.4
CH_3CO^+(s)	156	155.3	157.4
NO_2^-(s)	-45.2	-30.0	-25.4
NO_3^-(s)	-74.7	-61.4	-60.4
CN^-(s)	17.7	36.7	36.6
$H_3C\text{-}CH_2^-$(s)	35.1	53.5	52.1
$H_3C\text{-}N^-\text{-}CH_3$(s)	26.1	35.2	36.9
OH^-(s)	-33.2	11.0	14.9
$C_6H_5O^-$(s) (phenoxy)	-40.5	-28.5	-23.1

Table 13: Comparison between experimental gas-phase standard enthalpy of formation at 298.15 K and calculated gas-phase standard enthalpy of formation at 298.15 K for selected cations and anions. Calculation method: B3LYP/6-31G(d,p) corrected on an atomic basis. (s) stands for the singlet state.

Another *ab initio* method (G2) to determine the enthalpy of formation for anions was tested. This method is more precise but computationally can be time consuming. The enthalpy of formation is given by:

$$\Delta_f H^0{}_{298.15K\,(g)}(IL) = \left(627.51 \times \left(G2Enthalpy(IL) - \sum_i \alpha_i \times G2Enthalpy(i)\right)\right) + \sum_i \alpha_i \times \Delta_f H^0{}_{298.15K\,(g)}(i)$$

Here, α_i is the number of atoms *i* in the IL and G2Enthalpy denotes the enthalpy at 298 K of the molecule, calculated using the GAUSSIAN 03 software package. The units are Hartree.molecule^{-1} for G2Enthalpy, whereas $\Delta_f H°_{298.15\ K\ (g)}$ is in kcal mol^{-1}.

Table 14 compares the experimental enthalpy of formation values and the calculated ones for different anions. The results show good agreement between the calculated and the experimental values.

Compounds	G2Enthalpy	$\Delta_f H°_{298.15\ K\ (g)}$ of atom (kcal.mol^{-1})	Calculated $\Delta_f H°_{298.15\ K\ (g)}$ (kcal.mol^{-1})	Experimental $\Delta_f H°_{298.15\ K\ (g)}$ (kcal.mol^{-1}) [Mathieu et al., 2010 and Halim et al., 1986]
C	-37.785278	171.29		
H	-0.497639	52.1		
O	-74.980024	59.43		
N	-54.515599	112.97		
B	-24.599675	133.84		
CN^-(s)	-92.725481		17.8	17.7
NO_2^-(s)	-204.919145		-46.4	-45.2
NO_3^-(s)	-280.040762		-75.8	-74.7
OH^-(s)	-75.709467		-33.9	-33.2
$H_3C\text{-}CH_2^-$(s)	-78.95849		38.4	35.1
$H_3C\text{-}N^-\text{-}CH_3$(s)	-134.248824		29.6	26.1

Table 14: Comparison between experimental gas-phase standard enthalpy of formation at 298.15 K and calculated gas-phase standard enthalpy of formation at 298.15 K for different anions. Calculation method: G2.

2.3 Results

In this part, the enthalpy of formation and the thermodynamic data of the IL studied are presented. The enthalpy of formation of the cations are presented in Table 15, which have been determined via B3LYP/6-31G(d,p) calculations and corrected by using the Osmont method for energetic compounds. The anion values were determined via G2 calculations.

Due to excessive computational time encountered for the aprotic ionic liquids, only thermodynamic data of the separated ions have been calculated.

It must be noted that we were not able to determine the enthalpy of formation for $N(NO_2)(CN)^-$ due to convergence problems within the G2 method as implemented in the Gaussian 03 software package.

Compound	Molecule	Calculated $\Delta_f H°_{298.15\ K\ (g)}$ (kcal.mol^{-1})
1	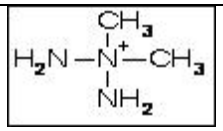	183.4
2	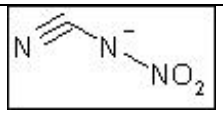	See text
3	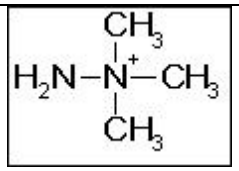	151.8
4	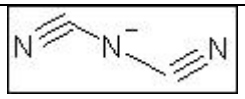	32.7
5	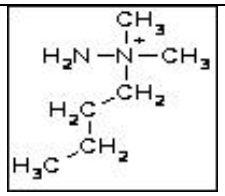	132.3
6	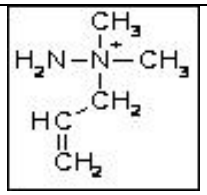	171.5
7	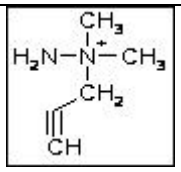	218.0
8	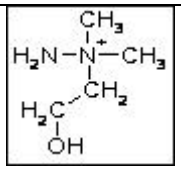	111.6
9	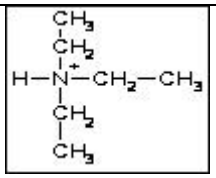	99.5
10	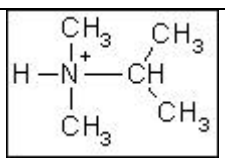	107.5

11	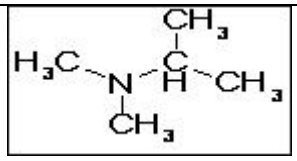	-18.9
12	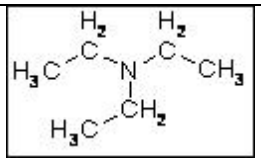	-24.0
13	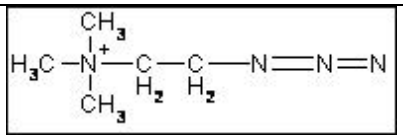	196.2
14	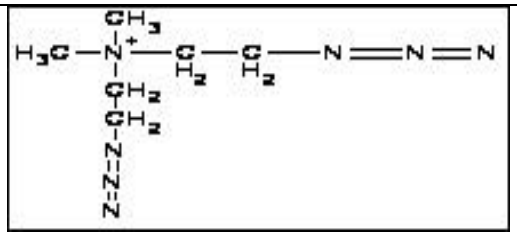	270.5
15	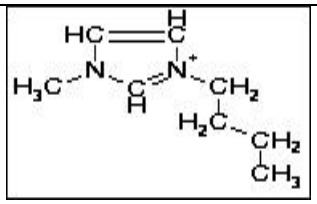	130.7
16	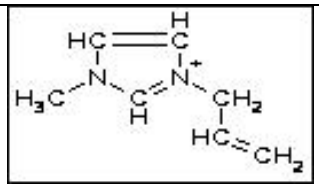	170.7
17	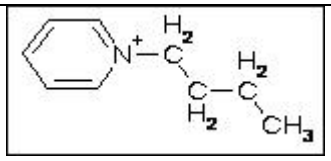	139.3
18	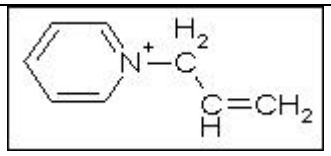	179.6
19	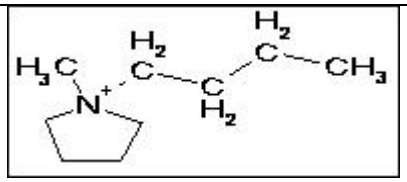	101.3
20	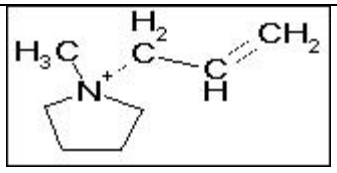	140.5

21	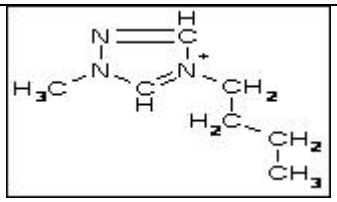	151.3
22	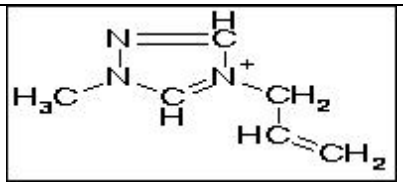	191.4
23	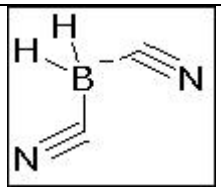	-15.3
24	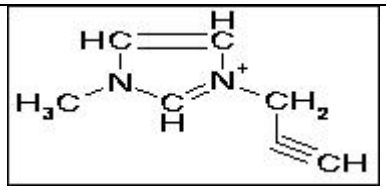	220.2
25	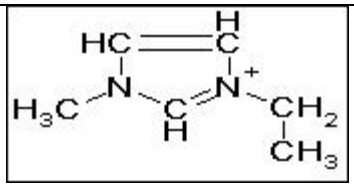	142.5
26	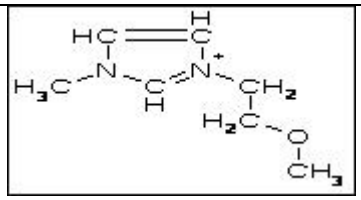	110.5

Table 15: Calculations of the gas-phase standard enthalpy of formation at 298.15 K for different ions of interest for ionic liquids studied in this report. Calculation methods: corrected B3LYP/6-31G(d,p) for the cations and molecules; and G2 method for the anions.

Once the standard enthalpy of formation at 298.15 K as well as the C_P, C_V and S had been calculated, the 14 coefficients in the NASA format needed for thermodynamic calculations were determined according to the CHEMKIN-NASA format.

These NASA polynomials have the form:

$$C_P/R = a1 + a2\ T + a3\ T^2 + a4\ T^3 + a5\ T^4$$

$$H/RT = a1 + a2\ T/2 + a3\ T^2\ /3 + a4\ T^3/4 + a5\ T^4/5 + a6/T$$

$$S/R = a1\ \ln(T) + a2\ T + a3\ T^2\ /2 + a4\ T^3\ /3 + a5\ T^4\ /4 + a7$$

Where a1, a2, a3, a4, a5, a6, and a7 are the numerical coefficients supplied in the NASA thermodynamic files. The first 7 numbers starting on the second line of each species entry (five of the second line and the first two of the third line) are the seven coefficients (a1 through a7, respectively) for the high-temperature range (above 1500 K, the upper boundary is specified on the first line of the species entry). The remaining seven numbers are the coefficients (a1 through a7, respectively) for the low-temperature range (below 1500 K, the lower boundary is specified on the first line of the species entry).

The thermodynamic data of the species studied here are given below. The species are named MOL1, MOL2, MOL3, etc. The correspondence between the molecules is given in Table 15. Thermodynamic data for $N(NO_2)(CN)^-$ (Molecule n°2) have not been determined.

MOL1 H 10C 2N 3 G 298.150 5000.000 1500.00 1
0.12221351E+02 0.27003260E-01-0.99627348E-05 0.17079181E-08-0.11138762E-12 2
0.85934737E+05-0.42110438E+02-0.56400683E+00 0.57280381E-01-0.36422690E-04 3
0.11771380E-07-0.15058781E-11 0.90199776E+05 0.26186977E+02 4

MOL3 H 11C 3N 2 G 298.150 5000.000 1500.000 1
0.12506042E+02 0.29490288E-01-0.10890801E-04 0.18664465E-08-0.12162023E-12 2
0.69541182E+05-0.44885430E+02-0.10450059E+01 0.58765690E-01-0.33305478E-04 3
0.87793139E-08-0.76556296E-12 0.74378328E+05 0.28557790E+02 4

MOL4 C 2N 3 G 298.150 5000.000 1500.000 1
8.39498290E+00 4.53143670E-03-1.81293070E-06 3.29552030E-10-2.24501790E-14 2
1.33068850E+04-1.66833200E+01 3.69004260E+00 1.70717050E-02-1.43469600E-05 3
5.89745910E-09-9.49972540E-13 1.47190690E+04 7.92532660E+00 4

MOL5 H 17C 6N 2 G 298.150 5000.000 1500.000 1
0.20769841E+02 0.46325712E-01-0.17189680E-04 0.29552207E-08-0.19297896E-12 2
0.55083923E+05-0.88213717E+02-0.29713969E+01 0.97424363E-01-0.56077011E-04 3
0.14811226E-07-0.12644377E-11 0.63580068E+05 0.40529523E+02 4

MOL6 H 13C 5N 2 G 298.150 5000.000 1500.000 1

0.17281353E+02 0.36143137E-01-0.13437319E-04 0.23154042E-08-0.15154042E-12 2
0.77194076E+05-0.68980441E+02-0.20951885E+01 0.81214599E-01-0.51909467E-04 3
0.16481108E-07-0.20236530E-11 0.83749462E+05 0.34831424E+02 4

MOL7 H 11C 5N 2 G 298.150 5000.000 1500.000 1
0.16535182E+02 0.31575764E-01-0.11778552E-04 0.20360063E-08-0.13362984E-12 2
0.10148196E+06-0.63303688E+02-0.16266850E+00 0.72173440E-01-0.48446302E-04 3
0.16586150E-07-0.22675481E-11 0.10693343E+06 0.25497909E+02 4

MOL8 H 13C 4N 2O 1 G 298.150 5000.000 1500.000 1
0.17374545E+02 0.35902592E-01-0.13305052E-04 0.22871019E-08-0.14941239E-12 2
0.46989499E+05-0.70084578E+02-0.19549970E+01 0.80494649E-01-0.50943720E-04 3
0.15925004E-07-0.19073303E-11 0.53570618E+05 0.33614265E+02 4

MOL9 H 16C 6N 1 G 298.150 5000.000 1500.000 1
1.82134750E+01 4.32403920E-02 -1.60232010E-05 2.75054700E-09-1.79354230E-13 2
3.96208820E+04-7.48831380E+01-3.15401830E+00 8.67997730E-02-4.61619800E-05 3
1.01808480E-08-4.23619110E-13 4.75409470E+04 4.18991630E+01 4

MOL10 H 14C 5N 1 G 298.150 5000.000 1500.000 1
1.56143130E+01 3.74427360E-02-1.38408510E-05 2.37154620E-09-1.54421660E-13 2
4.51906300E+04-6.14899080E+01-1.81484190E+00 7.22115700E-02-3.69007720E-05 3
7.41643810E-09-1.27910030E-13 5.17366300E+04 3.40534480E+01 4

MOL11 H 13C 5N 1 G 298.150 5000.000 1500.000 1
1.59482810E+01 3.47910660E-02-1.29295800E-05 2.22311060E-09-1.45094350E-13 2
-1.84222690E+04-6.30692110E+01-9.59869520E-01 6.71093780E-02-3.24778010E-05 3
5.23561280E-09 2.98754580E-13-1.19131880E+04 3.01472910E+01 4

MOL12 H 15C 6N 1 G 298.150 5000.000 1500.000 1

1.85598390E+01 4.05535670E-02-1.50935760E-05 2.59837650E-09-1.69756920E-13 2
-2.25364320E+04-7.60810400E+01-2.26125710E+00 8.18745290E-02-4.22125790E-05 3
8.33928440E-09-7.45779110E-14-1.46923830E+04 3.81366730E+01 4

MOL13 H 13C 5N 4 G 298.150 5000.000 1500.000 1
2.11309450E+01 3.83671830E-02-1.43254990E-05 2.47370000E-09-1.62055080E-13 2
8.77922240E+04-8.53840660E+01-5.90900300E-01 8.54137440E-02-5.04936990E-05 3
1.37136290E-08-1.22957220E-12 9.55325930E+04 3.22981140E+01 4

MOL14 H 14C 6N 7 G 298.150 5000.000 1500.000 1
0.29266684E+02 0.44981381E-01-0.16930399E-04 0.29415811E-08-0.19363340E-12 2
0.12167229E+06-0.12521235E+03-0.25915707E+00 0.11231959E+00-0.72871240E-04 3
0.22738680E-07-0.26489004E-11 0.13181224E+06 0.33478473E+02 4

MOL15 H 15C 8N 2 G 298.150 5000.000 1500.000 1
0.23633619E+02 0.44316180E-01-0.16588115E-04 0.28701773E-08-0.18833317E-12 2
0.53137611E+05-0.10119307E+03-0.50748197E+01 0.10959076E+00-0.70581446E-04 3
0.21853323E-07-0.25165423E-11 0.63019284E+05 0.53179294E+02 4

MOL16 H 11C 7N 2 G 298.150 5000.000 1500.000 1
2.01407130E+01 3.41313630E-02-1.28330030E-05 2.22960970E-09-1.46829910E-13 2
7.56107620E+04-8.22553380E+01-4.22537250E+00 9.34198090E-02-6.64336670E-05 3
2.35242240E-08-3.27461520E-12 8.35604630E+04 4.73094550E+01 4

MOL17 H 14C 9N 1 G 298.150 5000.000 1500.000 1
0.22887047E+02 0.42541565E-01-0.16001824E-04 0.27798010E-08-0.18299558E-12 2
0.57807766E+05-0.98611143E+02-0.70273065E+01 0.11350452E+00-0.78156131E-04 3
0.26488981E-07-0.34820330E-11 0.67773046E+05 0.61140793E+02 4

MOL18 H 10C 8N 1 G 298.150 5000.000 1500.000 1

0.19385432E+02 0.32357553E-01-0.12244457E-04 0.21384603E-08-0.14142111E-12 2
0.80444642E+05-0.80321391E+02-0.60966919E+01 0.96936218E-01-0.73449456E-04 3
0.27841274E-07-0.41753222E-11 0.88468817E+05 0.54212366E+02 4

MOL19 H 20C 9N 1 G 298.150 5000.000 1500.000 1
2.51021820E+01 5.63194830E-02-2.10361390E-05 3.63349540E-09-2.38086630E-13 2
3.65946780E+04-1.14534790E+02-8.25590260E+00 1.29996640E-01-7.94355540E-05 3
2.27986850E-08-2.30060050E-12 4.83208490E+04 6.56533820E+01 4

MOL20 H 16C 8N 1 G 298.150 5000.000 1500.000 1
0.21607868E+02 0.46141348E-01-0.17284782E-04 0.29936958E-08-0.19663707E-12 2
0.58673424E+05-0.95582664E+02-0.74028215E+01 0.11382253E+00-0.75285304E-04 3
0.24469191E-07-0.30588004E-11 0.68465705E+05 0.59770214E+02 4

MOL21 H 14C 7N 3 G 298.150 5000.000 1500.000 1
0.23383677E+02 0.41886809E-01-0.15683501E-04 0.27136129E-08-0.17803078E-12 2
0.63734166E+05-0.99096867E+02-0.44766222E+01 0.10463770E+00-0.66891146E-04 3
0.20342236E-07-0.22610795E-11 0.73390870E+05 0.50938069E+02 4

MOL22 H 10C 6N 3 G 298.150 5000.000 1500.000 1
0.19881811E+02 0.31710093E-01-0.11931202E-04 0.20734749E-08-0.13655142E-12 2
0.86239119E+05-0.80433040E+02-0.36417491E+01 0.88471133E-01-0.62723789E-04 3
0.21995312E-07-0.30147499E-11 0.93967638E+05 0.44830692E+02 4

MOL23 H 2B 1C 2N 2 G 298.150 5000.000 1500.000 1
1.04611980E+01 8.23196630E-03-3.24453210E-06 5.83262300E-10-3.93984190E-14 2
-1.19524750E+04-2.73473330E+01 3.47564280E+00 2.58450550E-02-1.98425640E-05 3
7.50902870E-09-1.11850340E-12-9.74261500E+03 9.56697690E+00 4

MOL24 H 9C 7N 2 G 298.150 5000.000 1500.000 1

1.93946860E+01 2.95388380E-02-1.11578610E-05 1.94645600E-09-1.28625530E-13 2
1.01429660E+05-7.59270610E+01-2.14987260E+00 8.39291620E-02-6.24863520E-05 3
2.33983040E-08-3.47713110E-12 1.08237480E+05 3.78967370E+01 4

MOL25 H 11C 6N 2 G 298.150 5000.000 1500.00 1
0.18124559E+02 0.33085667E-01-0.12386017E-04 0.21439698E-08-0.14075077E-12 2
0.62138460E+05-0.72551170E+02-0.37028381E+01 0.83822661E-01-0.55653614E-04 3
0.18054281E-07-0.22391805E-11 0.69526986E+05 0.44404675E+02 4

MOL26 H 13C 7N 2O 1 G 298.150 5000.000 1500.00 1
0.23062140E+02 0.39492745E-01-0.14793921E-04 0.25609108E-08-0.16808653E-12 2
0.43554033E+05-0.97103934E+02-0.39133912E+01 0.10105465E+00-0.65982974E-04 3
0.20701446E-07-0.24231499E-11 0.52813638E+05 0.47864867E+02 4

Because of excessive computational time, the enthalpy of formation and therefore, the thermodynamic data of ions pairs or neutral pairs were not calculated in this work.

3 Equilibrium Calculations

The third part of this report presents results obtained from the equilibrium calculations. At this time, only mixtures which were found to be hypergolic experimentally are considered here.

3.1 Initial conditions

The determination of the adiabatic Flame Temperature (T_F) and of the Adiabatic Isochoric Complete Combustion Pressure (P_{AICC}) was carried out via adiabatic constant volume calculations with the "Equilibrium Calculations" suite of the COSILAB software package [COSILAB, 2010].

The species taken into account for the equilibrium calculations are listed below:

- For H, C, N and O:

H, C, N, O, H+, OH-, H_2, CO, N_2O_4, CO_2, H_2O, N_2, O_3, OH, NO, NO_2, N_2O, H_2O_2, HO_2, CH_4, HNO_2, CH, HCN, CH_2, CH_3, CN, CN-, N_3-, N_3H, HNO, NH_3, CH_3O, CH_2OH, CH_3OH, C_2H_2, C_2H_4, C_3H_6, C_4H_8, HOCN, HCHO, CH_3CHO, HNO_3, C_2H_5OH, C_3H_8, C_2H_6, C_4H_{10}, HNCO, NO_2^-, NO_3^-

- For chlorine (Cl):

Cl, Cl^-, HCL, ClO_2, ClO, HOCl, Cl_2

- For boron (B):

B, B_2O_3, $BH_2(CN)_2^-$, BO, BH, BH_2, BH_3, BH_4, BH_5, B_2, B_2H, B_2H_2, B_2H_6, B_2O, B_2O_2

For all of these species, the thermodynamic data was taken from the database of Burcat [Goos et al., 2013].

All calculations were carried out with same starting conditions (initial temperature of 298.15 K and initial pressure of 1 Atm).

For the mixtures for which charged species are involved, the initial conditions are:

X(cation) = X(anion)

X(cation) + X(anion) + X(oxidant) =1

where X represents the mole fraction of the concerned species. X varies from 0 to 0.5.

For mixture where neutral species are considered:

X(neutral 1) = X(neutral 2)

X(neutral 1) + X(neutral 2)+ X(oxidant) =1

All of the mixtures considered are hypothetical and it is tenable that hypergolic ignition is also possible due to species present in the gas phase but formed by reactions taking place in the liquids. This possibility is examined in parts two and three of this report. Furthermore, the temperature of both the liquid and the gas is certainly higher than 298 K but neither the temperature nor the compositions are known when experimental hypergolic ignition is observed.

As seen in the first part of this report, ionic liquids can be divided into two classes, namely protic and aprotic ILs. The results obtained for each of these two classes are presented separately below.

3.2 Protic Ionic Liquid

Protic Ionic Liquids are ionic liquids for which the cation can transfer a proton (H+) to the anion to form two neutral compounds. As seen in the first part of this report, the chemical vapor above the ionic liquid can be composed of separated ions, separated neutrals, ion pairs, and pair of neutrals or a mixture of all of these. The chemical vapor above the IL/oxidant liquid system, once mixed, can also be composed of a combination of all of these as well as oxidant species (and its fragments). The nature of the vapor remains to be determined experimentally, both qualitatively and quantitatively. In this study, three different cases have been considered for equilibrium calculations:

- In the vapor, the cation and the anion both separated are present.

- In the vapor, two neutral molecules both separated are present.

- In the vapor, the cation, the anion and the neutral molecules all of them separated are present.

Two different protic ionic liquids were found to be hypergolic with N_2O_4 in the literature. These systems are:

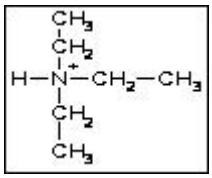

($NC_6H_{16}^+$) + N_3^- hypergolic with N_2O_4

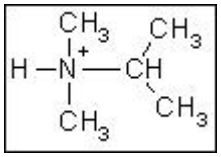

($NC_5H_{14}^+$) + N_3^- hypergolic with N_2O_4

The first mixture considered is $NC_6H_{16}^+ + N_3^-$ with N_2O_4. The results obtained for the mixtures with only the cation and the anion separated in the vapor are given in Figure 12 and Table 16.

As described in the second part of this report, a temperature criterion of 2700 K was proposed for determining the flammability limits of potential hypergolic systems. In this case, the lower flammability limit (LFL) and the upper flammability limit (UFL) are determined, respectively, for a mole fraction of the cation, X(cation), between 0.039 and 0.048 for the LFL and 0.310 and 0.315 for the UFL.

It can be seen, that at the beginning with an increase of the mole fraction of the cation, the flame temperature (T_F) and the adiabatic isochoric complete combustion pressure (P_{AICC}) rise until they reached their maximum for a mole fraction of cation around 0.140. At this point T_F is around 4200 K and the P_{AICC} is around 57 Atm. Then when the mole fraction continues to increase, T_F and the P_{AICC} decrease over the remaining composition domain.

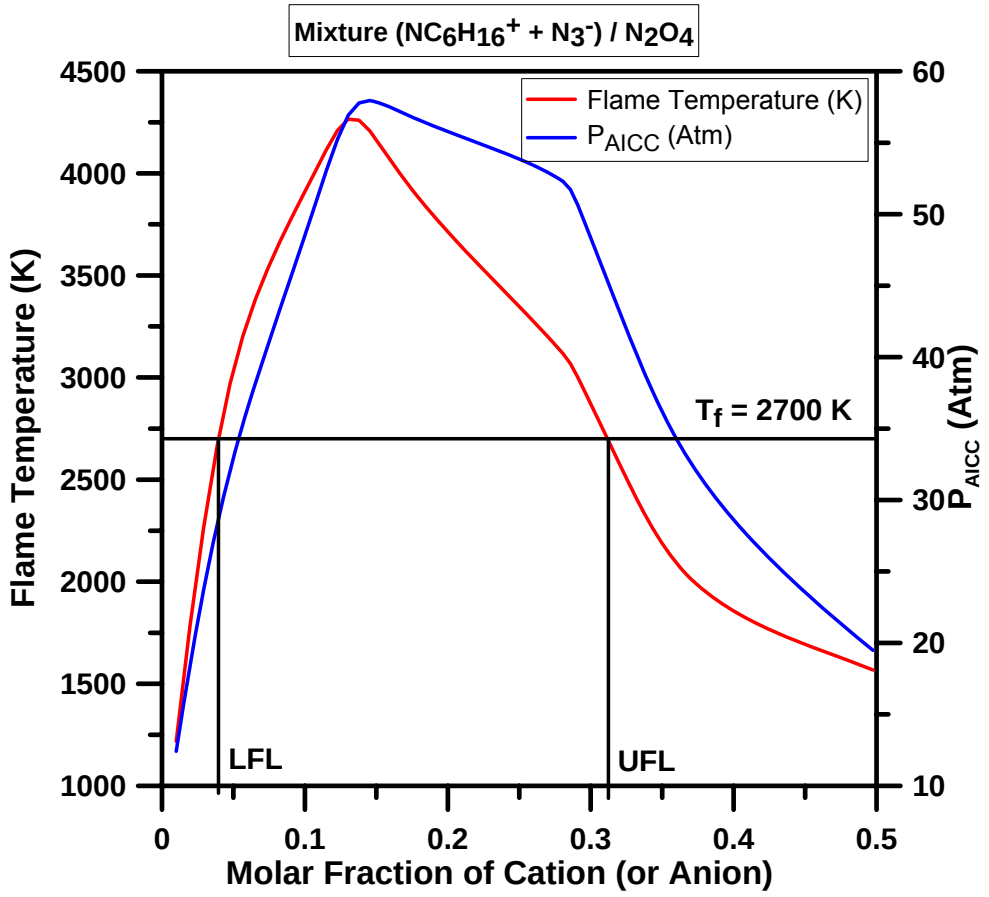

Figure 12: Flame temperature and P_{AICC} for different $NC_6H_{16}^+ + N_3^-$ / N_2O_4 mixtures at 298.15 K and 1 Atm.

Mixture	Cation 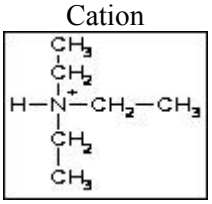 $NC_6H_{16}^+$	Anion N_3^-	Oxidant N_2O_4
Stoichiometric Equation	1 $[NC_6H_{16}^+ N_3^-]$ + 5 N_2O_4 → 6 CO_2 + 8 H_2O + 7 N_2		
Initial Conditions	P =1 Atm ; T = 298.15 K $X(NC_6H_{16}^+) = X(N_3^-)$ $X(NC_6H_{16}^+) + X(N_3^-) + X(N_2O_4) = 1$		
Lower Flammability Limit (LFL)	0.039 (T_F = 2661 K ; P_{AICC} = 28.2 Atm)	< $X(NC_6H_{16}^+)$ < < $X(N_3^-)$ <	0.048 (T_F = 2969 K ; P_{AICC} = 32.0 Atm)
Upper Flammability Limit (UFL)	0.310 (T_F = 2720 K ; P_{AICC} = 45.7 Atm)	< $X(NC_6H_{16}^+)$ < < $X(N_3^-)$ <	0.315 (T_F = 2650 K ; P_{AICC} = 44.5 Atm
P_{AICC} Max Composition	57.9 Atm ($X(Ca^+)$= 0.145)	**T_F Max Composition**	4266 K ($X(Ca^+)$= 0.130)

Table 16: Equilibrium Calculations results for the $NC_6H_{16}^+ + N_3^- / N_2O_4$ system. $X(Ca^+)$ is the mole fraction of cation.

In Figure 13 and in Table 17 are the results if we consider the chemical vapor above the ionic liquid composed of neutral compounds. The mixture can be represented as:

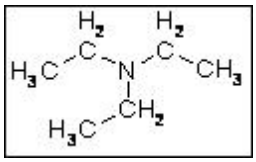 (NC_6H_{15}) + HN_3 with N_2O_4

A diminution in the value of the UFL can be observed compared to the value obtained with the mixtures with charged species. On the contrary, no change is noted in the value for LFL. The UFL is now encompassed between 0.259 and 0.265, leading to a reduction of the flammability domain compared to the one observed for the charged species. The maximum flame temperature and P_{AICC} are obtained for mixtures with a mole fraction $X(Ca^+)$ around 0.130.

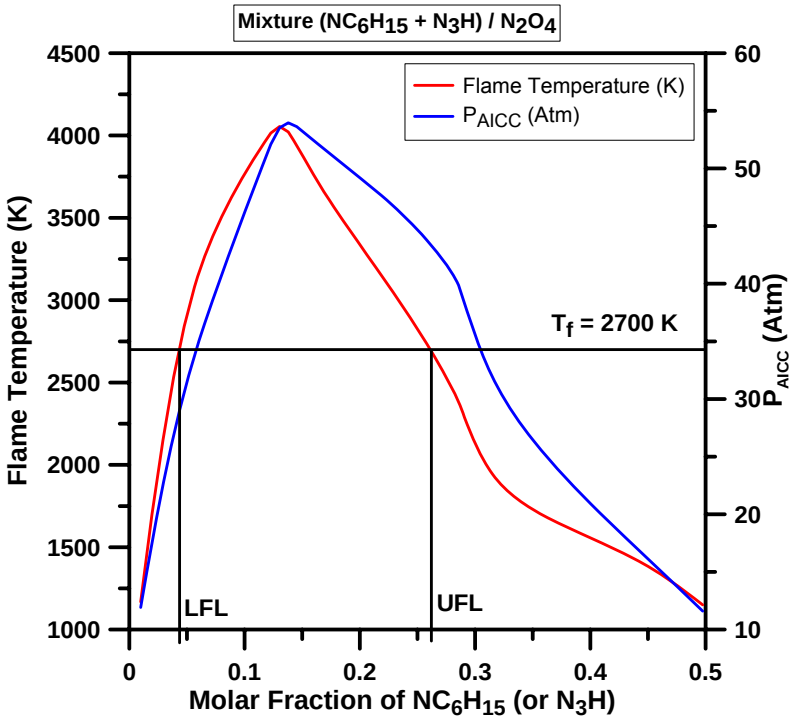

Figure 13: Flame temperature and P_{AICC} for different NC_6H_{15} + HN_3 / N_2O_4 mixtures at 298.15 K and 1 Atm.

Mixture	Neutral 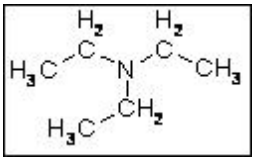 NC_6H_{15}	Neutral HN_3	Oxidant N_2O_4
Stoichiometric Equation	1 [NC_6H_{15} N_3H] + 5 N_2O_4 → 6 CO_2 + 8 H_2O + 7 N_2		
Initial Conditions	P =1 Atm ; T = 298.15 K $X(NC_6H_{15}) = X(HN_3)$ $X(NC_6H_{15}) + X(HN_3) + X(N_2O_4) = 1$		
Lower Flammability Limit (LFL)	0.039 (T_F = 2534 K ; P_{AICC} = 26.8 Atm)	< $X(NC_6H_{15})$ < < $X(HN_3)$ <	0.048 (T_F = 2842 K ; P_{AICC} = 30.6 Atm)
Upper Flammability Limit (UFL)	0.259 (T_F = 2722 K ; P_{AICC} = 43.7 Atm)	< $X(NC_6H_{15})$ < < $X(HN_3)$ <	0.265 (T_F = 2658 K ; P_{AICC} = 43.0 Atm)
P_{AICC} Max Composition	54.0 Atm (X(Ne)= 0.138)	**T_F Max Composition**	4055 K (X(Ne)= 0.130)

Table 17: Equilibrium Calculations results for the NC_6H_{15} + HN_3 / N_2O_4 system. X(Ne) is the mole fraction of neutrals.

The chemical vapor above the ionic liquid can be composed of a mixture of charged and neutrals species. The mixture is then supposed to be:

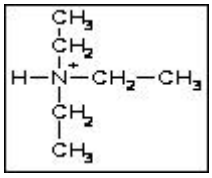

($NC_6H_{16}^+$) + N_3^- +

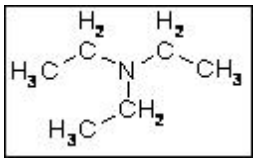

(NC_6H_{15}) + HN_3 and this mixture may be hypergolic with N_2O_4

In our study, we have considered that the mole ratio between the neutral and the charged species is equal to one. The initial conditions are the following:

$$X(NC_6H_{16}^+) = X(N_3^-) = X(NC_6H_{15}) = X(HN_3)$$

$$X(NC_6H_{16}^+) + X(N_3^-) + X(NC_6H_{15}) + X(HN_3) + X(N_2O_4) = 1$$

The results obtained for this mixture are presented in Figure 14 and in Table 18. The lower flammability limit is obtained for a mole fraction of $NC_6H_{16}^+$ between 0.019 and 0.024, and the upper flammability limit is between 0.143 and 0.145. The maximum flame temperature of the system is equal to 4164 K and is obtained for a mole fraction equal to 0.065.

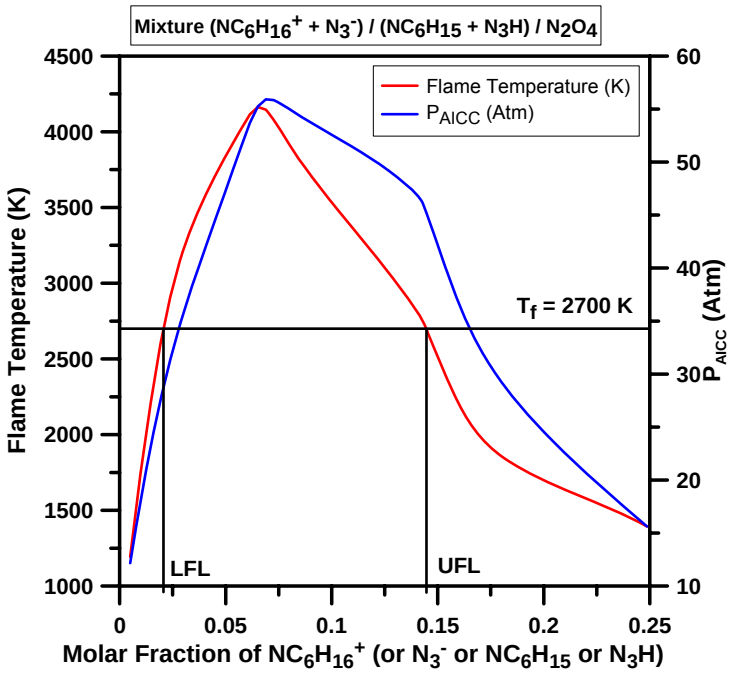

Figure 14: Flame temperature and P_{AICC} for different NC_6H_{15} + HN_3 + $NC_6H_{16}^+$ + N_3^- / N_2O_4 mixtures at 298.15 K and 1 Atm.

Mixture	Neutral 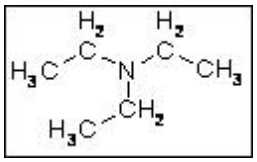 NC_6H_{15}	Neutral HN_3	Cation 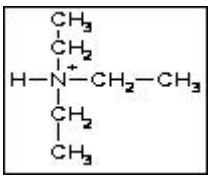 $NC_6H_{16}^+$	Anion N_3^-	Oxidant N_2O_4
Stoichiometric Equation	1 $[NC_6H_{16}^+ N_3^-]$ +1 $[NC_6H_{15}\ HN_3]$ + 10 N_2O_4 → 12 CO_2 + 16 H_2O + 14 N_2				
Initial Conditions	P =1 Atm ; T = 298.15 K $X(NC_6H_{16}^+) = X(N_3^-) = X(NC_6H_{15}) = X(HN_3)$ $X(NC_6H_{16}^+) + X(N_3^-) + X(NC_6H_{15}) + X(HN_3) + X(N_2O_4) = 1$				
Lower Flammability Limit (LFL)	0.019 (T_F = 2599 K ; P_{AICC} = 27.5 Atm)	< $X(NC_6H_{15})$ < < $X(HN_3)$ or $X(NC_6H_{16}^+)$ or $X(N_3^-)$ <		0.024 (T_F = 2907 K ; P_{AICC} = 31.3 Atm)	
Upper Flammability Limit (UFL)	0.143 (T_F = 2751 K ; P_{AICC} = 46.1 Atm)	< $X(NC_6H_{15})$ < < $X(HN_3)$ or $X(NC_6H_{16}^+)$ or $X(N_3^-)$ <		0.145 (T_F = 2671 K ; P_{AICC} = 44.9 Atm)	
P_{AICC} Max Composition	55.9 Atm (X(Ne)= 0.069)	**T_F Max Composition**		4164 K (X(Ne)= 0.065)	

Table 18: Equilibrium calculations results for the NC_6H_{15} + HN_3 + $NC_6H_{16}^+$ + N_3^- / N_2O_4 system.

Like the above system, for the second reported hypergol case, three different test compositions of the chemical vapor above the ionic liquid once mixed with the oxidizer (charged species, neutral species, and a mixture of both charged and neutral species) were similarly considered.

The results for the charged species are given in Table 19. The system considered is:

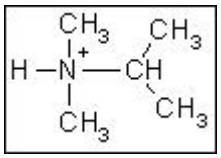 ($NC_5H_{14}^+$) + N_3^- with N_2O_4

The lower flammability limit is obtained at a mole fraction of cation (or anion) between 0.039 and 0.048, and the upper flammability limit at a mole fraction of cation (or anion) between 0.342 and 0.346. For a mixture with neutral species NC_5H_{13} and HN_3 (results given in Table 20), the flammability domain is smaller. Indeed, the LFL is obtained for a mole fraction of the neutral species between 0.048 and 0.057 and the UFL is between 0.286 and 0.291. For the mixtures with the charged species, the maximum flame temperature is equal to 4310 K for a mole fraction of cation equal to 0.153 (see Table 19). For the mixture with

neutral species, this maximum flame temperature drops to 4064 K for almost the same mole fraction. This behavior is also observed for the value of the maximum P_{AICC}.

Mixture	Cation 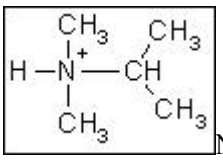 $NC_5H_{14}^+$	Anion N_3^-	Oxidant N_2O_4
Stoichiometric Equation	1 $[NC_5H_{14}^+ N_3^-]$ + 17/4 N_2O_4 → 5 CO_2 + 7 H_2O + 25/4 N_2		
Initial Conditions	P =1 Atm ; T = 298.15 K $X(NC_5H_{14}^+) = X(N_3^-)$ $X(NC_5H_{14}^+) + X(N_3^-) + X(N_2O_4) = 1$		
Lower Flammability Limit (LFL)	0.039 (T_F = 2482 K ; P_{AICC} = 26.0 Atm)	< $X(NC_5H_{14}^+)$ < < $X(N_3^-)$ <	0.048 (T_F = 2797 K ; P_{AICC} = 29.6 Atm)
Upper Flammability Limit (UFL)	0.342 (T_F = 2749 K ; P_{AICC} = 43.0 Atm)	< $X(NC_5H_{14}^+)$ < < $X(N_3^-)$ <	0.346 (T_F = 2690 K ; P_{AICC} = 42.0 Atm
P_{AICC} Max Composition	57.0 Atm ($X(Ca^+)$= 0.160)	**T_F Max Composition**	4310 K ($X(Ca^+)$= 0.153)

Table 19: Equilibrium calculations results for the $NC_5H_{14}^+ + N_3^- / N_2O_4$ system.

Mixture	Neutral 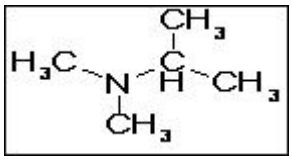 NC_5H_{13}	Neutral N_3H	Oxidant N_2O_4
Stoichiometric Equation	1 $[NC_5H_{13} N_3H]$ + 17/4 N_2O_4 → 5 CO_2 + 7 H_2O + 25/4 N_2		
Initial Conditions	P =1 Atm ; T = 298.15 K $X(NC_5H_{13}) = X(N_3H)$ $X(NC_5H_{13}) + X(N_3H) + X(N_2O_4) = 1$		
Lower Flammability Limit (LFL)	0.048 (T_F = 2646 K ; P_{AICC} = 28.0 Atm)	< $X(NC_5H_{13})$ < < $X(N_3H)$ <	0.057 (T_F = 2897 K ; P_{AICC} = 31.0 Atm)
Upper Flammability Limit (UFL)	0.286 (T_F = 2700 K ; P_{AICC} = 41.2 Atm)	< $X(NC_5H_{13})$ < < $X(N_3H)$ <	0.291 (T_F = 2642 K ; P_{AICC} = 40.6 Atm)

P_{AICC} Max Composition	52.5 Atm (X(Ne)= 0.153)	**T_F Max Composition**	4064 K (X(Ne)= 0.145)

Table 20: Equilibrium calculations results for the NC_5H_{13} + HN_3 / N_2O_4 system.

The results obtained for a mixture of charged and neutral species are given in Table 21. The initial conditions are given below:

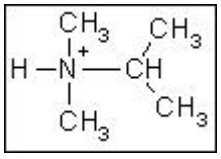 ($NC_5H_{14}^+$) + N_3^- + 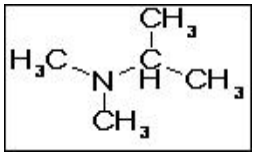 (NC_5H_{13}) + HN_3 hypergolic with N_2O_4

- $X(NC_5H_{14}^+) = X(N_3^-) = X(NC_5H_{13}) = X(HN_3)$
- $X(NC_5H_{14}^+) + X(N_3^-) + X(NC_5H_{13}) + X(HN_3) + X(N_2O_4) = 1$

For this mixture, the lower flammability limit is obtained for a mole fraction between 0.019 and 0.024, and between 0.158 and 0.160 for the upper flammability limit.

The maximum flame temperature is obtained for a mole fraction of 0.073 and is equal to 4191 K. This value is between the one obtained for the mixture with charged species (4310 K) and the one obtained for the mixture with neutral species (4064 K).

Mixture	Neutral 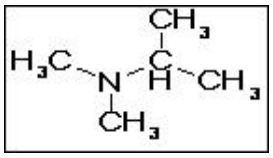 NC_5H_{13}	Neutral HN_3	Cation 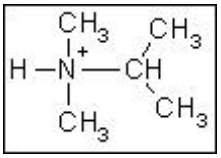 $NC_5H_{14}^+$	Anion N_3^-	Oxidant N_2O_4
Stoichiometric Equation	1 [$NC_5H_{14}^+$ N_3^-] +1 [NC_5H_{13} HN_3] + 17/2 N_2O_4 → 10 CO_2 + 14 H_2O + 25/2 N_2				
Initial Conditions	P =1 Atm ; T = 298.15 K $X(NC_5H_{14}^+) = X(N_3^-) = X(NC_5H_{13}) = X(HN_3)$ $X(NC_5H_{14}^+) + X(N_3^-) + X(NC_5H_{13}) + X(HN_3) + X(N_2O_4) = 1$				
Lower Flammability Limit (LFL)	0.019 (T_F = 2411 K ; P_{AICC} = 25.2 Atm)	< $X(NC_5H_{13})$ < < $X(HN_3)$ or $X(NC_5H_{14}^+)$ or $X(N_3^-)$ <		0.024 (T_F = 2723 K ; P_{AICC} = 28.8 Atm)	
Upper Flammability Limit (UFL)	0.158 (T_F = 2740 K ; P_{AICC} = 43.1 Atm)	< $X(NC_5H_{13})$ < < $X(HN_3)$ or $X(NC_5H_{14}^+)$ or $X(N_3^-)$ <		0.160 (T_F = 2660 K ; P_{AICC} = 41.8 Atm)	
P_{AICC} Max Composition	54.7 Atm ($X(Ca^+)$= 0.076)	**T_F Max Composition**		4191 K ($X(Ca^+)$= 0.073)	

Table 21: Equilibrium calculations results for the $NC_5H_{14}^+ + N_3^- + NC_5H_{13} + HN_3 / N_2O_4$ system.

3.3 Aprotic Ionic Liquid

For these ionic liquids, only mixtures in which the cation and the anion are separated in the vapor are considered.

For these ionic liquids, the results will be presented for each series of cations.

3.3.1 N'N-dimethyltriazanium cations

The first ionic liquid tested is the one with a N'N-dimethyltriazanium cation 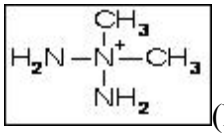
($N_3C_2H_{10}^+$). The results obtained for the system $N_3C_2H_{10}^+$ / $N(CN)_2^-$ which is hypergolic with N_2O_4 are presented in Figure 15 and in Table 22.

The results show that the flame temperature is above 2700 K for the entire domain. According to the criterion proposed, this mixture is hypergolic for any initial composition (pure IL or pure oxidizer excluded). The maximum flame temperature is equal to 4450 K and is obtained for a mole fraction equal to 0.187. The maximum value for the P_{AICC} is equal to 58.3 Atm and is obtained for a mole fraction equal to 0.206.

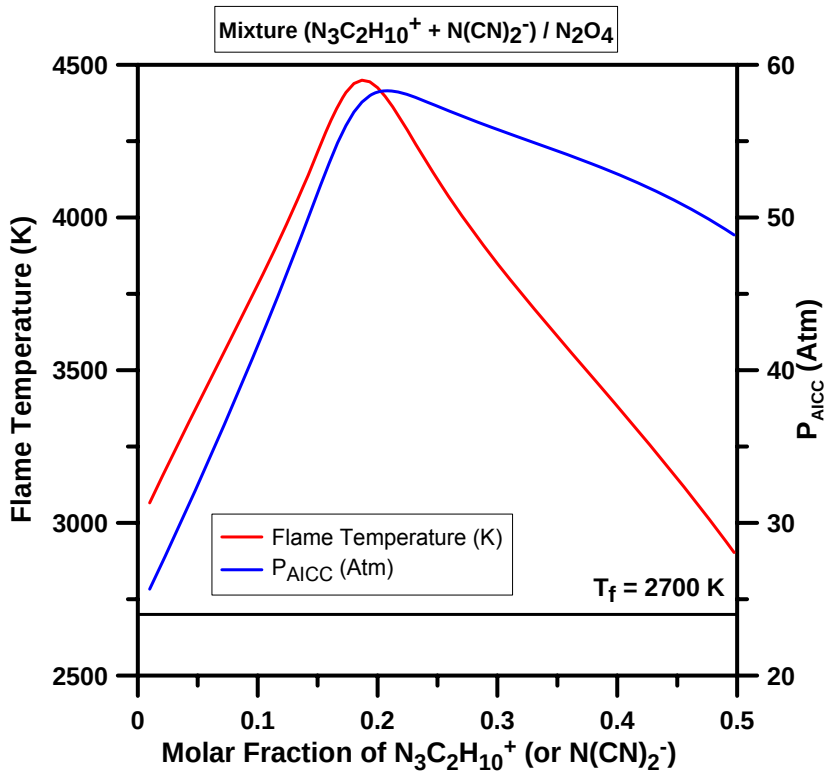

Figure 15: Flame temperature and P_{AICC} for different $N_3C_2H_{10}^+ + N(CN)_2^- / N_2O_4$ mixtures at 298.15 K and 1 Atm.

Mixture	Cation	Anion	Oxidant

	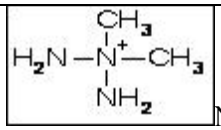 $N_3C_2H_{10}^+$	$N(CN)_2^-$	N_2O_4
Stoichiometric Equation	1 $[N_3C_2H_{10}^+ N(CN)_2^-]$ + 13/4 N_2O_4 → 4 CO_2 + 5 H_2O + 25/4 N_2		
Initial Conditions	P =1 Atm ; T = 298.15 K $X(N_3C_2H_{10}^+) = X(N(CN)_2^-)$ $X(N_3C_2H_{10}^+) + X(N(CN)_2^-) + X(N_2O_4) = 1$		
Lower Flammability Limit (LFL)	0	< $X(N_3C_2H_{10}^+)$ < < $X(N(CN)_2^-)$ <	9.90E-03 (T_F = 3066 K ; P_{AICC} = 25.7 Atm)
Upper Flammability Limit (UFL)	0.497 (T_F = 2903 K ; P_{AICC} = 48.9 Atm)	< $X(N_3C_2H_{10}^+)$ < < $X(N(CN)_2^-)$ <	0.500
P_{AICC} Max Composition	58.3 Atm ($X(Ca^+)$= 0.206)	**T_F Max Composition**	4450 K ($X(Ca^+)$= 0.187)

Table 22: Equilibrium calculations results for the $N_3C_2H_{10}^+$ + $N(CN)_2^-$ / N_2O_4 system.

Results obtained for the system $N_3C_2H_{10}^+$ / $N(CN)_2^-$ which is hypergolic with HNO_3 are given in Table 23. Like the previous case, the flame temperature is above 2700 K for the entire domain tested. For this system the maximum P_{AICC} is obtained for a mixture with a mole fraction of cation (or anion) equal to 0.497. The maximum flame temperature is equal to 3902 K and is obtained when the mole fraction of the cation is 0.115. This value is lower than the one obtained for the system with N_2O_4.

Mixture	Cation 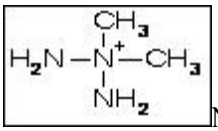 $N_3C_2H_{10}^+$	Anion $N(CN)_2^-$	Oxidant HNO_3
Stoichiometric Equation	1 $[N_3C_2H_{10}^+ N(CN)_2^-]$ + 26/5 HNO_3 → 4 CO_2 + 38/5 H_2O + 28/5 N_2		
Initial Conditions	P =1 Atm ; T = 298.15 K $X(N_3C_2H_{10}^+) = X(N(CN)_2^-)$ $X(N_3C_2H_{10}^+) + X(N(CN)_2^-) + X(HNO_3) = 1$		
Lower Flammability Limit (LFL)	0	< $X(N_3C_2H_{10}^+)$ < < $X(N(CN)_2^-)$ <	9.90E-03 (T_F = 2724 K ; P_{AICC} = 20.3 Atm)
Upper Flammability	0.497	< $X(N_3C_2H_{10}^+)$ < <	0.500

Limit (UFL)	(T_F = 2895 K ; P_{AICC} = 48.7 Atm)	$X(N(CN)_2^-)$ <	
P_{AICC} Max Composition	48.7 Atm ($X(Ca^+)$= 0.497)	**T_F Max Composition**	3902 K ($X(Ca^+)$= 0.115)

Table 23: Equilibrium calculations results for the $N_3C_2H_{10}^+$ + $N(CN)_2^-$ / HNO_3 system.

The anion $N(CN)_2^-$ was replaced by NO_3^-. For the ionic liquid $N_3C_2H_{10}^+$ / NO_3^- which is hypergolic with HNO_3, the results are presented in Table 24. On the contrary to the previous cases just presented above, this mixture is not hypergolic for the entire domain. The lower flammability limit is obtained for a mole fraction of cation between 9.90E-03 and 0.020. However, the upper flammability limit is between 0.497 and 0.500 for the cation mole fraction. The maximum flame temperature is equal to 3904 K for a mole fraction of cation (or anion) equal to 0.160.

The results obtained for the $N_3C_2H_{10}^+$ NO_3^- ionic liquid with N_2O_4 are presented in Table 25. For the entire domain, the adiabatic flame temperature at constant volume is above 2700 K. As seen before for the mixture with the $N(CN)_2^-$ anion, higher flame temperatures are obtained with N_2O_4 compared to HNO_3. For this mixture, the maximum flame temperature is equal to 4344 K which is 400 K higher than the one obtained for the mixture with HNO_3.

Mixture	Cation 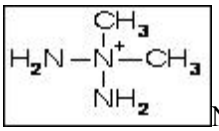 $N_3C_2H_{10}^+$	Anion NO_3^-	Oxidant HNO_3
Stoichiometric Equation	1 [$N_3C_2H_{10}^+$ NO_3^-] + 12/5 HNO_3 → 2 CO_2 + 31/5 H_2O + 16/5 N_2		
Initial Conditions	P =1 Atm ; T = 298.15 K $X(N_3C_2H_{10}^+) = X(NO_3^-)$ $X(N_3C_2H_{10}^+) + X(NO_3^-) + X(HNO_3) = 1$		
Lower Flammability Limit (LFL)	9.90E-03 (T_F = 2675 K ; P_{AICC} = 19.8 Atm)	< $X(N_3C_2H_{10}^+)$ < < $X(NO_3^-)$ <	0.020 (T_F = 2769 K ; P_{AICC} = 21.2 Atm)
Upper Flammability Limit (UFL)	0.497 (T_F = 3385 K ; P_{AICC} = 54.1 Atm)	< $X(N_3C_2H_{10}^+)$ < < $X(NO_3^-)$ <	0.500
P_{AICC} Max Composition	54.1 Atm ($X(Ca^+)$= 0.497)	**T_F Max Composition**	3904 K ($X(Ca^+)$= 0.160)

Table 24: Equilibrium calculations results for the $N_3C_2H_{10}^+$ + NO_3^- / HNO_3 system.

Mixture	Cation 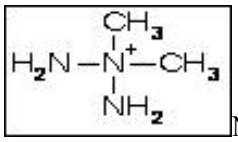 $N_3C_2H_{10}^+$	Anion NO_3^-	Oxidant N_2O_4
Stoichiometric Equation	1 $[N_3C_2H_{10}^+ NO_3^-]$ + 3/2 N_2O_4 → 2 CO_2 + 5 H_2O + 7/2 N_2		
Initial Conditions	P = 1 Atm ; T = 298.15 K $X(N_3C_2H_{10}^+) = X(NO_3^-)$ $X(N_3C_2H_{10}^+) + X(NO_3^-) + X(N_2O_4) = 1$		
Lower Flammability Limit (LFL)	0	$< X(N_3C_2H_{10}^+) < < X(NO_3^-) <$	9.90E-03 (T_F = 3036 K ; P_{AICC} = 25.2 Atm)
Upper Flammability Limit (UFL)	0.497 (T_F = 3390 K ; P_{AICC} = 54.2 Atm)	$< X(N_3C_2H_{10}^+) < < X(NO_3^-) <$	0.500
P_{AICC} Max Composition	58.2 Atm ($X(Ca^+)$= 0.270)	**T_F Max Composition**	4344 K ($X(Ca^+)$= 0.242)

Table 25: Equilibrium calculations results for the $N_3C_2H_{10}^+$ + NO_3^- / N_2O_4 system.

The N'N-dimethyltriazanium cation was also tested with the chloride anion (Cl^-). This ionic liquid is reported hypergolic with N_2O_4. The results obtained for this mixture are given in Table 26.

For this mixture, the flame temperature is above 2700 K for the entire domain. The maximum P_{AICC} and flame temperature are equal, respectively, to 55.7 Atm and 4509 K for mole fractions of cation equal to 0.224 and 0.206.

In summary, for this cation, hypergolicity is predicted for almost the entire domain for all the systems tested.

Mixture	Cation 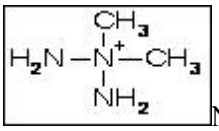 $N_3C_2H_{10}^+$	Anion Cl^-	Oxidant N_2O_4
Stoichiometric Equation	1 $[N_3C_2H_{10}^+ Cl^-]$ + 11/4 N_2O_4 → 2 CO_2 + 1 ClO_2 + 5 H_2O + 17/4 N_2		
Initial Conditions	P = 1 Atm ; T = 298.15 K $X(N_3C_2H_{10}^+) = X(Cl^-)$ $X(N_3C_2H_{10}^+) + X(Cl^-) + X(N_2O_4) = 1$		
Lower Flammability Limit (LFL)	0	< $X(N_3C_2H_{10}^+)$ < < $X(Cl^-)$ <	0.020 (T_F = 3107 K ; P_{AICC} = 26.6 Atm)
Upper Flammability Limit (UFL)	0.497 (T_F = 3249 K ; P_{AICC} = 47.1 Atm)	< $X(N_3C_2H_{10}^+)$ < < $X(Cl^-)$ <	0.500
P_{AICC} Max Composition	55.7 Atm ($X(Ca^+)$= 0.224)	**T_F Max Composition**	4509 K ($X(Ca^+)$= 0.206)

Table 26: Equilibrium calculations results for the $N_3C_2H_{10}^+$ + Cl^- / N_2O_4 system.

3.3.2 N'N-dimethylhydrazinium cations

In this part, the N'N-dimethylhydrazinium cation with different alkyl substituents was tested.

The first ionic liquid tested, shown below, is reported hypergolic with HNO_3.

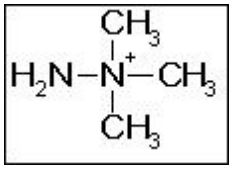

($N_2C_3H_{11}^+$) + $N(CN)_2^-$

For this case, the results are given in Figure 16 and in Table 27. Hypergolicity is predicted until a mole fraction of cation (or anion) between 0.371 and 0.375 (the upper flammability limit). The maximum flame temperature is found for a mole fraction of cation equal to 0.099 and is equal to 3795 K.

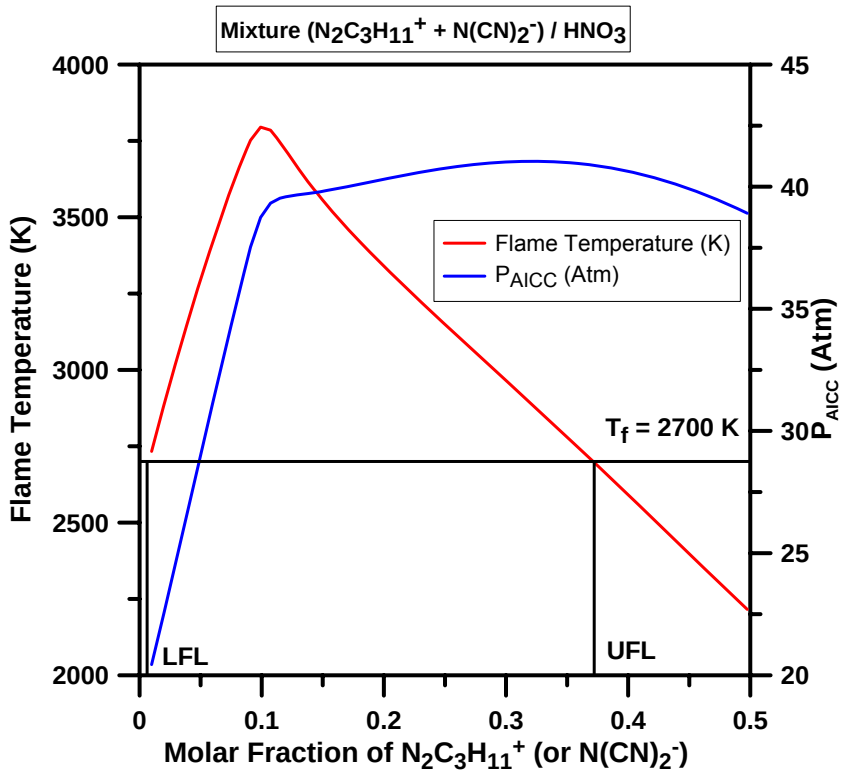

Figure 16: Flame temperature and P_{AICC} for different $N_2C_3H_{11}^+$ + $N(CN)_2^-$ / HNO_3 mixtures at 298.15 K and 1 Atm.

Mixture	Cation 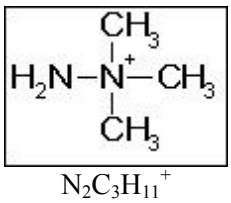 $N_2C_3H_{11}^+$	Anion $N(CN)_2^-$	Oxidant HNO_3
Stoichiometric Equation	1 [$N_2C_3H_{11}^+$ $N(CN)_2^-$] + 93/15 HNO_3 → 5 CO_2 + 43/5 H_2O + 84/15 N_2		
Initial Conditions	P =1 Atm ; T = 298.15 K $X(N_2C_3H_{11}^+) = X(N(CN)_2^-)$ $X(N_2C_3H_{11}^+) + X(N(CN)_2^-) + X(HNO_3) = 1$		

Lower Flammability Limit (LFL)	0	< $X(N_2C_3H_{11}^+)$ < < $X(N(CN)_2^-)$ <	9.90E-03 (T_F = 2734 K ; P_{AICC} = 20.4 Atm)
Upper Flammability Limit (UFL)	0.371 (T_F = 2701 K ; P_{AICC} = 40.9 Atm)	< $X(N_2C_3H_{11}^+)$ < < $X(N(CN)_2^-)$ <	0.375 (T_F = 2686 K ; P_{AICC} = 40.9 Atm)
P_{AICC} Max Composition	41.0 Atm ($X(Ca^+)$= 0.320)	**T_F Max Composition**	3795 K ($X(Ca^+)$= 0.099)

Table 27: Equilibrium calculations results for the $N_2C_3H_{11}^+$ + $N(CN)_2^-$ / HNO_3 system.

In Table 28 are the results for the ionic liquid $N_2C_3H_{11}^+$ / $BH_2(CN)_2^-$ which was found hypergolic with HNO_3. Compared to the above case, the dicyanamide anion was replaced by the dicyanoborate anion. For this system, the upper flammability limit was found for a mole fraction of cation between 0.291 and 0.296 (with P_{AICC} around 38 Atm). The presence of the dicyanoborate anion instead of the dicyanamide anion leads to a decrease of the flammability domain for this IL.

Mixture	Cation 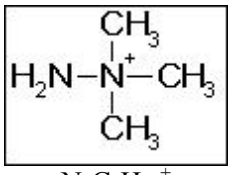 $N_2C_3H_{11}^+$	Anion $BH_2(CN)_2^-$	Oxidant HNO_3
Stoichiometric Equation	1 [$N_2C_3H_{11}^+$ $BH_2(CN)_2^-$] + 36/5 HNO_3 → 5 CO_2 + 1/2 B_2O_3 + 101/10 H_2O + 56/10 N_2		
Initial Conditions	P =1 Atm ; T = 298.15 K $X(N_2C_3H_{11}^+) = X(BH_2(CN)_2^-)$ $X(N_2C_3H_{11}^+) + X(BH_2(CN)_2^-) + X(HNO_3) = 1$		
Lower Flammability Limit (LFL)	0	< $X(N_2C_3H_{11}^+)$ < < $X(BH_2(CN)_2^-)$ <	9.90E-03 (T_F = 2746 K ; P_{AICC} = 20.6 Atm)
Upper Flammability Limit (UFL)	0.291 (T_F = 2716 K ; P_{AICC} = 37.9 Atm)	< $X(N_2C_3H_{11}^+)$ < < $X(BH_2(CN)_2^-)$ <	0.296 (T_F = 2694 K ; P_{AICC} = 37.8 Atm)
P_{AICC} Max Composition	38.1 Atm ($X(Ca^+)$= 0.237)	**T_F Max Composition**	3716 K ($X(Ca^+)$= 0.083)

Table 28: Equilibrium calculations results for the $N_2C_3H_{11}^+$ + $BH_2(CN)_2^-$ / N_2O_4 system.

In Table 29 and 30 are the results for the 1-butyl-N'N-dimethylhydrazinium cation based ionic liquids. The first system tested is with the dicyanamide anion (Table 29) and the second one with the dicyanoborate anion (Table 30). Both of these ionic liquids are hypergolic with WFNA.

For these two systems, hypergolicity (T_F above 2700 K) is predicted. For the mixture with the dicyanamide anion, the upper flammability limit is found for a mole fraction of cation between 0.194 and 0.200. As seen before, the presence of the dicyanoborate anion induces smaller flammability domain. The upper flammability limit is found for mole fraction of cation between 0.174 and 0.180.

For these two cases, the maximum flame temperature is around 3600 K for small values of mole fraction of cation.

Mixture	Cation 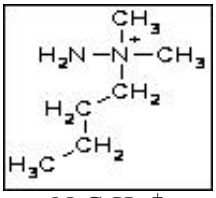 $N_2C_6H_{17}^+$	Anion $N(CN)_2^-$	Oxidant HNO_3
Stoichiometric Equation	1 [$N_2C_6H_{17}^+$ $N(CN)_2^-$] + 49/5 HNO_3 → 8 CO_2 + 67/5 H_2O + 37/5 N_2		
Initial Conditions	P =1 Atm ; T = 298.15 K $X(N_2C_6H_{17}^+) = X(N(CN)_2^-)$ $X(N_2C_6H_{17}^+) + X(N(CN)_2^-) + X(HNO_3) = 1$		
Lower Flammability Limit (LFL)	0	< $X(N_2C_6H_{17}^+)$ < < $X(N(CN)_2^-)$ <	9.90E-03 (T_F = 2790 K ; P_{AICC} = 21.4 Atm)
Upper Flammability Limit (UFL)	0.194 (T_F = 2723 K ; P_{AICC} = 39.6 Atm)	< $X(N_2C_6H_{17}^+)$ < < $X(N(CN)_2^-)$ <	0.200 (T_F = 2683 K ; P_{AICC} = 39.6 Atm)
P_{AICC} Max Composition	39.7 Atm ($X(Ca^+)$= 0.174)	**T_F Max Composition**	3646 K ($X(Ca^+)$= 0.065)

Table 29: Equilibrium calculations results for the $N_2C_6H_{17}^+$ + $N(CN)_2^-$ / HNO_3 system.

Mixture	Cation 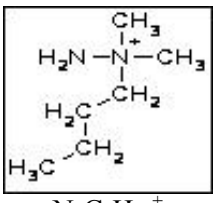 $N_2C_6H_{17}^+$	Anion $BH_2(CN)_2^-$	Oxidant HNO_3
Stoichiometric Equation	1 [$N_2C_6H_{17}^+$ $BH_2(CN)_2^-$] + 54/5 HNO_3 → 8 CO_2 + 1/2 B_2O_3 + 149/10 H_2O + 37/5 N_2		
Initial Conditions	P =1 Atm ; T = 298.15 K $X(N_2C_6H_{17}^+) = X(BH_2(CN)_2^-)$ $X(N_2C_6H_{17}^+) + X(BH_2(CN)_2^-) + X(HNO_3) = 1$		
Lower Flammability Limit (LFL)	0	$< X(N_2C_6H_{17}^+) < < X(BH_2(CN)_2^-) <$	9.90E-03 (T_F = 2803 K ; P_{AICC} = 21.6 Atm)
Upper Flammability Limit (UFL)	0.174 (T_F = 2710 K ; P_{AICC} = 38.1 Atm)	$< X(N_2C_6H_{17}^+) < < X(BH_2(CN)_2^-) <$	0.180 (T_F = 2665 K ; P_{AICC} = 38.0 Atm)
P_{AICC} Max Composition	38.2 Atm ($X(Ca^+)$= 0.145)	**T_F Max Composition**	3605 K ($X(Ca^+)$= 0.057)

Table 30: Equilibrium calculations results for the $N_2C_6H_{17}^+$ + $BH_2(CN)_2^-$ / HNO_3 system.

1-allyl-N'N-dimethylhydrazinium cation based ionic liquids are reported hypergolic with WFNA with two different anions: the nitrocyanamide anion (see Table 31) and the dicyanoborate anion (see Table 32).

These two mixtures are predicted hypergolic. For the dicyanamide anion based ILs, the upper flammability limit is predicted to be equal to a mole fraction of cation between 0.291 and 0.296. As seen for the other N'N-dimethylhydrazinium cation based ILs, the replacement of the $N(CN)_2^-$ by $BH_2(CN)_2^-$ leads to a decrease of the flammability domain (UFL : 0.242 < X(cation) < 0.248 ; see Table 32).

Mixture	Cation 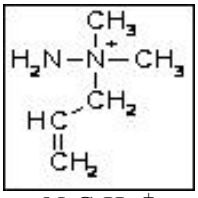 $N_2C_5H_{13}^+$	Anion $N(CN)_2^-$	Oxidant HNO_3
Stoichiometric Equation	1 $[N_2C_5H_{13}^+ N(CN)_2^-]$ + 41/5 HNO_3 → 7 CO_2 + 53/5 H_2O + 33/5 N_2		
Initial Conditions	P =1 Atm ; T = 298.15 K $X(N_2C_5H_{13}^+) = X(N(CN)_2^-)$ $X(N_2C_5H_{13}^+) + X(N(CN)_2^-) + X(HNO_3) = 1$		
Lower Flammability Limit (LFL)	0	< $X(N_2C_5H_{13}^+)$ < < $X(N(CN)_2^-)$ <	9.90E-03 (T_F = 2772 K ; P_{AICC} = 21.0 Atm)
Upper Flammability Limit (UFL)	0.291 (T_F = 2719 K ; P_{AICC} = 42.2 Atm)	< $X(N_2C_5H_{13}^+)$ < $X(N(CN)_2^-)$	0.296 (T_F = 2697 K ; P_{AICC} = 42.2 Atm)
P_{AICC} Max Composition	42.2 Atm ($X(Ca^+)$= 0.286)	**T_F Max Composition**	3767 K ($X(Ca^+)$= 0.083)

Table 31: Equilibrium calculations results for the $N_2C_5H_{13}^+$ + $N(CN)_2^-$ / HNO_3 system.

Mixture	Cation 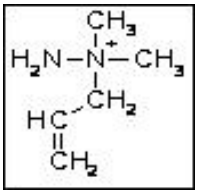 $N_2C_5H_{13}^+$	Anion $BH_2(CN)_2^-$	Oxidant HNO_3
Stoichiometric Equation	1 $[N_2C_5H_{13}^+ BH_2(CN)_2^-]$ + 46/5 HNO_3 → 7 CO_2 + 1/2 B_2O_3 + 121/10 H_2O + 33/5 N_2		
Initial Conditions	P =1 Atm ; T = 298.15 K $X(N_2C_5H_{13}^+) = X(BH_2(CN)_2^-)$ $X(N_2C_5H_{13}^+) + X(BH_2(CN)_2^-) + X(HNO_3) = 1$		
Lower Flammability Limit (LFL)	0	$< X(N_2C_5H_{13}^+) < < X(BH_2(CN)_2^-) <$	9.90E-03 (T_F = 2784 K ; P_{AICC} = 21.2 Atm)
Upper Flammability Limit (UFL)	0.242 (T_F = 2716 K ; P_{AICC} = 39.6 Atm)	$< X(N_2C_5H_{13}^+) < < X(BH_2(CN)_2^-) <$	0.248 (T_F = 2687 K ; P_{AICC} = 39.6 Atm)
P_{AICC} Max Composition	39.6 Atm ($X(Ca^+)$= 0.225)	**T_F Max Composition**	3700 K ($X(Ca^+)$= 0.074)

Table 32: Equilibrium calculations results for the $N_2C_5H_{13}^+$ + $BH_2(CN)_2^-$ / HNO_3 system.

1-(2-propargyl)-N'N-dimethylhydrazinium cation based ionic liquids were found hypergolic with WFNA with two different anions: the nitrocyanamide anion (see Table 33) and the dicyanoborate anion (see Table 34). For these two cases, the systems are predicted hypergolic. For the dicyanamide anion based IL, the upper flammability limit was found for a mole fraction of cation between 0.415 and 0.419.

For the $N_2C_5H_{11}^+$ / $BH_2(CN)_2^-$ ionic liquid, the upper limit was found for a mole fraction of cation between 0.315 and 0.320. For this cation, replacement of the $N(CN)_2^-$ anion by the $BH_2(CN)_2^-$ anion again induces a decrease of the flammability domain.

Mixture	Cation 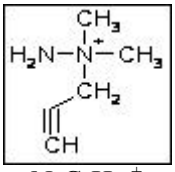 $N_2C_5H_{11}^+$	Anion $N(CN)_2^-$	Oxidant HNO_3
Stoichiometric Equation	1 [$N_2C_5H_{11}^+$ $N(CN)_2^-$] + 39/5 HNO_3 → 7 CO_2 + 47/5 H_2O + 32/5 N_2		
Initial Conditions	P =1 Atm ; T = 298.15 K $X(N_2C_5H_{11}^+) = X(N(CN)_2^-)$ $X(N_2C_5H_{11}^+) + X(N(CN)_2^-) + X(HNO_3) = 1$		
Lower Flammability Limit (LFL)	0	< $X(N_2C_5H_{11}^+)$ < < $X(N(CN)_2^-)$ <	9.90E-03 (T_F = 2775 K ; P_{AICC} = 20.9 Atm)
Upper Flammability Limit (UFL)	0.415 (T_F = 2715 K ; P_{AICC} = 46.7 Atm)	< $X(N_2C_5H_{11}^+)$ < < $X(N(CN)_2^-)$ <	0.419 (T_F = 2692 K ; P_{AICC} = 46.4 Atm)
P_{AICC} Max Composition	48.4 Atm ($X(Ca^+)$= 0.398)	**T_F Max Composition**	3892 K ($X(Ca^+)$= 0.091)

Table 33: Equilibrium calculations results for the $N_2C_5H_{11}^+$ + $N(CN)_2^-$ / HNO_3 system.

Mixture	Cation 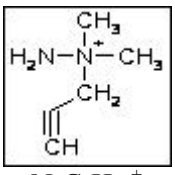 $N_2C_5H_{11}^+$	Anion $BH_2(CN)_2^-$	Oxidant HNO_3
Stoichiometric Equation	1 $[N_2C_5H_{11}^+ BH_2(CN)_2^-]$ + 44/5 HNO_3 → 7 CO_2 + 1/2 B_2O_3 + 109/10 H_2O + 32/5 N_2		
Initial Conditions	P =1 Atm ; T = 298.15 K $X(N_2C_5H_{11}^+) = X(BH_2(CN)_2^-)$ $X(N_2C_5H_{11}^+) + X(BH_2(CN)_2^-) + X(HNO_3) = 1$		
Lower Flammability Limit (LFL)	0	< $X(N_2C_5H_{11}^+)$ < < $X(BH_2(CN)_2^-)$ <	9.90E-03 (T_F = 2787 K ; P_{AICC} = 21.1 Atm)
Upper Flammability Limit (UFL)	0.315 (T_F = 2720 K ; P_{AICC} = 42.7 Atm)	< $X(N_2C_5H_{11}^+)$ < < $X(BH_2(CN)_2^-)$ <	0.320 (T_F = 2688 K ; P_{AICC} = 42.5 Atm)
P_{AICC} Max Composition	42.8 Atm ($X(Ca^+)$= 0.296)	**T_F Max Composition**	3792 K ($X(Ca^+)$= 0.083)

Table 34: Equilibrium calculations results for the $N_2C_5H_{13}^+$ + $BH_2(CN)_2^-$ / HNO_3 system.

The last N'N-dimethylhydrazinium cation under consideration in this study is the 1-(2-hydroxyethyl)-N'N-dimethylhydrazinium cation. Together with a dicyanamide anion, this ionic liquid was reported hypergolic with nitric acid (HNO_3).

The system is predicted to be hypergolic. The upper flammability limit was found for a mole fraction of cation between 0.286 and 0.291 (see Table 35).

Mixture	Cation 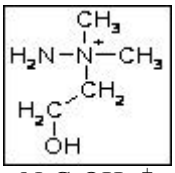 $N_2C_4OH_{13}^+$	Anion $N(CN)_2^-$	Oxidant HNO_3
Stoichiometric Equation	1 $[N_2C_4OH_{13}^+ N(CN)_2^-]$ + 7 HNO_3 → 6 CO_2 + 10 H_2O + 6 N_2		
Initial Conditions	P =1 Atm ; T = 298.15 K $X(N_2C_4OH_{13}^+) = X(N(CN)_2^-)$ $X(N_2C_4OH_{13}^+) + X(N(CN)_2^-) + X(HNO_3) = 1$		
Lower Flammability Limit (LFL)	0	< $X(N_2C_4OH_{13}^+)$ < < $X(N(CN)_2^-)$ <	9.90E-03 (T_F = 2746 K ; P_{AICC} = 20.7 Atm)
Upper Flammability Limit (UFL)	0.286 (T_F = 2705 K ; P_{AICC} = 41.4 Atm)	< $X(N_2C_4OH_{13}^+)$ < < $X(N(CN)_2^-)$ <	0.291 (T_F = 2683 K ; P_{AICC} = 41.4 Atm)
P_{AICC} Max Composition	41.4 Atm ($X(Ca^+)$= 0.281)	**T_F Max Composition**	3695 K ($X(Ca^+)$= 0.091)

Table 35: Equilibrium calculations results for the $N_2C_4OH_{13}^+$ + $N(CN)_2^-$ / HNO_3 system.

For the N'N-dimethylhydrazinium cations, different alkyl substituents were considered (methyl, butyl, allyl, propargyl, and hydroxyethyl). For the ionic liquid with a dicyanamide anion, the impact on the flammability domains of these alkyl substituents in the cation is as follows: butyl < hydroxyethyl < allyl < methyl < propargyl.

3.3.3 Cations with an azide function

Different ionic liquids with a cation containing an azide function were studied and reported hypergolic with HNO_3.

The first system tested is given below:

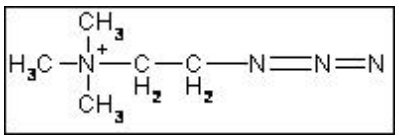 ($N_4C_5H_{13}^+$) + $N(CN)_2^-$ with HNO_3

The results obtained for this are given in Figure 17 and in Table 37. Again, hypergolicity is predicted. When the mole fraction of the cation increases, the flame temperature rises until it reaches a maximum (3771 K) at a mole fraction of 0.083. Then, the flame temperature decreases and the upper flammability is predicted for a mole fraction of cation between 0.310 and 0.315.

A second similar ionic liquid is also reported hypergolic with HNO_3. The ionic liquid is:

Cation: 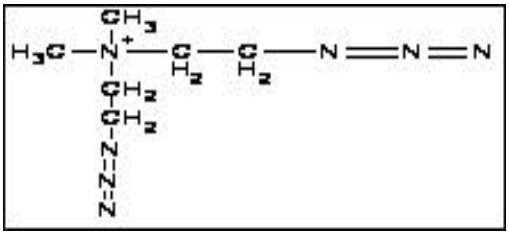 ($N_7C_6H_{14}^+$) ; Anion: $N(CN)_2^-$

The trends predicted for the previous system are also predicted here. The results for this system are given in Table 37.

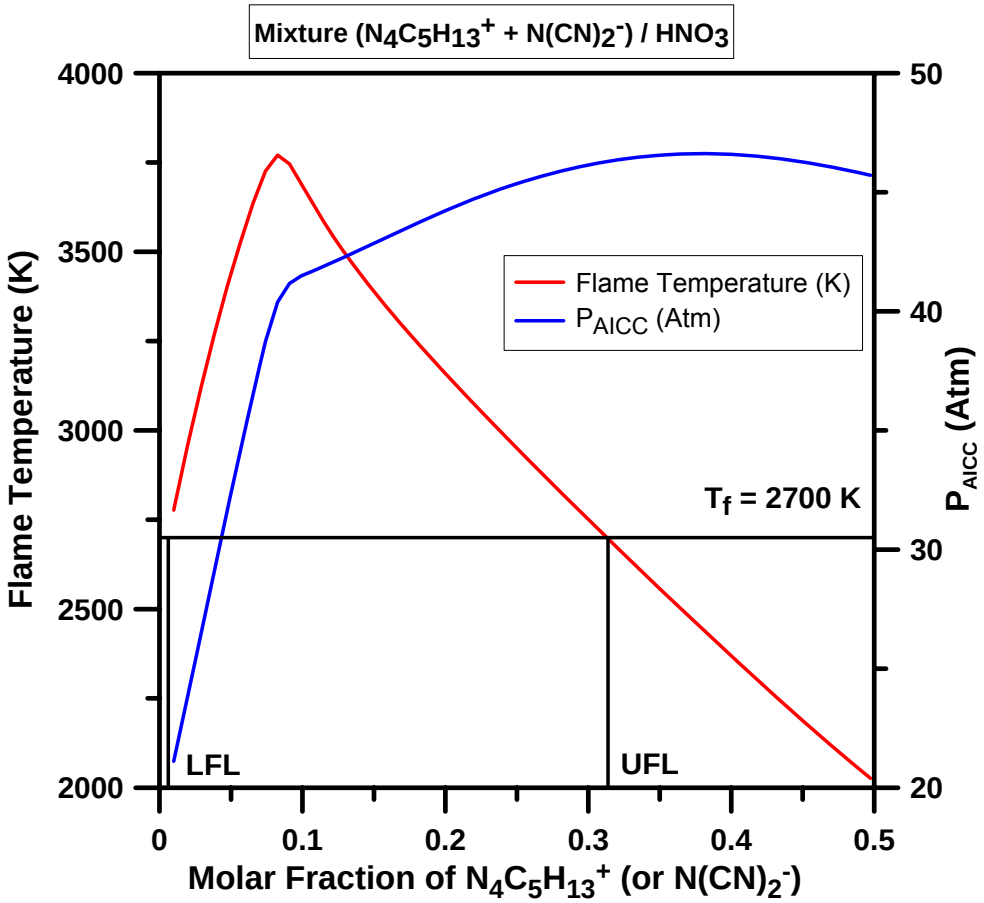

Figure 17: Flame temperature and P_{AICC} for different $N_4C_5H_{13}^+$ + $N(CN)_2^-$ / HNO_3 mixtures at 298.15 K and 1 Atm.

Mixture	Cation 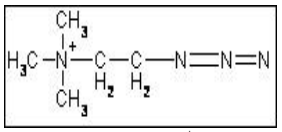 $N_4C_5H_{13}^+$	Anion $N(CN)_2^-$	Oxidant HNO_3
Stoichiometric Equation	$1\ [N_4C_5H_{13}^+\ N(CN)_2^-] + 41/5\ HNO_3 \rightarrow 7\ CO_2 + 53/5\ H_2O + 38/5\ N_2$		
Initial Conditions	P =1 Atm ; T = 298.15 K $X(N_4C_5H_{13}^+) = X(N(CN)_2^-)$ $X(N_4C_5H_{13}^+) + X(N(CN)_2^-) + X(HNO_3) = 1$		
Lower Flammability Limit (LFL)	0	$< X(N_4C_5H_{13}^+) < < X(N(CN)_2^-) <$	9.90E-03 (T_F = 2777 K ; P_{AICC} = 21.1 Atm)
Upper Flammability Limit (UFL)	0.310 (T_F = 2710 K ; P_{AICC} = 46.3 Atm)	$< X(N_4C_5H_{13}^+) < < X(N(CN)_2^-) <$	0.315 (T_F = 2692 K ; P_{AICC} = 46.3 Atm)
P_{AICC} Max Composition	46.6 Atm ($X(Ca^+)$= 0.379)	**T_F Max Composition**	3771 K ($X(Ca^+)$= 0.083)

Table 36: Equilibrium calculations results for the $N_4C_5H_{13}^+ + N(CN)_2^- / HNO_3$ system.

Mixture	Cation	Anion	Oxidant

	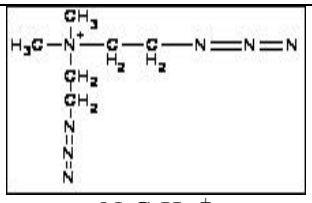 $N_7C_6H_{14}^+$	$N(CN)_2^-$	HNO_3
Stoichiometric Equation	1 [$N_7C_6H_{14}^+$ $N(CN)_2^-$] + 46/5 HNO_3 → 8 CO_2 + 58/5 H_2O + 48/5 N_2		
Initial Conditions	P =1 Atm ; T = 298.15 K $X(N_7C_6H_{14}^+) = X(N(CN)_2^-)$ $X(N_7C_6H_{14}^+) + X(N(CN)_2^-) + X(HNO_3) = 1$		
Lower Flammability Limit (LFL)	0	< $X(N_7C_6H_{14}^+)$ < < $X(N(CN)_2^-)$ <	9.90E-03 (T_F = 2810 K ; P_{AICC} = 21.6 Atm)
Upper Flammability Limit (UFL)	0.363 (T_F = 2707 K ; P_{AICC} = 58.7 Atm)	< $X(N_7C_6H_{14}^+)$ < < $X(N(CN)_2^-)$ <	0.367 (T_F = 2696 K ; P_{AICC} = 58.8 Atm)
P_{AICC} Max Composition	63.1 Atm ($X(Ca^+)$= 0.497)	**T_F Max Composition**	3807 K ($X(Ca^+)$= 0.074)

Table 37: Equilibrium calculations results for the $N_7C_6H_{14}^+$ + $N(CN)_2^-$ / HNO_3 system.

3.3.4 Imidazolium cations

As previously discussed in the first part of the report, different alkyl substituted 1-methylimidazolium cation-based ionic liquids have been reported hypergolic with white fuming nitric acid.

The first system tested was the 3-butyl-1-methylimidazolium cation-based ionic liquid. Two different anions were considered: the dicyanamide anion (see Figure 18 and Table 38) and the dicyanoborate anion (see Table 39).

For both of these systems, the flame temperature is above 2700 K for a given domain of compositions. For the ionic liquid with the dicyanamide anion, the upper flammability limit is found for a mole fraction of cation between 0.174 and 0.180. For the ionic liquid with the dicyanoborate anion, the UFL is found for a mole fraction of cation between 0.153 and 0.160. As was seen before for the N'N-dimethylhydrazinium cations, replacement of the $N(CN)_2^-$ anion by the $BH_2(CN)_2^-$ anion leads to a smaller flammability domain.

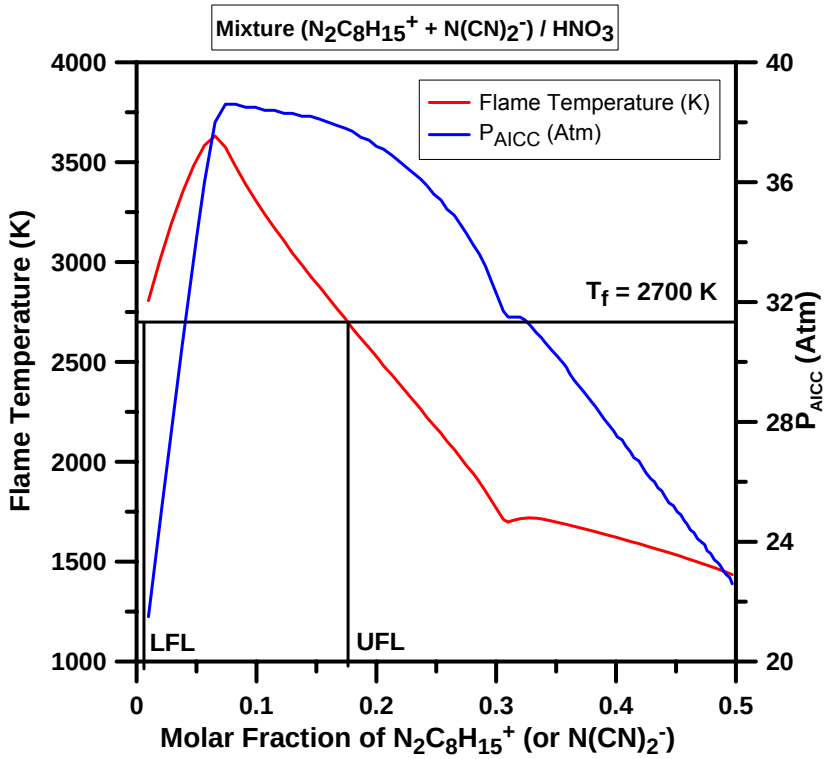

Figure 18: Flame temperature and P_{AICC} for different $N_2C_8H_{15}^+$ + $N(CN)_2^-$ / HNO_3 mixtures at 298.15 K and 1 Atm.

Mixture	Cation 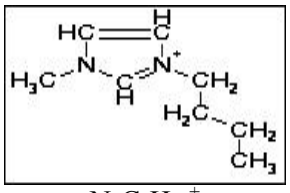 $N_2C_8H_{15}^+$	Anion $N(CN)_2^-$	Oxidant HNO_3
Stoichiometric Equation	1 [$N_2C_8H_{15}^+$ $N(CN)_2^-$] + 46/5 HNO_3 → 8 CO_2 + 58/5 H_2O + 48/5 N_2		
Initial Conditions	P =1 Atm ; T = 298.15 K $X(N_2C_8H_{15}^+) = X(N(CN)_2^-)$ $X(N_2C_8H_{15}^+) + X(N(CN)_2^-) + X(HNO_3) = 1$		
Lower Flammability Limit (LFL)	0	< $X(N_2C_8H_{15}^+)$ < < $X(N(CN)_2^-)$ <	9.90E-03 (T_F = 2807 K ; P_{AICC} = 21.5 Atm)
Upper Flammability Limit (UFL)	0.174 (T_F = 2718 K ; P_{AICC} = 37.8 Atm)	< $X(N_2C_8H_{15}^+)$ < < $X(N(CN)_2^-)$ <	0.180 (T_F = 2668 K ; P_{AICC} = 37.7 Atm)
P_{AICC} Max Composition	38.6 Atm ($X(Ca^+)$= 0.74)	**T_F Max Composition**	3632 K ($X(Ca^+)$= 0.065)

Table 38: Equilibrium calculations results for the $N_2C_8H_{15}^+$ + $N(CN)_2^-$ / HNO_3 system.

Mixture	Cation 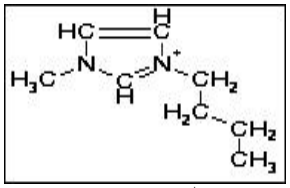 $N_2C_8H_{15}^+$	Anion $BH_2(CN)_2^-$	Oxidant HNO_3
Stoichiometric Equation	1 $[N_2C_8H_{15}^+ BH_2(CN)_2^-]$ + 12 HNO_3 → 10 CO_2 + 1/2 B_2O_3 + 145/10 H_2O + 8 N_2		
Initial Conditions	P =1 Atm ; T = 298.15 K $X(N_2C_8H_{15}^+) = X(BH_2(CN)_2^-)$ $X(N_2C_8H_{15}^+) + X(BH_2(CN)_2^-) + X(HNO_3) = 1$		
Lower Flammability Limit (LFL)	0	$< X(N_2C_8H_{15}^+) < < X(BH_2(CN)_2^-) <$	9.90E-03 (T_F = 2820 K ; P_{AICC} = 21.7 Atm)
Upper Flammability Limit (UFL)	0.153 (T_F = 2745 K ; P_{AICC} = 36.7 Atm)	$< X(N_2C_8H_{15}^+) < < X(BH_2(CN)_2^-)$,	0.160 (T_F = 2689 K ; P_{AICC} = 36.6 Atm)
P_{AICC} Max Composition	37.6 Atm ($X(Ca^+)$= 0.065)	**T_F Max Composition**	3600 K ($X(Ca^+)$= 0.057)

Table 39: Equilibrium calculations results for the $N_2C_8H_{15}^+$ + $BH_2(CN)_2^-$ / HNO_3 system.

Other alkyl substituents were tested for 1-methylimidazolium cation-based ionic liquids. 3-allyl-1-methylimidazolium cation-based ionic liquids were tested with two different anions: the dicyanamide anion (see Table 40) and the dicyanoborate anion (see Table 41). Both of these ionic liquids were found hypergolic experimentally with nitric acid.

The 3-propargyl-1-methylimidazolium / nitrocyanamide ionic liquid was also tested in this study (see Table 42) with nitric acid.

The lower flammability limits of these three ionic liquid are predicted for a mole fraction of cation (or anion) below 0.0099. For the 3-allyl-1-methylimidazolium cation-based ionic liquids, replacement of the $N(CN)_2^-$ anion by the $BH_2(CN)_2^-$ anion induces a decrease of the flammability domain (see Table 40 and Table 41).

For the 3-propargyl-1-methylimidazolium / nitrocyanamide ionic liquid, the upper flammability limit is found for a mole fraction of cation between 0.342 and 0.346.

Mixture	Cation	Anion	Oxidant

	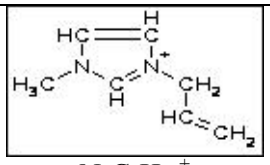 $N_2C_7H_{11}^+$	$N(CN)_2^-$	HNO_3
Stoichiometric Equation	1 [$N_2C_7H_{11}^+$ $N(CN)_2^-$] + 47/5 HNO_3 → 9 CO_2 + 51/5 H_2O + 36/5 N_2		
Initial Conditions	P =1 Atm ; T = 298.15 K $X(N_2C_7H_{11}^+) = X(N(CN)_2^-)$ $X(N_2C_7H_{11}^+) + X(N(CN)_2^-) + X(HNO_3) = 1$		
Lower Flammability Limit (LFL)	0	< $X(N_2C_7H_{11}^+)$ < < $X(N(CN)_2^-)$ <	9.90E-03 (T_F = 2789 K ; P_{AICC} = 21.1 Atm)
Upper Flammability Limit (UFL)	0.248 (T_F = 2719 K ; P_{AICC} = 39.3 Atm)	< $X(N_2C_7H_{11}^+)$ < < $X(N(CN)_2^-)$ <	0.254 (T_F = 2688 K ; P_{AICC} = 39.3 Atm)
P_{AICC} Max Composition	39.7 Atm ($X(Ca^+)$= 0.187)	**T_F Max Composition**	3743 K ($X(Ca^+)$= 0.083)

Table 40: Equilibrium calculations results for the $N_2C_7H_{11}^+$ + $N(CN)_2^-$ / HNO_3 system.

Mixture	Cation	Anion $BH_2(CN)_2^-$	Oxidant HNO_3

	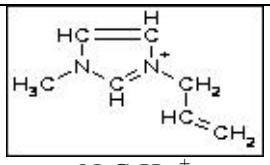 $N_2C_7H_{11}^+$		
Stoichiometric Equation	1 $[N_2C_7H_{11}^+ BH_2(CN)_2^-]$ + 52/5 HNO_3 → 9 CO_2 + 1/2 B_2O_3 + 117/10 H_2O + 36/5 N_2		
Initial Conditions	P =1 Atm ; T = 298.15 K $X(N_2C_7H_{11}^+) = X(BH_2(CN)_2^-)$ $X(N_2C_7H_{11}^+) + X(BH_2(CN)_2^-) + X(HNO_3) = 1$		
Lower Flammability Limit (LFL)	0	< $X(N_2C_7H_{11}^+)$ < < $X(BH_2(CN)_2^-)$ <	9.90E-03 (T_F = 2801 K ; P_{AICC} = 21.3 Atm)
Upper Flammability Limit (UFL)	0.213 (T_F = 2716 K ; P_{AICC} = 37.5 Atm)	< $X(N_2C_7H_{11}^+)$ < < $X(BH_2(CN)_2^-)$ <	0.219 (T_F = 2679 K ; P_{AICC} = 37.4 Atm)
P_{AICC} Max Composition	38.1 Atm ($X(Ca^+)$= 0.083)	**T_F Max Composition**	3676 K ($X(Ca^+)$= 0.074)

Table 41: Equilibrium calculations results for the $N_2C_7H_{11}^+$ + $BH_2(CN)_2^-$ / HNO_3 system.

Mixture	Cation	Anion $N(CN)_2^-$	Oxidant HNO_3

	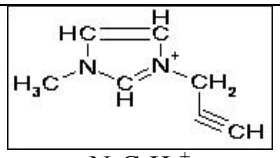 $N_2C_7H_9^+$		
Stoichiometric Equation	1 $[N_2C_7H_9^+ N(CN)_2^-]$ + 9 HNO_3 → 9 CO_2 + 9 H_2O + 7 N_2		
Initial Conditions	P =1 Atm ; T = 298.15 K $X(N_2C_7H_9^+) = X(N(CN)_2^-)$ $X(N_2C_7H_9^+) + X(N(CN)_2^-) + X(HNO_3) = 1$		
Lower Flammability Limit (LFL)	0	< $X(N_2C_7H_9^+)$ < < $X(N(CN)_2^-)$ <	9.90E-03 (T_F = 2792 K ; P_{AICC} = 21.0 Atm)
Upper Flammability Limit (UFL)	0.342 (T_F = 2722 K ; P_{AICC} = 42.7 Atm)	< $X(N_2C_7H_9^+)$ < < $X(N(CN)_2^-)$ <	0.346 (T_F = 2682 K ; P_{AICC} = 42.1 Atm)
P_{AICC} Max Composition	44.0 Atm ($X(Ca^+)$= 0.329)	**T_F Max Composition**	3873 K ($X(Ca^+)$= 0.091)

Table 42: Equilibrium calculations results for the $N_2C_7H_9^+$ + $N(CN)_2^-$ / HNO_3 system.

For the 1-methylimidazolium cation-based ionic liquids, different alkyl substituents were tested (butyl, allyl, and propargyl). For the ionic liquid with a dicyanamide anion, the impact on the flammability domain of these alkyl substituents in the cation is as follows: butyl < allyl < propargyl.

3.3.5 Pyridinium cations

Two different pyridinium cation-based ionic liquids were studied in this work. The first one is composed of the 1-butylpyridinium cation and the dicyanoborate anion. This ionic liquid has been found experimentally hypergolic with HNO_3. The results obtained from the equilibrium calculations are given in Figure 19 and in Table 43.

The lower flammability limit of this system is found for a mole fraction of cation (or anion) below 0.0099. The upper flammability limit is obtained for a mole fraction between 0.153 and 0.160.

The maximum flame temperature is equal to 3600 K and is obtained for a small amount of ionic liquid (mole fraction = 0.057). The same trend is predicted for the 1-allylpyridinium cation-based ionic liquid (T_F Max = 3700 K for a mole fraction = 0.065) (see Table 44).

The ionic liquid ($NC_8H_{10}^+$ + $BH_2(CN)_2^-$) was also determined hypergolic experimentally with HNO_3. For this system, the lower flammability limit was also found for a mole fraction of cation (or anion) below 0.0099. However, we observed an increase of the

upper flammability limit. It is predicted at a mole fraction of cation between 0.213 and 0.219 (see Table 44).

As seen previously for imidazolium and N'N-dimethylhydrazinium cations the presence of the allyl substituent instead of the butyl substituent in the cation leads to an increase of the hypergolicity domain.

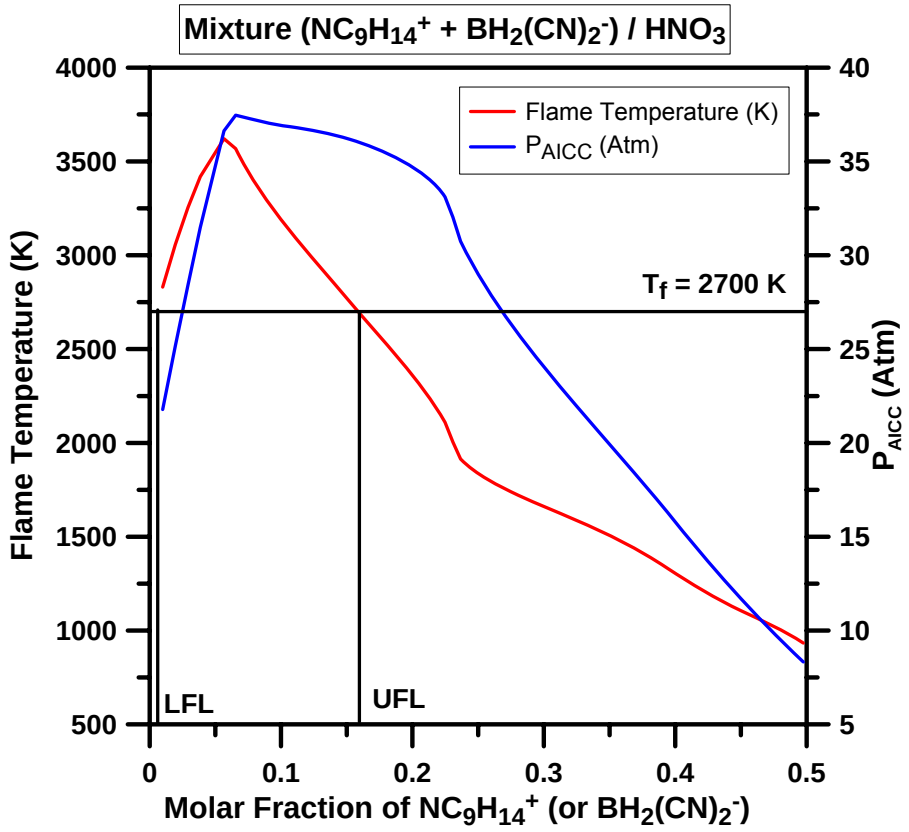

Figure 19: Flame temperature and P_{AICC} for different $NC_9H_{14}^+$ + $BH_2(CN)_2^-$ / HNO_3 mixtures at 298.15 K and 1 Atm.

Mixture	Cation	Anion $BH_2(CN)_2^-$	Oxidant HNO_3

	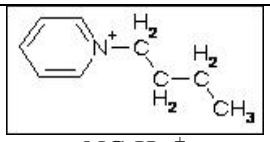 $NC_9H_{14}^+$		
Stoichiometric Equation	$1\ [NC_9H_{14}^+\ BH_2(CN)_2^-] + 63/5\ HNO_3 \rightarrow 11\ CO_2 + 1/2\ B_2O_3 + 143/10\ H_2O + 39/5\ N_2$		
Initial Conditions	P =1 Atm ; T = 298.15 K $X(NC_9H_{14}^+) = X(BH_2(CN)_2^-)$ $X(NC_9H_{14}^+) + X(BH_2(CN)_2^-) + X(HNO_3) = 1$		
Lower Flammability Limit (LFL)	0	$< X(NC_9H_{14}^+) < < X(BH_2(CN)_2^-) <$	9.90E-03 (T_F = 2830 K ; P_{AICC} = 21.8 Atm)
Upper Flammability Limit (UFL)	0.153 (T_F = 2751 K ; P_{AICC} = 36.2 Atm)	$< X(NC_9H_{14}^+) < < X(BH_2(CN)_2^-) <$	0.160 (T_F = 2694 K ; P_{AICC} = 36.0 Atm)
P_{AICC} Max Composition	37.5 Atm ($X(Ca^+)$= 0.065)	**T_F Max Composition**	3622 K ($X(Ca^+)$= 0.057)

Table 43: Equilibrium calculations results for the $NC_9H_{14}^+$ + $BH_2(CN)_2^-$ / HNO_3 system.

Mixture	Cation	Anion $BH_2(CN)_2^-$	Oxidant HNO_3

	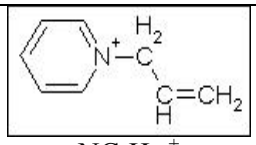 $NC_8H_{10}^+$		
Stoichiometric Equation	1 [$NC_8H_{10}^+$ $BH_2(CN)_2^-$] + 11 HNO_3 → 10 CO_2 + 1/2 B_2O_3 + 115/10 H_2O + 7 N_2		
Initial Conditions	P =1 Atm ; T = 298.15 K $X(NC_8H_{10}^+) = X(BH_2(CN)_2^-)$ $X(NC_8H_{10}^+) + X(BH_2(CN)_2^-) + X(HNO_3) = 1$		
Lower Flammability Limit (LFL)	0	< $X(NC_8H_{10}^+)$ < < $X(BH_2(CN)_2^-)$ <	9.90E-03 (T_F = 2812 K ; P_{AICC} = 21.3 Atm)
Upper Flammability Limit (UFL)	0.213 (T_F = 2718 K ; P_{AICC} = 36.7 Atm)	< $X(NC_8H_{10}^+)$ < < $X(BH_2(CN)_2^-)$ <	0.219 (T_F = 2676 K ; P_{AICC} = 36.6 Atm)
P_{AICC} Max Composition	37.8 Atm ($X(Ca^+)$= 0.083)	**T_F Max Composition**	3700 K ($X(Ca^+)$= 0.065)

Table 44: Equilibrium calculations results for the $NC_8H_{10}^+$ + $BH_2(CN)_2^-$ / HNO_3 system.

3.3.6 N-methylpyrrololidinium cations

Different N-methylpyrrololidinium cation-based ionic liquids are reported hypergolic experimentally with nitric acid.

The first ones tested here are 1-butyl-N-methylpyrrolidinium cation-based ionic liquids with different anions (the dicyanamide anion $N(CN)_2^-$ (see Figure 20 and Table 45) and the dicyanoborate anion (see Table 46)). Equilibrium calculations were carried out for these two ionic liquids with HNO_3 as the oxidant.

For both systems, for a given domain of compositions, the flame temperature is above 2700 K and therefore the mixture is predicted hypergolic. The lower flammability limit is found for a mole fraction of cation below 0.0099. For the $NC_9H_{20}^+$ + $N(CN)_2^-$ ionic liquid, the upper flammability is predicted for a mole fraction of cation between 0.138 and 0.145. For the $NC_9H_{20}^+$ + $BH_2(CN)_2^-$ ionic liquid, the upper flammability limit was found for a mole fraction between 0.123 and 0.130. As has been seen before for N-methylpyrrololidinium cation-based ionic liquids, replacement of the $N(CN)_2^-$ anion by the $BH_2(CN)_2^-$ anion leads to a smaller flammability domain.

For both of these systems, the maximum flame temperature was similar and around 3550 K, and was observed for small mole fraction of cation (around 0.05 - 0.06) (see Table 45 and Table 46).

Equilibrium calculations for 1-allyl-N-methylpyrrolidinium cation dicyanoborate anion ionic liquid ($NC_8H_{16}^+$ + $BH_2(CN)_2^-$) were also carried out. Like with the previous systems, the lower flammability limit was found for mole fraction of cation below 0.0099 (see Table 47). For this ionic liquid, the upper flammability limit was found for a mole fraction between 0.160 and 0.167. As seen previously for the other cations, the presence of the allyl substituent instead of the butyl substituent in the cation again leads to an increase of the hypergolicity domain.

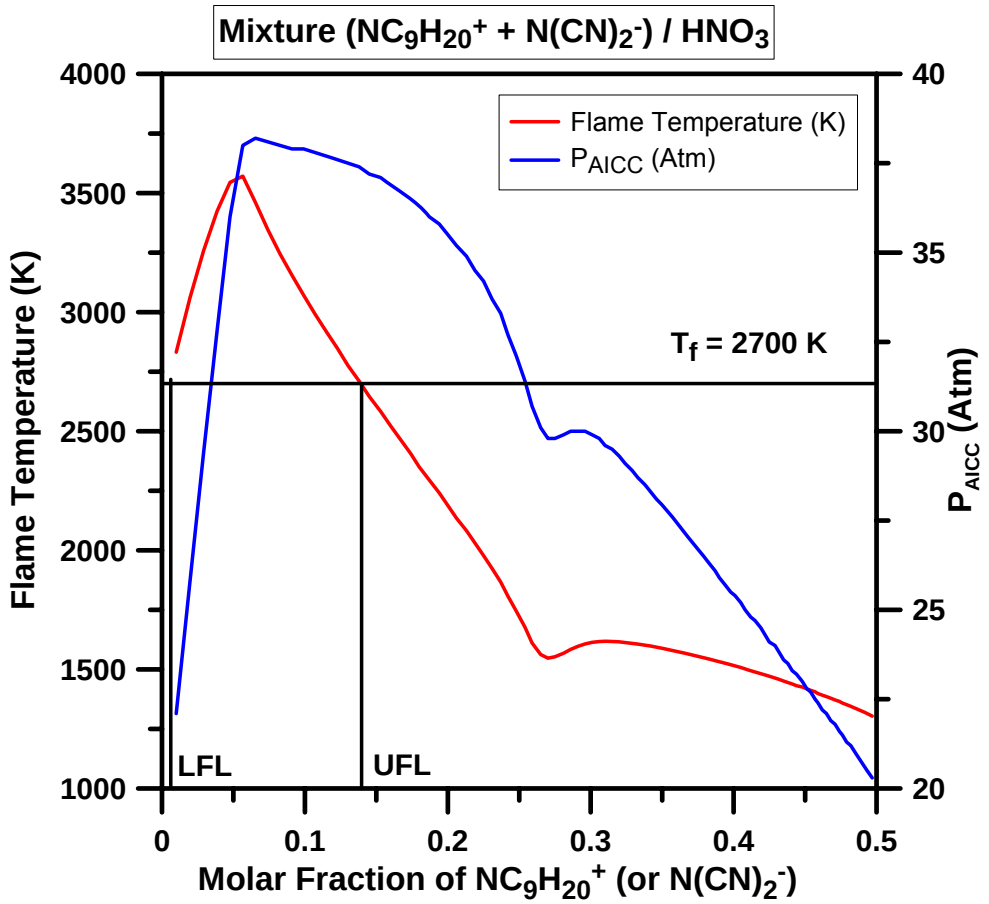

Figure 20: Flame temperature and P_{AICC} for different $NC_9H_{20}^+$ + $N(CN)_2^-$ / HNO_3 mixtures at 298.15 K and 1 Atm.

Mixture	Cation	Anion	Oxidant

	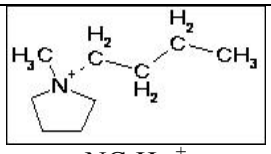 $NC_9H_{20}^+$	$N(CN)_2^-$	HNO_3
Stoichiometric Equation	1 $[NC_9H_{20}^+ N(CN)_2^-]$ + 64/5 HNO_3 → 11 CO_2 + 82/5 H_2O + 42/5 N_2		
Initial Conditions	P =1 Atm ; T = 298.15 K $X(NC_9H_{20}^+) = X(N(CN)_2^-)$ $X(NC_9H_{20}^+) + X(BH_2(CN)_2^-) + X(HNO_3) = 1$		
Lower Flammability Limit (LFL)	0	< $X(NC_9H_{20}^+)$ < < $X(N(CN)_2^-)$ <	9.90E-03 (T_F = 2832 K ; P_{AICC} = 22.1 Atm)
Upper Flammability Limit (UFL)	0.138 (T_F = 2710 K ; P_{AICC} = 37.4 Atm)	< $X(NC_9H_{20}^+)$ < < $X(N(CN)_2^-)$ <	0.145 (T_F = 2646 K ; P_{AICC} = 37.2 Atm)
P_{AICC} Max Composition	38.2 Atm ($X(Ca^+)$= 0.065)	**T_F Max Composition**	3571 K ($X(Ca^+)$= 0.057)

Table 45: Equilibrium calculations results for the $NC_9H_{20}^+$ + $N(CN)_2^-$ / HNO_3 system.

Mixture	Cation	Anion $BH_2(CN)_2^-$	Oxidant HNO_3

	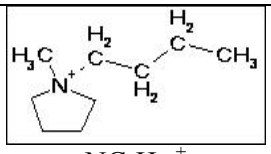 $NC_9H_{20}^+$		
Stoichiometric Equation	1 $[NC_9H_{20}^+ BH_2(CN)_2^-]$ + 69/5 HNO_3 → 11 CO_2 + 1/2 B_2O_3 + 179/10 H_2O + 42/5 N_2		
Initial Conditions	P =1 Atm ; T = 298.15 K $X(NC_9H_{20}^+) = X(BH_2(CN)_2^-)$ $X(NC_9H_{20}^+) + X(BH_2(CN)_2^-) + X(HNO_3) = 1$		
Lower Flammability Limit (LFL)	0	< $X(NC_9H_{20}^+)$ < < $X(BH_2(CN)_2^-)$ <	9.90E-03 (T_F = 2845 K ; P_{AICC} = 22.3 Atm)
Upper Flammability Limit (UFL)	0.123 (T_F = 2748 K ; P_{AICC} = 36.5 Atm)	< $X(NC_9H_{20}^+)$ < < $X(BH_2(CN)_2^-)$ <	0.130 (T_F = 2677 K ; P_{AICC} = 36.4 Atm)
P_{AICC} Max Composition	37.5 Atm ($X(Ca^+)$= 0.057)	**T_F Max Composition**	3559 K ($X(Ca^+)$= 0.048)

Table 46: Equilibrium calculations results for the $NC_9H_{20}^+$ + $BH_2(CN)_2^-$ / HNO_3 system.

Mixture	Cation	Anion $BH_2(CN)_2^-$	Oxidant HNO_3

	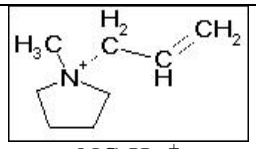 $NC_8H_{16}^+$		
Stoichiometric Equation	1 $[NC_8H_{16}^+ BH_2(CN)_2^-]$ + 61/5 HNO_3 → 10 CO_2 + 1/2 B_2O_3 + 151/10 H_2O + 38/5 N_2		
Initial Conditions	P =1 Atm ; T = 298.15 K $X(NC_8H_{16}^+) = X(BH_2(CN)_2^-)$ $X(NC_8H_{16}^+) + X(BH_2(CN)_2^-) + X(HNO_3) = 1$		
Lower Flammability Limit (LFL)	0	< $X(NC_8H_{16}^+)$ < < $X(BH_2(CN)_2^-)$ <	9.90E-03 (T_F = 2826 K ; P_{AICC} = 21.8 Atm)
Upper Flammability Limit (UFL)	0.160 (T_F = 2730 K ; P_{AICC} = 37.2 Atm)	< $X(NC_8H_{16}^+)$ < < $X(BH_2(CN)_2^-)$ <	0.167 (T_F = 2677 K ; P_{AICC} = 37.1 Atm)
P_{AICC} Max Composition	37.8 Atm ($X(Ca^+)$= 0.065)	**T_F Max Composition**	3626 K ($X(Ca^+)$= 0.057)

Table 47: Equilibrium calculations results for the $NC_8H_{16}^+$ + $BH_2(CN)_2^-$ / HNO_3 system.

3.3.7 N-methyltriazolium cations

Two different N-methyltriazolium cation-based ionic liquids have been studied in this work. The first one is the ionic liquid composed of the 4-butyl-1-methyl-1,2,4-triazolium cation and the dicyanoborate anion. This ionic liquid ($N_3C_7H_{14}^+$ + $BH_2(CN)_2^-$) is reported hypergolic with HNO_3. The results obtained from the equilibrium calculations are given in Figure 21 and in Table 48.

The lower flammability limit of this system is found for a mole fraction of cation (or anion) below 0.0099. The upper flammability limit is obtained for a mole fraction between 0.180 and 0.187.

The maximum flame temperature is equal to 3600 K and is obtained for a small amount of ionic liquid (mole fraction = 0.065). The same can be noted for the 4-allyl-1-methyl-1,2,4-triazolium cation-based ionic liquid (T_F Max = 3700 K for a mole fraction = 0.074) (see Table 44).

This ionic liquid ($N_3C_6H_{10}^+$ + $BH_2(CN)_2^-$) was also determined hypergolic experimentally with HNO_3. For this system, the lower flammability limit was also found for a mole fraction of cation (or anion) below 0.0099. However, we predict an increase of the upper flammability limit. This time, it was determined at a mole fraction of cation between 0.254 and 0.259 (see Table 49).

As seen previously for the other cations, presence of the allyl substituent instead of the butyl substituent in the cation leads to an increase of the hypergolicity domain.

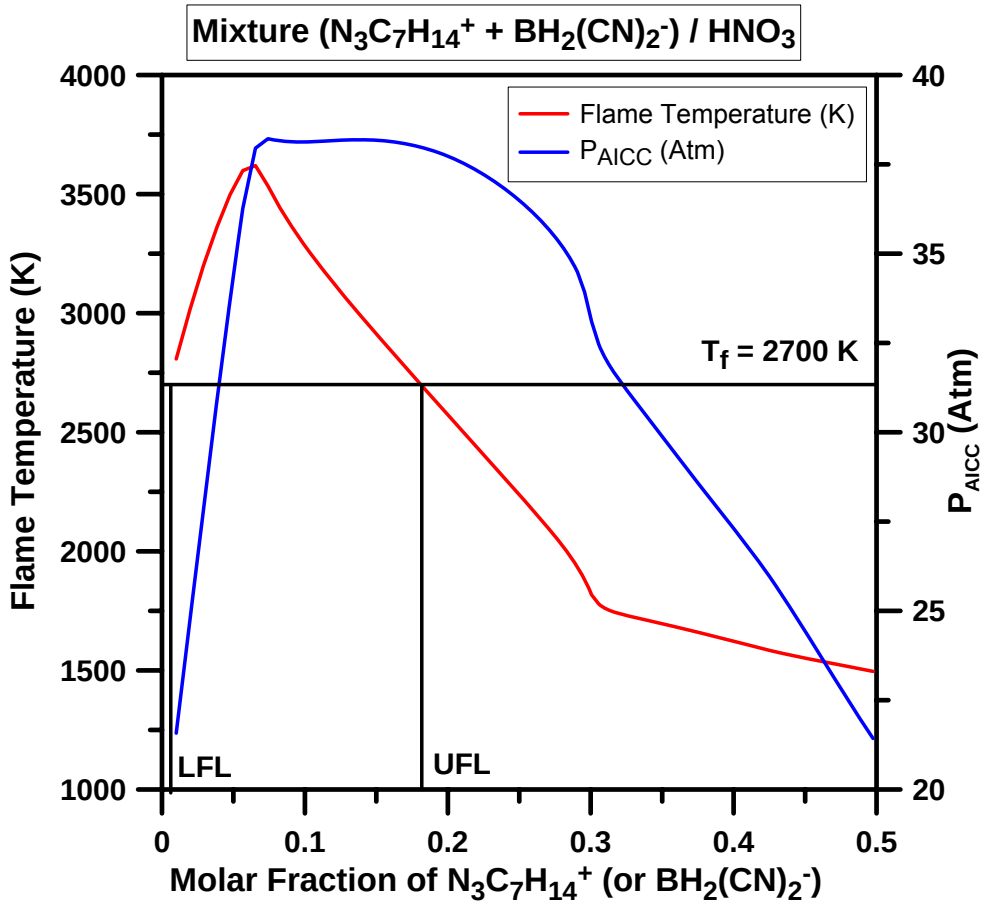

Figure 21: Flame temperature and P_{AICC} for different $N_3C_7H_{14}^+$ + $BH_2(CN)_2^-$ / HNO_3 mixtures at 298.15 K and 1 Atm.

Mixture	Cation	Anion $BH_2(CN)_2^-$	Oxidant HNO_3

	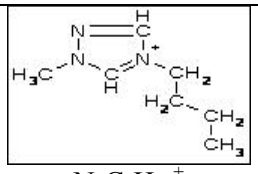 $N_3C_7H_{14}^+$		
Stoichiometric Equation	$1\ [N_3C_7H_{14}^+\ BH_2(CN)_2^-] + 11\ HNO_3 \rightarrow 9\ CO_2 + 1/2\ B_2O_3 + 135/10\ H_2O + 8\ N_2$		
Initial Conditions	P =1 Atm ; T = 298.15 K $X(N_3C_7H_{14}^+) = X(BH_2(CN)_2^-)$ $X(N_3C_7H_{14}^+) + X(BH_2(CN)_2^-) + X(HNO_3) = 1$		
Lower Flammability Limit (LFL)	0	$< X(N_3C_7H_{14}^+) < < X(BH_2(CN)_2^-) <$	9.90E-03 (T_F = 2808 K ; P_{AICC} = 21.6 Atm)
Upper Flammability Limit (UFL)	0.180 (T_F = 2706 K ; P_{AICC} = 38.0 Atm)	$< X(N_3C_7H_{14}^+) < < X(BH_2(CN)_2^-) <$	0.187 (T_F = 2661 K ; P_{AICC} = 37.9 Atm)
P_{AICC} Max Composition	38.2 Atm ($X(Ca^+)$= 0.074)	**T_F Max Composition**	3620 K ($X(Ca^+)$= 0.065)

Table 48: Equilibrium calculations results for the $N_3C_7H_{14}^+$ + $BH_2(CN)_2^-$ / HNO_3 system.

Mixture	Cation	Anion	Oxidant

	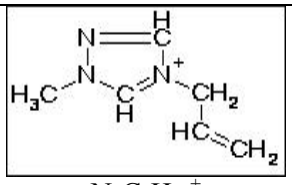 $N_3C_6H_{10}^+$	$BH_2(CN)_2^-$	HNO_3
Stoichiometric Equation	1 $[N_3C_6H_{10}^+ BH_2(CN)_2^-]$ + 47/5 HNO_3 → 8 CO_2 + 1/2 B_2O_3 + 107/10 H_2O + 36/5 N_2		
Initial Conditions	P =1 Atm ; T = 298.15 K $X(N_3C_6H_{10}^+) = X(BH_2(CN)_2^-)$ $X(N_3C_6H_{10}^+) + X(BH_2(CN)_2^-) + X(HNO_3) = 1$		
Lower Flammability Limit (LFL)	0	< $X(N_3C_6H_{10}^+)$ < < $X(BH_2(CN)_2^-)$ <	9.90E-03 (T_F = 2789 K ; P_{AICC} = 21.1 Atm)
Upper Flammability Limit (UFL)	0.254 (T_F = 2719 K ; P_{AICC} = 39.5 Atm)	< $X(N_3C_6H_{10}^+)$ < < $X(BH_2(CN)_2^-)$ <	0.259 (T_F = 2692 K ; P_{AICC} = 39.4 Atm)
P_{AICC} Max Composition	39.5 Atm ($X(Ca^+)$= 0.225)	**T_F Max Composition**	3722 K ($X(Ca^+)$= 0.074)

Table 49: Equilibrium calculations results for the $N_3C_6H_{10}^+$ + $BH_2(CN)_2^-$ / HNO_3 system.

Conclusions and future work

This work presents a numerical method devoted to the prediction of hypergolic mixture flammability limits. A flame temperature criterion can be used to determine flammability limits of MMH/NTO hypergolic mixtures and other non-ionic fuel/oxidant systems. In this part were also presented the ionic liquids which were found hypergolic experimentally with the oxidants N_2O_4 and HNO_3. The determination of the thermodynamic data of cations, anions and neutrals in the gas phase was presented.

The results obtained from the equilibrium calculations for both protic and aprotic ionic liquids are presented in the third section of this part. For all of the systems considered, we were able to determine flammability limits. All of the systems reported experimentally to be hypergolic are also predicted hypergolic for a given domain of compositions using our numerical approach of adiabatic Flame Temperature (T_F). Some of these systems are predicted hypergolic for almost the entire domain of compositions. However, complementary calculations are needed to assess these results.

Refinements to this approach are also needed since the gas-phase compositions considered here for the systems are somewhat simplistic. It is tenable then to examine more complex gas-phase compositions in which species formed in the liquid-phase reactions are also considered. Such species may be isocyanic acid (HNCO), HCN, NH_3, etc., some of which have been experimentally observed during the pre-ignition phase.

New insight concerning the mixtures already studied in this report may be gained via the determination of thermodynamic data for ion pairs for aprotic ionic liquids, and neutral pairs for protic ionic liquids. Additional ionic liquid systems can be also examined by considering other alkyl substituents (e.g. methoxymethyl) in the already studied cations (imidazolium, triazolium, N'N-dimethylhydrazinium, etc.).

Finally, this thermodynamic approach of predicting flammability envelopes could be fully developed into a time-resolved chemical kinetics model, which implicitly couples the dynamics of the initial liquid-phase chemistry to the subsequent gas-phase chemistry to predict ignition delay times under realistic experimental conditions. The last points are examined in parts two and three of the present report.

References

Armstrong J.P., et al., 2007, Vapourisation of Ionic Liquids, Phys. Chem. Chem. Phys., Vol. 9, p. 982-990

Baranyai K.J. et al., 2004, Thermal Degradation of Ionic Liquids at Elevated Temperatures, Aus. J. Chem., Vol. 57, p. 145-147

Catoire, L. et al., Chemical Kinetic Model for Monomethylhydrazine/Nitrogen Tetraoxide Gas-Phase Combustion and Hypergolic Ignition, 2004, J. Propulsion and Power, Vol. 20, p. 87-92

Catoire L. et al., Hypergolicity with Ionic Liquids, 2008, Interim report, Contract FA8655-07-M-4009 EOARD

Catoire L. et al., Chemical Kinetics Interpretation of Hypergolicity of Ionic Liquid-Based Systems, 2009, Final report, Contract FA8655-07-M-4009 EOARD

Catoire L., Method for Predicting Hypergolic Mixture Flammability Project, 2012

COSILAB, Chemical Equilibrium, Basics of and Techniques for Computing Chemical Equilibria, Rotexo, Document RX-D-0003 from August 2, 2010

Earle M.J. et al., 2006, The Distillation and Volatility of Ionic Liquids, Nature, Vol. 439, p. 831-834

Emel'yanenko V.N. et al., 2007, The Gaseous Enthalpy of Formation of the Ionic Liquid 1-Butyl-3-methylimidazolium Dicyanamide from Combustion Calorimetry, Vapor Pressure Measurements, and *Ab Initio* Calculations, J. Am. Chem. Soc., Vol. 129, p. 3930-3937

Fredlake et al, Thermophysical Propoerties of Imidazolium-Based Ionic Liquids, 2004, J. Chem. Eng. Data, Vol. 49, p. 954-964

Gao H. et al., Hypergolic Ionic Liquids with the 2,2-Dialkyltriazanium Cation, 2009, Angew. Chem. Int. Ed., Vol. 48, p. 2792-2795

Goos E., et al., Ideal Gas Thermochemical Database with updates from Active Thermochemical Tables, mirrored at <http://garfield.chem.elte.hu/Burcat/burcat.html> ; December 2013

Halim H. et al., MINDO/3 and MNDO Calculations of Closed- and Open-Shell Cations Containing C, H, N, and O, J. Comp. Chem, 1986, Vol. 7, p. 93-104

He L. et al., Nitrocyanamide-Based Ionic Liquids and Their Potential Applications as Hypergolic Fuels, 2010, Chem. Eur. J., Vol. 16, p. 5736-5743

Joo et al., Inorganic or Organic Azide-containing Hypergolic Ionic Liquids, 2010, Inorg. Chem., Vol. 49, p. 3282-3288

Leal J.P. et al., 2007, The Nature of Ionic Liquids in the Gas Phase, J. Phys. Chem. A, Vol. 111, p. 6176-6182

Mathieu D. et al., Formation Enthalpies of Ions: Routine Prediction Using Atom Equivalents, 2010, J. Chem. Theory. Comput. Vol. 6, p. 2126-2139

Osmont A., Elaboration d'une méthode théorique de calcul des enthalpies de formation en phase gazeuse et condense de s molécules et radicaux de masse molaire élevée – Application à l'énergétique, 2007, Ph.D. Thesis, University of Orléans

Osmont A. et al., *Ab initio* quantum chemical predictions of enthalpies of formation, heat capcities, and entropies of gas-phase energetic compounds, 2007, Combustion and Flame, Vol. 151, p. 262-273

Pucheault M, Liquides Ioniques, 2010, http://perso.univrennes1.fr/mathieu.pucheault/_PDF/Publis/2010_Pucheault_Dunod.pdf

Schmidt M.W. et al, 2005, Triazolium-Based Energetic Ionic Liquids, J. Phys. Chem. A, Vol. 109, p. 7285-7295

Schneider et al., Ionic Liquids as Hypergolic Fuels, 2008, Energy and Fuels, Vol. 22, p. 2871-2872

Schneider S. et al., Green Bipropellants: Hydrogen-Rich Ionic Liquids that are Hypergolic with Hydrogen Peroxide, 2011, Angew. Chem. Int. Ed., Vol. 50, p. 5886-5888

Smiglak M. et al., The second evolution of ionic liquids: from solvents and separations to advanced materials – Energetic examples from the ionic liquid cookbook, 2007, Acc. Chem. Res., Vol. 40., p. 1182-1192

Strasser D. et al., 2007, Photoelectron Spectrum of Isolated Ion-Pairs in Ionic Liquid Vapor, J. Phys. Chem. A, Vol. 111, p. 3191-3195

Van Valkenburg et al., Thermochemistry of Ionic Liquid Heat-Transfer Fluids, 2005, Thermochimica Acta, Vol. 425, p. 181-188

Wang K. et al., Boronium-Cation based Ionic Liquids as Hypergolic Fluids, 2012, Chem. Eur. J., Vol. 18, p. 16931-16937

Zhang Y. et al., Hypergolic N,N-dimethylhydrazinium ionic liquids, 2010, Chem. Eur. J., Vol. 16, p. 3114-3120

Zhang Y. et al., Dicyanoborate-Based Ionic Liquids as Hypergolic Fluids, 2011a, Angew. Chem. Int. Ed., Vol. 50, p. 935-937

Zhang Y. et al, Minireview: Ionic Liquids as Hypergolic Fuels, 2010b, Angew. Chem. Int. Ed., Vol. 50, p. 9554-9562

Zorn D.D. et al, 2006, Electronic Structure Studies of Tetrazolium-Based Ionic Liquids, J. Phys. Chem. B, Vol. 110, p. 11110-11119

List of Symbols, Abbreviations and Acronyms

An or An^-: Anion

Ca or Ca^+: Cation

IL(s): Ionic Liquid(s)

LFL: lower flammability limit

Ne: Neutral species

(s): singlet spectral term

UFL: upper flammability limit

WFNA: White Fuming Nitric Acid (Pure nitric acid: HNO_3)

X: Mole fraction

Part two:

CHEMICAL KINETICS AND DYNAMICS OF HYPERGOLIC IGNITION OF ILs BASED SYSTEMS

Table of Contents

List of Figures

1. Introduction

In the frame for searching new hypergolic (auto-igniting) propellant systems, it is necessary to discuss their reactions in both the liquid and gas phases. In practical hypergolic applications, propellant fuels and oxidants are liquids and upon contact, reactions occur in the liquid phase and also in the gas phase above the liquids. One point which seems clear is that ignition occurs in the gas phase even if the reactants come into contact as liquids. The issue of interest is related to the understanding of the qualitative and quantitative compositions of both phases when ignition occurs. Several hypotheses can be proposed. For instance, both liquids vaporize upon contact and therefore the igniting gas phase is composed of the fuel and oxidant as is. This is tenable for non-ionic propellants because the vapor pressures of both liquids are already high as is the case for the gas phase ignition of monomethyl hydrazine (MMH) and nitrogen tetroxide (NTO) [Catoire, 2006]. For ionic liquids (ILs)/oxidant combinations, this is also tenable but less obvious because ILs have negligible vapor pressure at room temperature. Nevertheless, experimental observations have shown that isocyanic acid (HNCO) is present in the gas phase for the 1-butyl-3-methylimidazolium dicyanamide/white fuming nitric acid (BMIM-dca/WFNA) system when ignition occurs; presumably HNCO is formed during liquid phase reactions (see Figure 1), which means that reactions in the liquid phase together with reactions in the gas phase are playing a role during the ignition process.

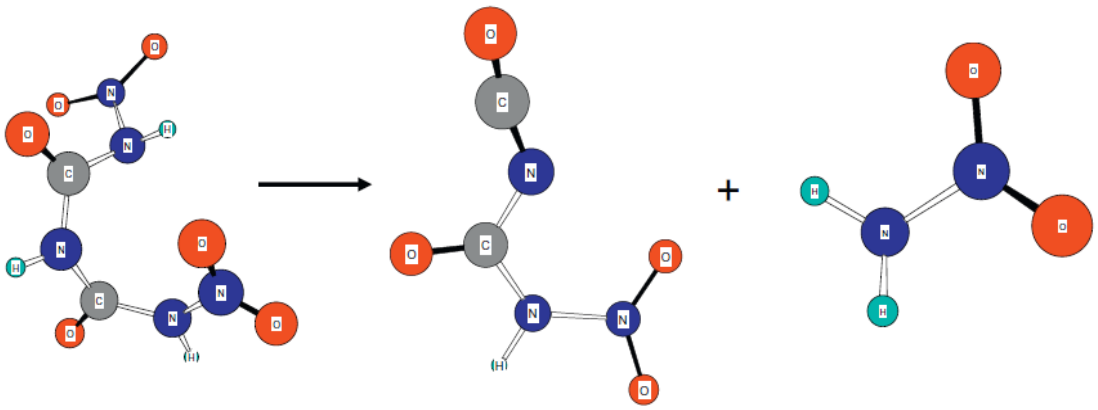

Figure 1. Interpretation of hypergolic ignition of BMIM-dca with WFNA. The two species formed from the liquid phase intermediate further decompose to give gaseous HNCO, which is present when hypergolic ignition occurs [Catoire, 2012].

For some non-ionic liquid/oxidant hypergolic systems one elementary reaction in the liquid phase and one elementary reaction in the gas phase have been shown to be sufficient to explain ignition [Zhang, 2015]. However, as underlined by the authors, their approach is far from being detailed and hence more work is needed to conclude unambiguously about this issue. These non-ionic liquid/oxidant combinations are complex systems because chemical reaction dynamics both in the liquid phase and the gas phase and their inter-coupling need to be examined. Furthermore, in drop-test experiments in which a liquid droplet of fuel falls into a volume of liquid oxidant, the chemical dynamics at the liquid interfaces also needs to be examined. One other issue of interest concerns the existence, or not, of ions in the gas phase; either formed in the gas phase or originating from the ionic liquid phase and their potential role on ignition. All of these features are developed in this report to allow for a deeper understanding of the role they play in controlling the composition of the mixture formed before ignition occurs. This approach may also allow for a discussion on the ignition delay, which is known to be an important parameter in practical hypergolic devices. Briefly, if the

ignition delay is too long, the IL/oxidant combination is of no interest in real bipropellant applications even if its theoretical specific impulse is promising.

2. Chemical reaction dynamics for liquid hydrazines/liquid NTO (or liquid HNO_3) hypergolic ignition

Daimon et al. [Daimon, 1984], Tanaka et al. [Tanaka, 1985], and Daimon et al. [Daimon, 1991] observed a N_2H_4 droplet falling into a NTO pool (see Figure 2) and a NTO droplet falling into a N_2H_4 pool (see Figure 3). In both cases, they found that a layer of NTO was vaporized upon contact. Their interpretations of the visualizations given in Figures 2 and 3 are reported in Figures 4 and 5, respectively. In the first case, ignition is supposed to be due to gas-gas reactions at the interface of the two liquids whereas in the second case, NTO vapor penetrates into the liquid hydrazine and, although not evoked explicitly by the authors, however, a gas-liquid interface is formed.

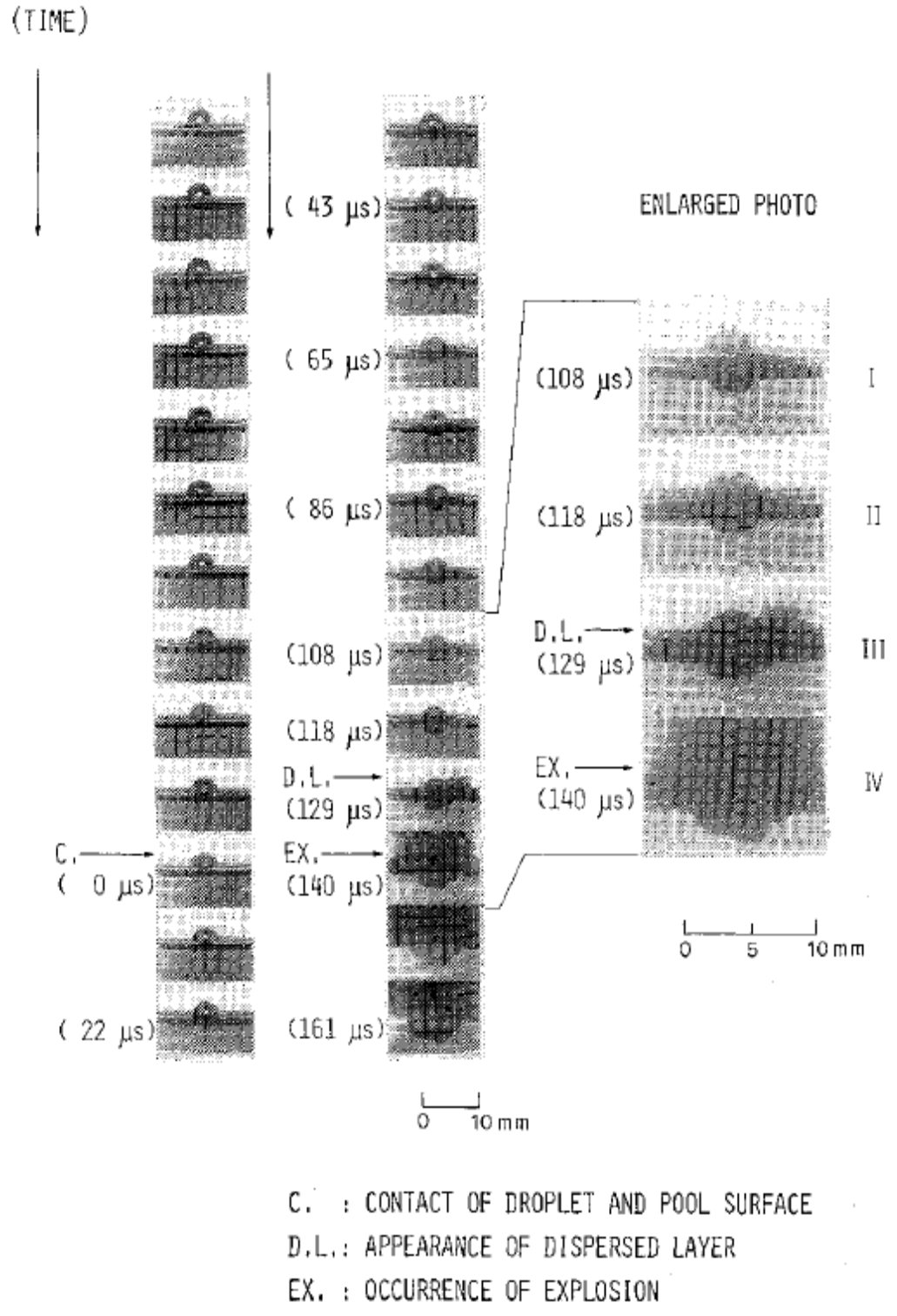

Figure 2. High speed motion pictures (92900 frames per second) of the contact of a N_2H_4 droplet falling into a NTO pool.

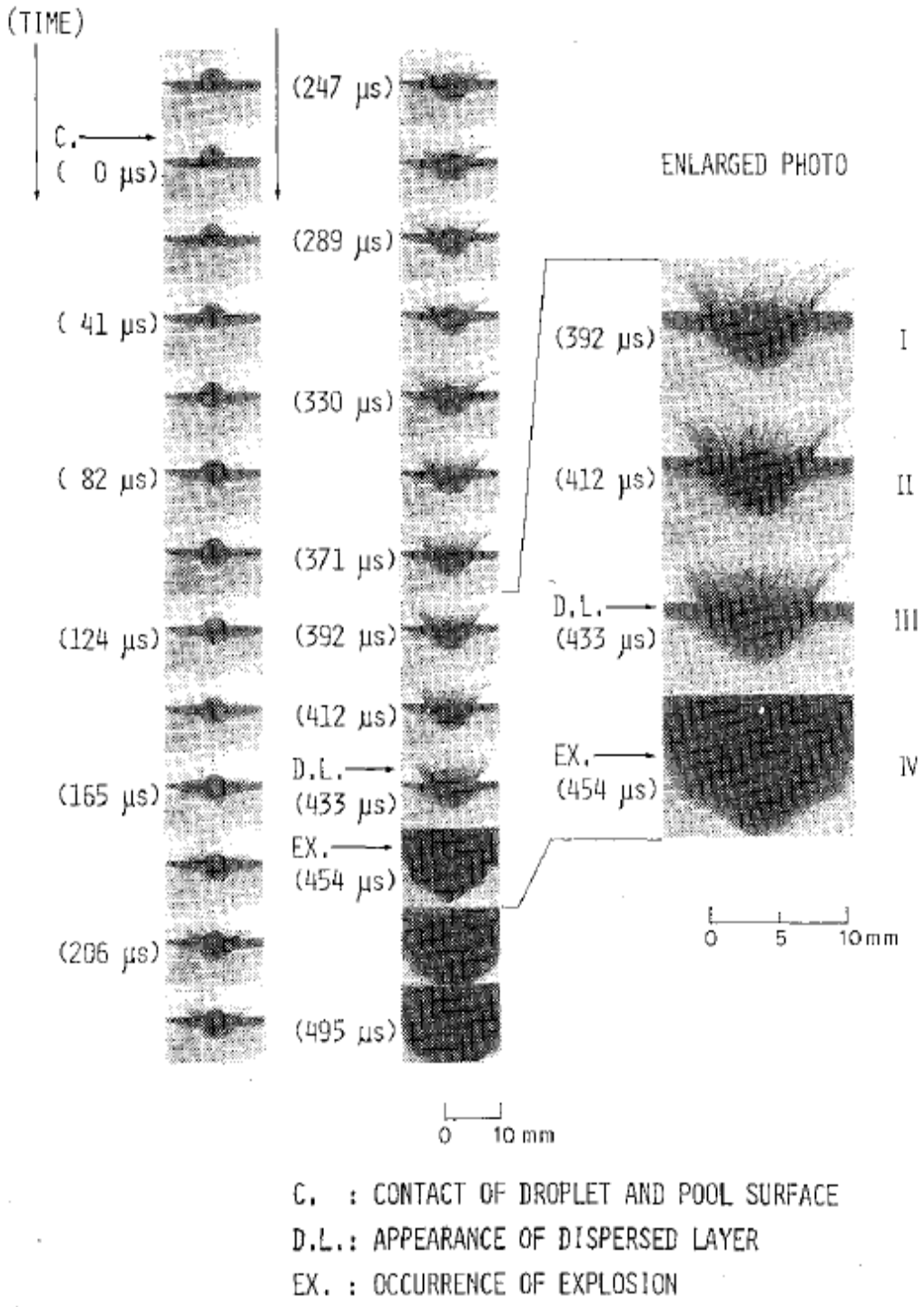

Figure 3. High speed motion pictures (48500 frames per second) of the contact of a NTO droplet falling into a hydrazine pool.

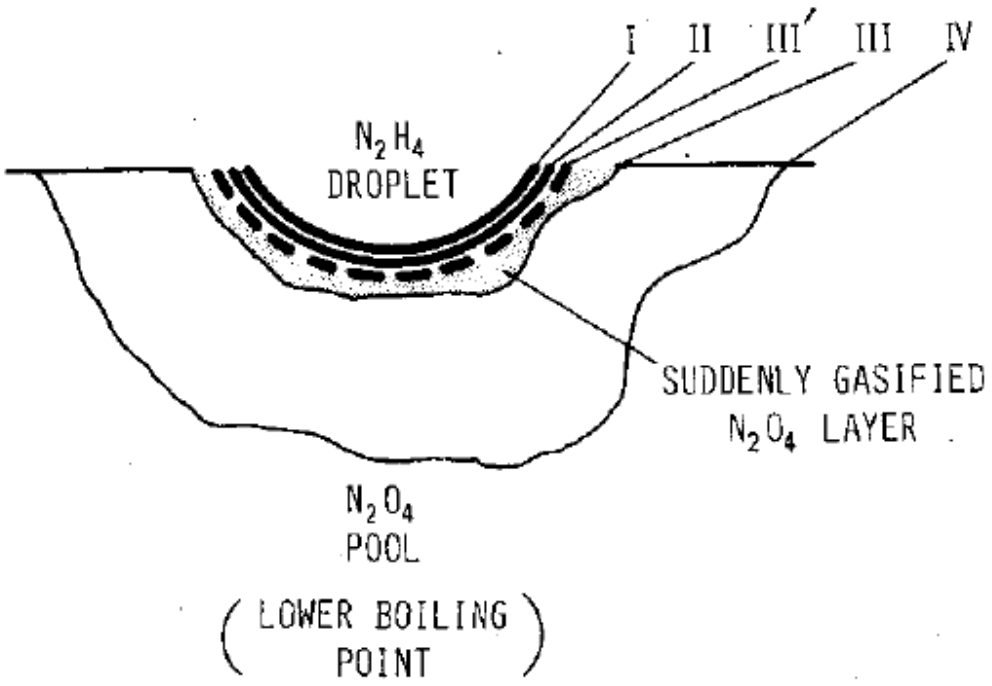

Figure 4. Interpretation of Tanaka et al. [Tanaka, 1985] to explain hypergolic ignition when a droplet of hydrazine is falling into a pool of liquid NTO.

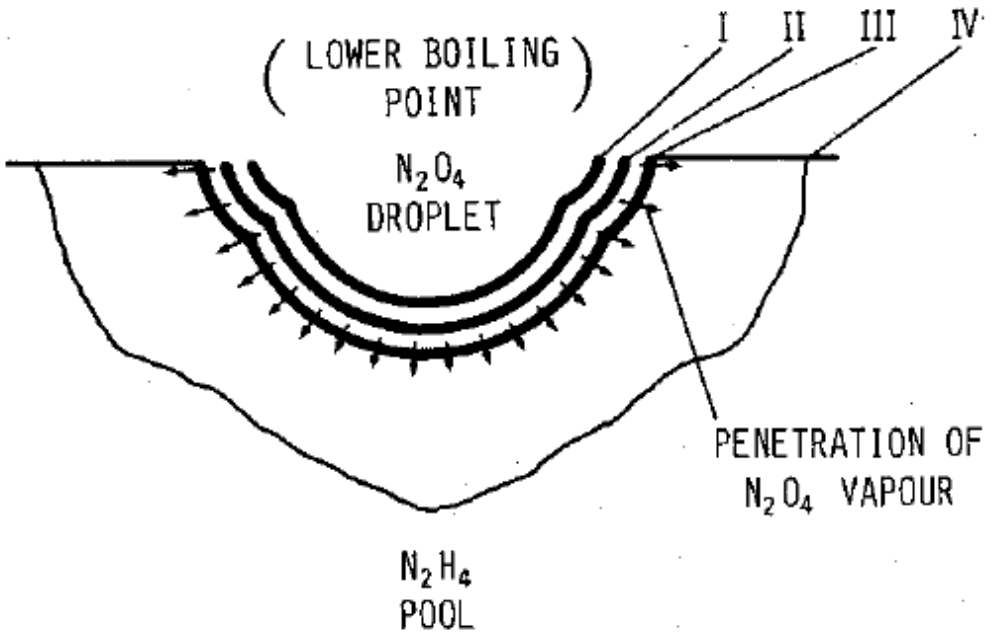

Figure 5. Interpretation of Tanaka et al. [Tanaka, 1985] to explain hypergolic ignition when a droplet of NTO is falling into a pool of liquid hydrazine.

For N_2H_4 and its methylated derivatives MMH and UDMH (unsymmetrical dimethyl hydrazine) and for two oxidizers NTO and FNA (fuming nitric acid) it is reported that the explosion phenomena observed can be classified into three categories [Daimon, 1991]:

- In the case of hydrazine/NTO, sudden gasification of a superheated liquid layer formed at the boundary of the two liquids occurs spontaneously and a detonation-like reaction proceeds in the reactive mixture produced.

- In the cases of MMH/NTO and UDMH/NTO, sudden gasification is caused by the shock from a local ignition source and a turbulent-combustion reaction proceeds in the reactive mixture produced.

- In the cases of hydrazine type fuels/FNA, sudden gasification occurs spontaneously as in the case of hydrazine/NTO, but it is not augmented by a chemical reaction and in these cases the observed explosion is weak.

In all these cases, the vapor layer, which is formed between the reactive fuel droplet and the liquid pool, plays an important role for the occurrence of the explosion. The composition of this layer (pure oxidant, pure fuel or mixture of both) is not clearly discussed and all these studies do not identify unambiguously the chemical cause of ignition or explosion. The sections below are devoted to chemical dynamics and kinetics in the gas phase, in the liquid phase, at the gas-liquid interface, and at the liquid-liquid interface to obtain a deeper understanding of the hypergolic ignition phenomenon.

3. Chemical reaction dynamics and kinetics for gas/gas hypergolic ignition

Wasko [Wasko, 1963], Chuan and Wiber [Chuan, 1967], and Miyajima and Sakamoto [Miyajima, 1973] observed gas phase N_2H_4/NTO hypergolic ignitions, and Catoire et al. [Catoire, 2004 & 2006] studied gas phase MMH/NTO hypergolic ignitions (see Figure 6) and provided a detailed MMH/NTO chemical kinetics model to interpret the observed room-temperature and low-pressure self-ignition.

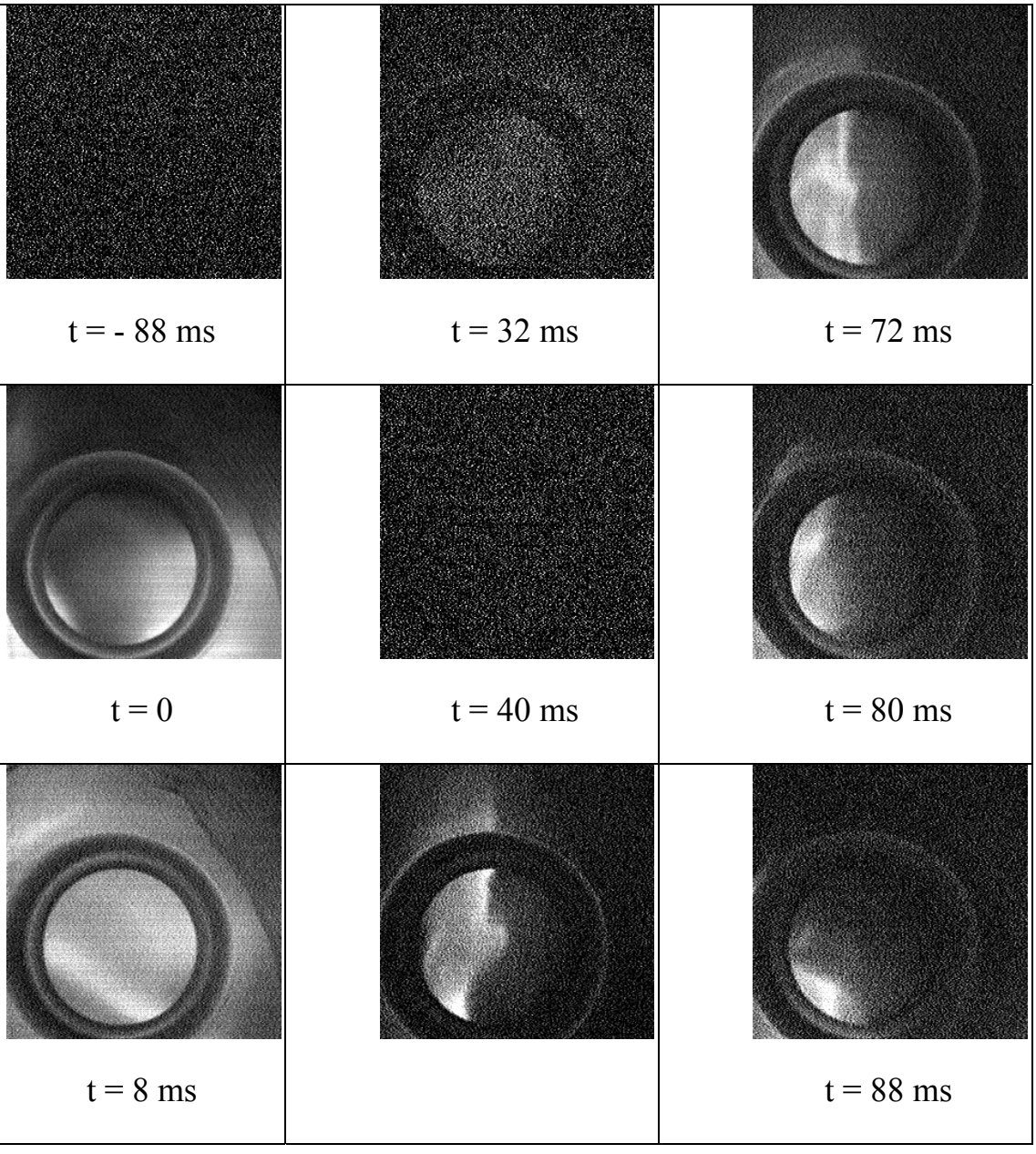

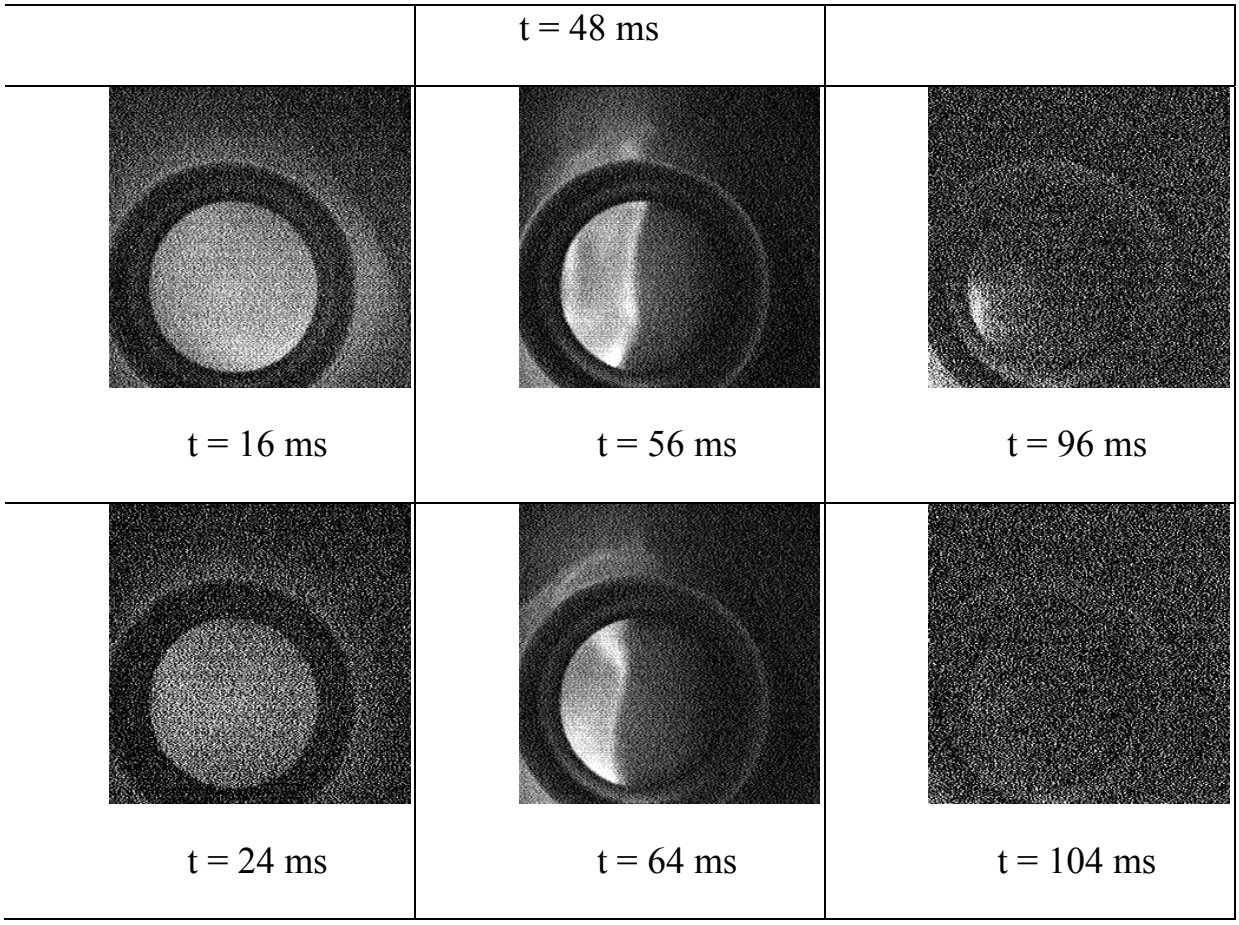

Figure 6. Hypergolic ignition observed when a jet of gaseous NTO enters into a volume occupied by gaseous MMH [Catoire, 2006].

A two-stage ignition occurs. Initially, a flame appears followed by its extinction. After some delay, a second flame appears. This two-step ignition is very interesting as it suggests that something happens as soon as the reactants come into contact showing that the interfaces probably play an important role both in the production of reactive species and in the production of heat. Very recently, Daimon et al. [Daimon, 2014] provide a detailed chemical kinetics model for pure gas phase N_2H_4/NTO hypergolic ignition. Zhang et al. [Zhang, 2015] studied theoretically the reaction of azido-N,N-dimethylethanamine (DMAZ) and pure nitric acid. Two important low-temperature reactions pathways were identified for DMAZ/HNO_3 ignition; one in the liquid phase and one in the gas phase. In the liquid phase, it was proton

transfer from the nitric acid to the amine nitrogen of DMAZ. In the gas phase, it was the reaction between DMAZ and NO_2. Similarly, Catoire et al. [Catoire, 2012] have discussed the role of isocyanic acid formed in the liquid phase on the kinetics of gas phase ignition.

To conclude, it appears that processes at interfaces may play a major role in sustaining hypergolic ignition. Both interface types, gas-gas and gas-liquid, need to be considered. For non-ionic liquid/liquid oxidant systems, reactions in the gas phase are probably of major importance, whereas for IL/liquid oxidant systems, the issue of which phases are important remains to be worked out and is further examined herein.

4. Chemical reaction dynamics in the gas phase

The types of reactions in the gas phase are generally well known and are not exhaustively presented here. Generally, only neutral species (molecules, radicals and atoms) are involved. Even if ions exist in the gas phase, they are much less numerous than neutral species and their kinetics role is generally negligible and therefore neglected in non-ionic liquid/oxidant systems. For NTO and WFNA as oxidants, NO_2 molecules react with gas phase molecules of the neat fuel or with product species either formed from liquid phase reactions or from the initial reaction between the fuel and NO_2. For ILs/oxidant systems, the existence of ions however must be discussed. If one assumes that the vapor phase from ILs plays a role, four possibilities exist. Above the liquid phase, ion pairs can exist, or separated ions can exist, or neutral pairs can exist, or finally separated neutrals can exist. Experimental findings and theoretical calculations are reported in the literature on this issue. It appears that ionic liquids have to be divided into two classes; protic ionic liquids and aprotic ionic liquids.

Protic Ionic Liquids

According to Earle and co-workers, for protic ionic liquids, an equilibrium exists between ionic and non-ionic species [Earle, 2006]:

$$BH^+_{(\ell)} + X^-_{(\ell)} \leftrightarrow B_{(\ell)} + HX_{(\ell)} \leftrightarrow B_{(g)} + HX_{(g)}$$

where (ℓ) represents the liquid phase and (g) represents the gas phase. Calculations on protic triazolium-based energetic ionic liquids show that the neutral pair is of lower energy than the ionic pair [Schmidt, 2005]. Separation of the species in the ion pair requires a significant amount of energy and therefore the ionic pair once formed will transfer one proton to form a neutral pair. This proton transfer is therefore fundamental for the decomposition of the triazolium-based ILs considered. However, Baranyai et al. did not observe the formation of species according to the proton transfer process, and therefore, they questioned this mechanism [Baranyai, 2004]. On the other hand, Zorn et al. deduced from their calculations on protic tetrazolium-based ionic liquids that when a cation is paired with an oxygen rich anion, an isolated gas phase ion pair was not generally found to be stable [Zorn, 2006]. In fact, a proton transfers barrierlessly from the cation to the anion to form a neutral pair. This result is also consistent with the experimental findings of Leal and co-workers, who reported that the gas phase above a protic ionic liquid is composed of separated neutral molecules [Leal, 2007].

Aprotic Ionic Liquids

Calculations carried out by Emel'yanenko et al. on the gas phase equilibrium:

$$\text{ion pair} \leftrightarrow \text{separated ions}$$

for 1-butyl-3-methylimidazolium dicyanamide indicate that dissociation of the ion pair is marginal [Emel'yanenko, 2007]. Experimental and theoretical works reported by Strasser

et al. suggest that the vapor pressure of an aprotic ionic liquid (1-ethyl-3-methylimidazolium bis(trifluoromethylsulfonyl)imide) is composed of isolated ion pairs [Strasser, 2007]. The formation of clusters of ion pairs was reported to be negligible. This conclusion is supported by another experimental work performed by Leal et al., who found that the gas phase is composed of only isolated ion pairs and that their experimental observations did not support the formation of ion clusters [Leal, 2007]. For aprotic ionic liquids, the only possible mechanism for volatilization, according to Earle et al., is as ion pairs, isolated or as clusters [Earle, 2006]. Armstrong et al. performed an analysis of the vapor pressure of 1-ethyl-3-methylimidazolium ethylsulfate by mass spectrometry [Armstrong, 2007]. They deduced from their experiments that the vapor pressure of these ionic liquids was due to ion pairs, although they did not observe directly these ion pairs because the ionized ion pair (formed in the ionization chamber of the mass spectrometer by electron bombardment) was unstable and, therefore, fragmentation occurred in their experiments. One other finding by Armstrong et al. is that clusters of ion pairs do not seem to form in the gas phase [Armstrong, 2007].

5. Gas diffusion in bulk liquids

Condensed phase concentration of a gaseous species is limited by its solubility in the liquid of interest. At equilibrium, the Henry's law, $k_h = c_i/p_i$, links partial pressure p_i of a species i to its liquid phase concentration c_i. Henry's constants k_h are available for many gases (H_2, He, Ne, etc.) in many solvents (alkanes, alcohols, etc.). However, Henry's law describes the steady state but for real reacting systems it is doubtful that this equilibrium is reached due to diffusion limitations. The diffusion inside the bulk is linked to the interfacial area which can be "natural" (planar interface between gas and liquid) or "forced" (as it is

probably the case when a droplet free falls into a pool). In both cases, the diffusion process can be expressed using a film model such as the Whitman model presented in Figure 7 for a reacting system. Furthermore, a competition between diffusion into the bulk and consumption in the interface may lead to smaller concentrations that are finally reached in the bulk. Thus it could well be a fact that the reaction phenomenon in the bulk is somehow negligible before ignition, i.e., everything happens in the interface and this finally leads to ignition.

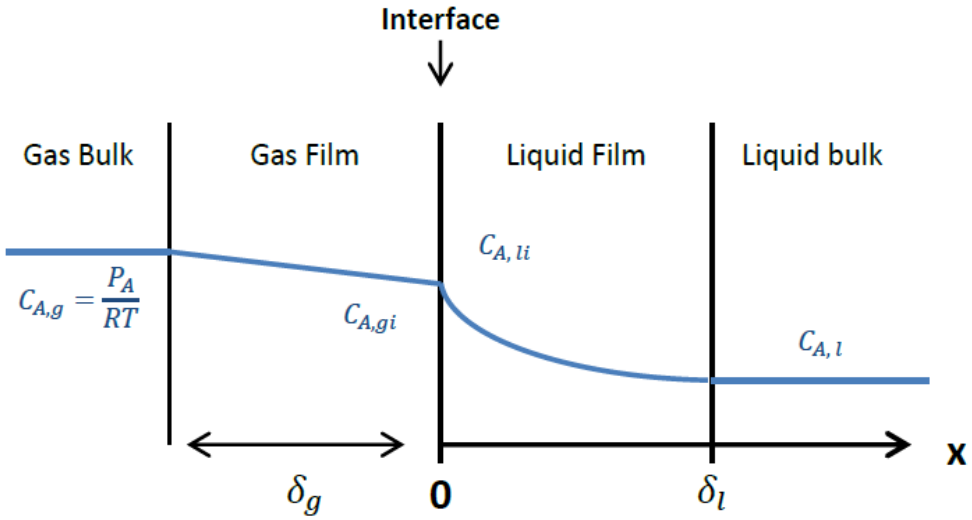

Figure 7. Whitman model for a reacting system consuming the species A in the liquid phase. P_A is the partial pressure of species *A*. *g*, *l* and *i* stand for gas, liquid and interface, respectively.

6. Chemical reaction dynamics in solution (in liquids)

For the problem at hand, it is essential to have an understanding of the nature of chemical reactions in solution. Much less is known about the reaction dynamics in liquids at

the microscopic level than about the dynamics of gas phase reactions. This statement [Schroeder, 1987] was valid 30 years ago and is most certainly valid today [Elles, 2006], and also because in recent decades, *ab initio* computations of gas phase thermochemistry and rate coefficients have become routine activities. Some concepts derived from gas phase studies are also valid for reactions in solution, but on the other hand, many characteristics of the dynamics in liquids are not important for the gas phase and therefore the liquid does not behave like a gas of high density [Schroeder, 1987]. For instance, solvent molecules can affect the motion of reactants in a minor to a profound manner [Elles, 2006]. The effects of a solvent on a reaction rate may be either chemical or physical. If the solvent molecules participate directly in the reaction mechanism, the effect is chemical. If the role of the solvent is merely to modify the interaction between reacting species, its effect may be termed physical. A reaction between two molecules in a solution/liquid can be thought as occurring in three well defined steps:

(1) diffusion of the molecules to each other

(2) the actual chemical transformation

(3) diffusion of the products away from each other

The first way in which a solvent medium can affect a reaction rate is via the modification of the activation energy by stabilization of the transition state as illustrated in Figure 8.

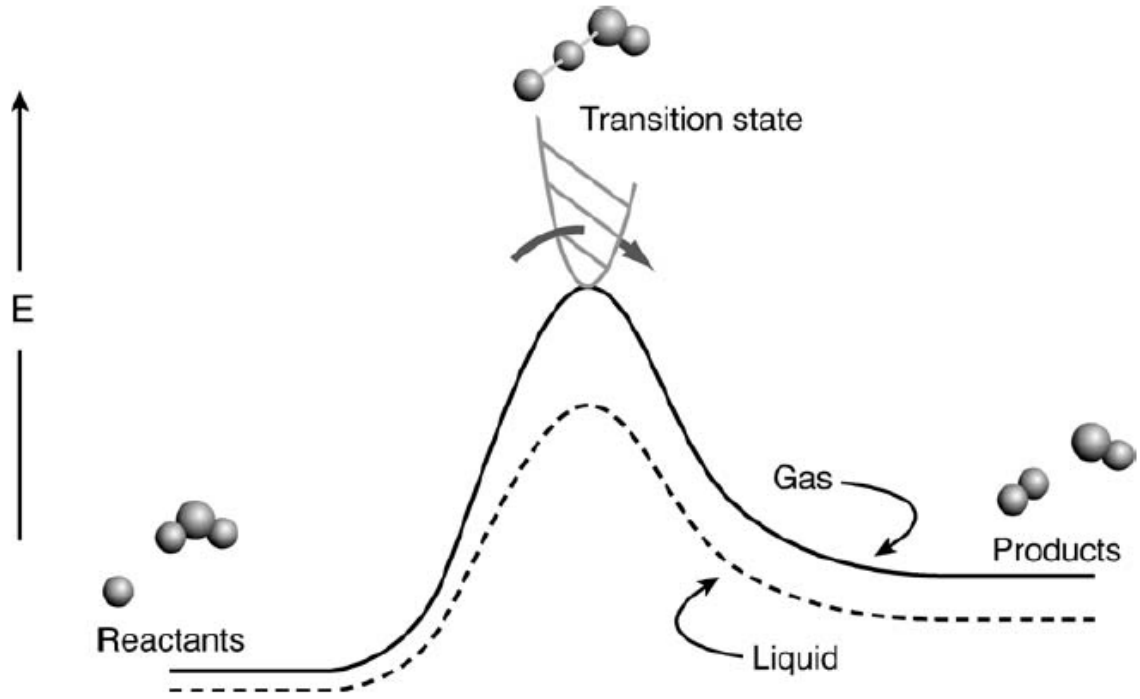

Figure 8. Energy diagram for a bimolecular reaction in the gas phase and in solution [Elles, 2006].

If activation energies are impacted, it means that both thermochemistry and kinetics are impacted as shown in Figure 9. Solvents can also play a role by initiating reactions, stabilizing intermediates (both ionic and radical), and moderating the collisions between molecules. In fact, the collision frequency is lower in solution than in the gas phase because solvent molecules get in the way, but the net effect is that the presence of a solvent often increases the rate of a reaction, especially the reaction rates of ions. Generally, solvents have only a small effect on reactions of neutral species.

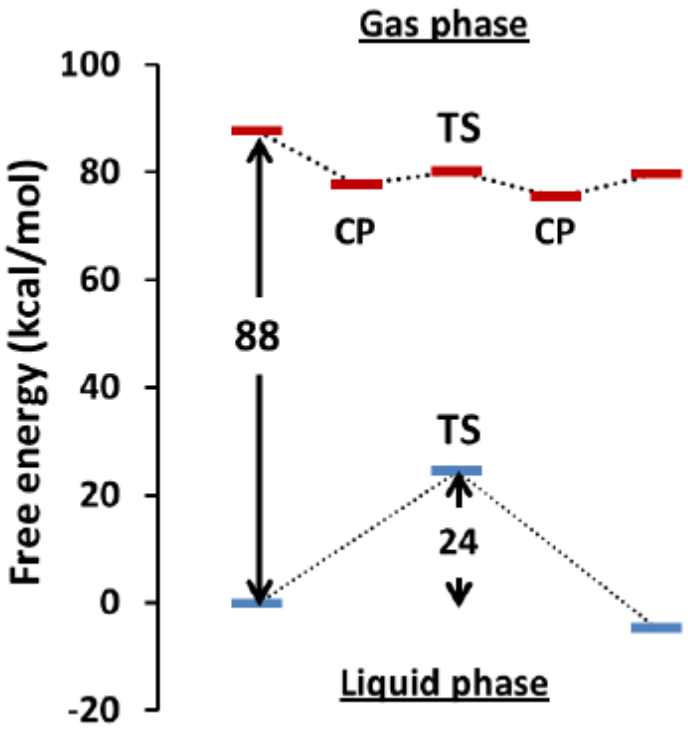

Figure 9. Energy changes for the reaction $Cl^- + CH_3Br \rightarrow CH_3Cl + Br^-$ in gas phase and in liquid phase (DMF). CP and TS stand for complex and transition state, respectively. Data are from Reichardt and Welton [Reichardt, 2011].

The impact of solvation on thermochemistry and kinetics has been discussed by Jalan et al. [Jalan, 2010] among others. To treat these issues, two approaches are possible. The first one deals with experimental measurements, which continues to be the preferred approach. The second one consists of applying solvent corrections to the gas phase data. This treatment is presented herein in sections (A) and (B) below.

(A) Solvent effects: impact on the thermochemistry

Corrections are illustrated by the thermodynamic cycle given in Figure 10. It includes individual corrections applied from a real gas mixture to a concentrated solute in solvent. Corrections can be divided into four main steps [Orozco, 2000]:

(1) ideal state corrections in which gases and liquids are "moved" from concentrated to diluted conditions

(2) cavity formation corrections

(3) Van der Waals corrections (also called dispersion-repulsion forces) and

(4) electrostatic contributions, which refer to the charge distribution in the solvent.

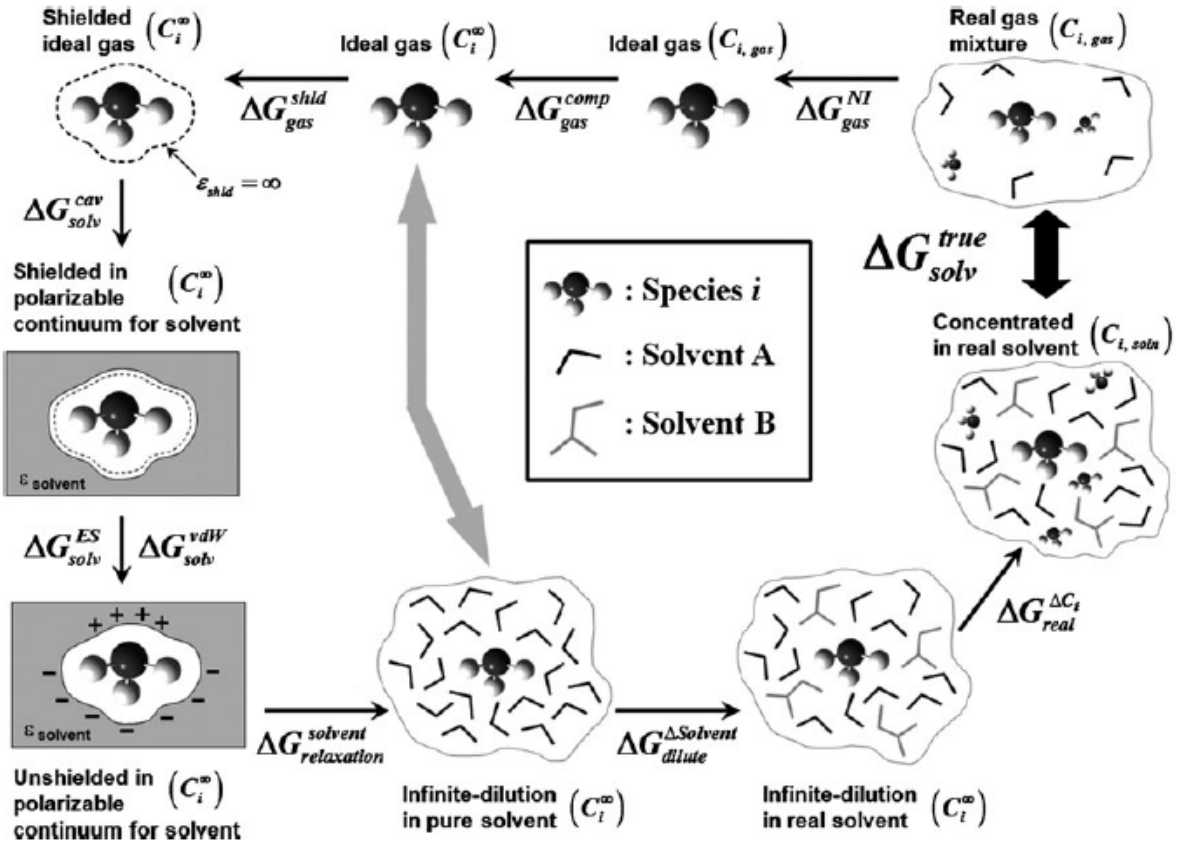

Figure 10. Thermodynamic cycle representing a solvation process. Grey arrows represent what is commonly computed; the free energy change between ideal gas to diluted solute in solvent. Diagram from Jalan et al. [Jalan, 2010].

The accuracy of the results obtained is indeed a function of each correction, which can be evaluated separately by using molecular modeling or corrected collectively by using semi-empirical methods. The accuracy of the methods depends on the description of the solute-solvent interactions in both semi-empirical methods with solute-solvent descriptors and in computational modeling methods using different solvent description theories. The level of description of solvation in molecular modeling is presented in Figure 11. These solvation models can be divided into two approaches. In the first one, solvent molecules surrounding solutes are represented explicitly (see Figures 11 a, b, and c). In the second one, a continuum model is used to model all (Figure 11f) or part of the solvent (Figures 11d and e).

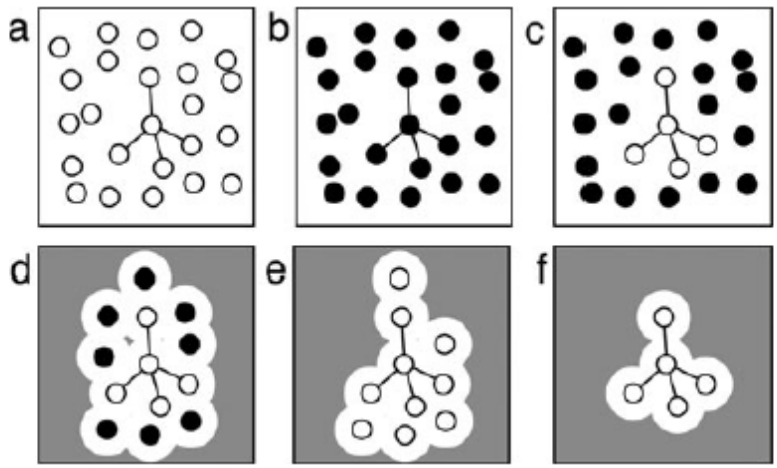

Figure 11. Solvent model illustration for discrete (a) to continuum models (f) [Jalan, 2010]. Grey represents continuum dielectric.

In these two approaches, molecules can be either described using quantum mechanics (QM) or molecular mechanics (MM). Evaluations of these methods and their accuracies are reported in Jalan et al. [Jalan, 2010]. As is usual in modeling studies, accuracy of results and computational costs need to be balanced. The number of electrons in the molecules that are

included in the model is the main limiting factor. For this reason, semi-empirical methods, like the LSER (linear solvation energy relation) method described hereafter, are still widely used. These methods require fewer parameters that are based on the physical properties of both the solute and solvent to obtain solvation corrections. Many solute/solvent pairs can be investigated and the solvation correction is obtained using a small set of equations.

However, only stable species parameters can be obtained experimentally and calculations are still required for radicals and other short lifetime species. The liquid phase thermochemistry can be calculated in two steps using the LSER method. The first one (Eq. 5), requires calculating G_{liq}, the liquid phase free energy of the species estimated by applying free energy of solvation correction ΔG_{solv}, to its gas phase free energy G_{gas}. ΔG_{solv} is obtained by using Eq. 6 and the partition coefficient $K_{vapor\text{-}solvent}$ of a given solute/solvent pair. The LSER method based on Abraham et al.'s models (Eq. 7) [Abraham, 2010] provides an estimation of this partition coefficient at 298 K. In Eq. 7, the first set is referring to solute descriptors (E, S, A, B, and L) and the second to solvent descriptors (c, e, s, a, b, and I). The next step is to calculate the enthalpy of solvation ΔH_{solv} at 298 K, using Mintz's model also based on Abraham et al.'s model just described (Eq. 8). With Mintz's model, the solute descriptors remain the same and the new solvent descriptors (c', a', b', e', s', and I') are obtained through another empirical correlation. It is then possible to obtain ΔS_{solv} according to $\Delta G = \Delta H - T\Delta S$. ΔG_{solv} can be expressed as a function of temperature following Eq. 9, wherein ΔH_{solv} and ΔS_{solv} are assumed to be temperature independent. These assumptions provide good agreement (with root mean square error of 0.5 kcal/mol) for many systems as presented by Jalan et al. [Jalan, 2013] with over 900 data points.

$$G_{liq} = G_{gas} + \Delta G_{solv} \quad \textit{Eq. 5}$$

$$\Delta G_{solv} = -RT \ln(K_{vapor-solvent}) \quad \textit{Eq. 6}$$

$$log\ K_{vapor-solvent} = c + eE + sS + aA + bB + IL \quad \textit{Eq. 7}$$

$$\Delta H_{solv}(298\ K) = c' + a'A + b'B + e'E + s'S + I'L \quad \textit{Eq. 8}$$

$$\Delta G_{solv}(T) = \Delta H_{solv}(298\ K) - T\ \Delta S_{solv}(298\ K) \quad \textit{Eq. 9}$$

In Eqs. 7 and 8, the sS and s'S terms correspond to the electrostatic interactions, the eE and e'E account for residual contributions from dipolarity/polarizability, the IL and I'L terms are related to the cavity formation and the dispersion interactions, aA, a'A and bB, b'B terms stand for the ability to donate protons and accept protons, respectively.

(B) Solvent effects: impact on the kinetics

Solvent effects may impact transition state theory (TST) calculations according to three different ways:

(1) by increasing or decreasing the activation energy E_a as presented in Figure 8. Many observations of kinetics solvent effects are presented in the literature where the rate constants may be increased or decreased compared to their gas phase values. Kinetics solvent effect is important for Menschutkin reactions as shown in Figure 12. It is relevant to reactions where ions are formed from neutral species. When the transition state (TS) is more polar than the reactants, the use of polar solvents stabilizes the TS and decreases the value of the activation energy E_a.

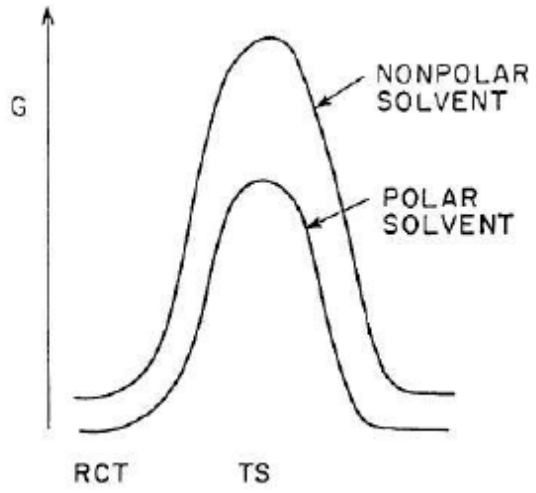

Figure 12. Solvent effect for Menschutkin reactions. A polar solvent stabilizes the transition state.

(2) by solvent friction.

As presented by Hynes [Hynes, 1985], solvents may impact the TS due to solvent friction. In case of competing reactions, any one reaction that is less impacted by solvent friction may become predominant compared to the situation observed in the gas phase.

(3) by local (at cage scale) diffusion-reaction competition.

Finally, solvents may greatly affect the mass transfer rates during reactions. The key feature is that the solvent slows down the diffusion rate of the reactants, which affects the collision rate. In addition, the solvent tends to trap the reactants in a solvent cage, which has a dramatic effect on the rate. Qualitative predictions of the effects of solvents on the rate are possible through Hughes-Ingold rules for ionic reactions [Masel, 2001]:

- if the TS for a reaction has a larger charge than the reactants do, then the rate of reaction will increase as the polarity of the solvent increases
- if the TS for a reaction has a smaller charge than the reactants, then the rate of reaction will decrease as the polarity of the solvent increases
- if the net charge remains the same, but the charge is dispersed, then there will be a small decrease in rate as the polarity of the solvent increases
- if the net charge remains the same, but the charge is localized, then there will be a small increase in rate as the polarity of the solvent increases

Semi-quantitative predictions are also possible through four key semi-quantitative models:

- the double-sphere model
- the single-sphere model
- Debye-Hückel theory
- Regular solution theory

Essential connections between chemical dynamics in gases and liquids are described by Elles and Crim [Elles, 2006]. Existing solution reaction types are: (a) radical recombinations, (b) precipitation reactions, (c) acid-base reactions, (d) electron transfer reactions, (e) oxidation-reduction or redox reactions, (f) inorganic exchange and substitution reactions, (g) organic exchange and substitution reactions, (h) elimination and decomposition reactions, (i) atom transfer reactions, (j) isomerization reactions, (k) charge transfers and isomerizations, and (l) tunneling reactions, which are further described below.

(a) Radical recombination reactions:

Radical recombination reactions are simple because they are generally barrierless. One example of such reactions is the iodine atom recombination:

$I + I \rightarrow I_2$.

(b) Precipitation reactions:

Precipitation reactions are reactions in which a precipitate is formed. All potential precipitates are considered by writing all possible combinations between cations and anions present in the liquids. Then solubility rules are used to determine which combinations are insoluble and able to precipitate.

(c) Acid-base reactions:

$H^+ + NH_3 \rightarrow NH_4^+$

(d) Electron transfer reactions:

$Fe^{2+} + Fe^{*3+} \rightarrow Fe^{3+} + Fe^{*2+}$ (isotopic exchange electron transfer reactions) where the asterisk denotes a radioactive isotope [Marcus, 1993].

(e) Oxidation-reduction or redox reactions:

$Fe^{2+} + Ce^{4+} \rightarrow Fe^{3+} + Ce^{3+}$ (electron transfer reactions between two different redox systems [Marcus, 1993])

(f) Inorganic exchange and substitution reactions:

$[Co(H_2O)_6]^{2+} + 4\ Cl^- \rightarrow [CoCl_4]^{2-} + 6\ H_2O$

(g) Organic exchange and substitution reactions:

These are the so called S_N1 and S_N2 reactions or nucleophilic substitution reations such as

$RBr + OH^- \rightarrow ROH + Br^-$

(h) Elimination and decomposition reactions:

(i) Atom transfer reactions:

Atom transfer reactions such as $AB + C \rightarrow A + BC$. It is the transfer of an atom or a group B from AB to form BC [Marcus, 1993].

$HI + Br \rightarrow I + HBr$

(j) Isomerization reactions:

(k) Charge transfers and isomerizations:

(l) Tunneling reactions:

7. Reactions in solution (in liquids) of excited states

Thomas provides a review on the reactions of excited states in liquids [Thomas, 1970]. The occurrence of excited states is not assessed in the liquid phase but excited OH radicals are certainly formed in the gas phase when H_2O_2 is used as an oxidant as well as excited NO_2 radicals are probably formed when the oxidant is NTO or WFNA. However, these reactions are probably marginal because usually species exist in their ground state. Excited state ion reactions are also observed such as:

$$O^+(^2D) + N_2 \rightarrow N_2^+ + O$$

8. Ion-molecule reactions

Finally, other ions (positive or negative) can also be formed upon heating due to exothermic reactions, independently from the ions initially present in the ILs. Various types of reactions are possible in the family of ion-molecule reactions in the gas phase [Ferguson, 1975]. Either chemically stable neutral gases or "unstable" neutrals such as atoms or free radicals in their ground state or excited species can participate. For instance, charge transfer reactions such as:

$$N_2^+ + O \rightarrow N_2 + O^+$$

generally compete with ion-atom interchange reaction such as:

$$N_2^+ + O \rightarrow NO^+ + N$$

or in associative-detachment reactions, where the energy to detach an electron is provided by the formation of a new bond between the reactants, may be fast such as in:

$$H^- + H \rightarrow H_2 + e^-$$

$$OH^- + H \rightarrow H_2O + e^-$$

and charge transfer reactions in doubly charged ions may be important such as in:

$$Ca^{2+} + NO \rightarrow Ca^{+} + NO^{+}$$

However, most ionic reactions occur in solutions or on solid catalysts. The major difference between a reaction in the gas phase and in solution is that the ionic species are stabilized by the presence of the solution resulting in ions that are much more stable than those in the gas phase. The ion is generally surrounded by a solvent cage. In order for a reaction to occur, one needs to first distort the ion cage so the reactants can get close enough to react. Because the exact nature of the distortion is unclear, it is at present, very difficult to accurately predict how much the value of the intrinsic barrier changes as a result of the solvent. Fortunately, the change in the intrinsic barrier does not really change the mechanism of a reaction. All of the same elementary reactions observed in the gas phase are also seen in solution phase. Olah et al. [Olah, 1997] showed that one can often predict mechanisms of reaction without considering the changes in the intrinsic barriers because of the solvent. It is just that the relative rates of reactions change in solution. Often, the intrinsic barriers to all of the reactions of a species are changed by a similar amount.

9. Chemical reactions at gas-liquid interfaces

As underlined by Benjamin, [Benjamin, 2015] chemical reactions that take place at the interface between a liquid and a second phase (vapor, another immiscible liquid or a solid) are of major interest. Ordinarily, the gas-liquid interface is generally considered to play the role of a "gateway" into the liquid, and is believed not to play the role of a reaction medium. However, it is shown in this report that the gas-liquid interface is a distinct region where often unique reactions can occur. Since Daimon et al. and Tanaka et al. have previously presented

evidence that a gas-liquid interface exists just before ignition, it may therefore be possible that reactions taking place in this region are the cause of ignition. It is clear that during the ignition delay, reactions occur in the liquid phase and that reactions occur in the gas phase, but the gas-liquid interface aspects have not been discussed at all in any of the previous papers on hypergolic ignition. It is therefore of interest to examine the processes at the gas-liquid interface, especially as to how gas phase species enter into the liquid phase and most importantly how they react. The contrary, the entering into the gas phase of a species formed in the liquid phase, is simple to understand; if the species formed is gaseous or has a high vapor pressure, it will be liberated as is into the gas phase.

a. Collision of a gas phase molecule with a liquid surface

Nathanson [Nathanson, 2004] has presented a review of experiments performed to clarify the role of the surface region during interfacial and bulk phase reactions. When a gas phase molecule collides with a liquid surface it can be sent back to the gas phase through inelastic scattering or it can be trapped, i.e., its kinetic energy is absorbed and it is able to bind to the surface. The probability of the trapping event depends on many parameters: the kinetic energy of the impinging molecule, the mass of this molecule and the ones at the surface, the liquid temperature, its surface tension, etc. Experiments have demonstrated that gas-liquid reactions can occur as soon as the gas phase molecule enters the interfacial region and this region is therefore a reaction medium.

b. Collision of a gas phase strong acid with a ionic liquid surface

Figure 13 illustrates the pathways observed after a gaseous acid, HX collides with the surface of a solution of deuterated sulfuric acid, D_2SO_4 in deuterated water, D_2O.

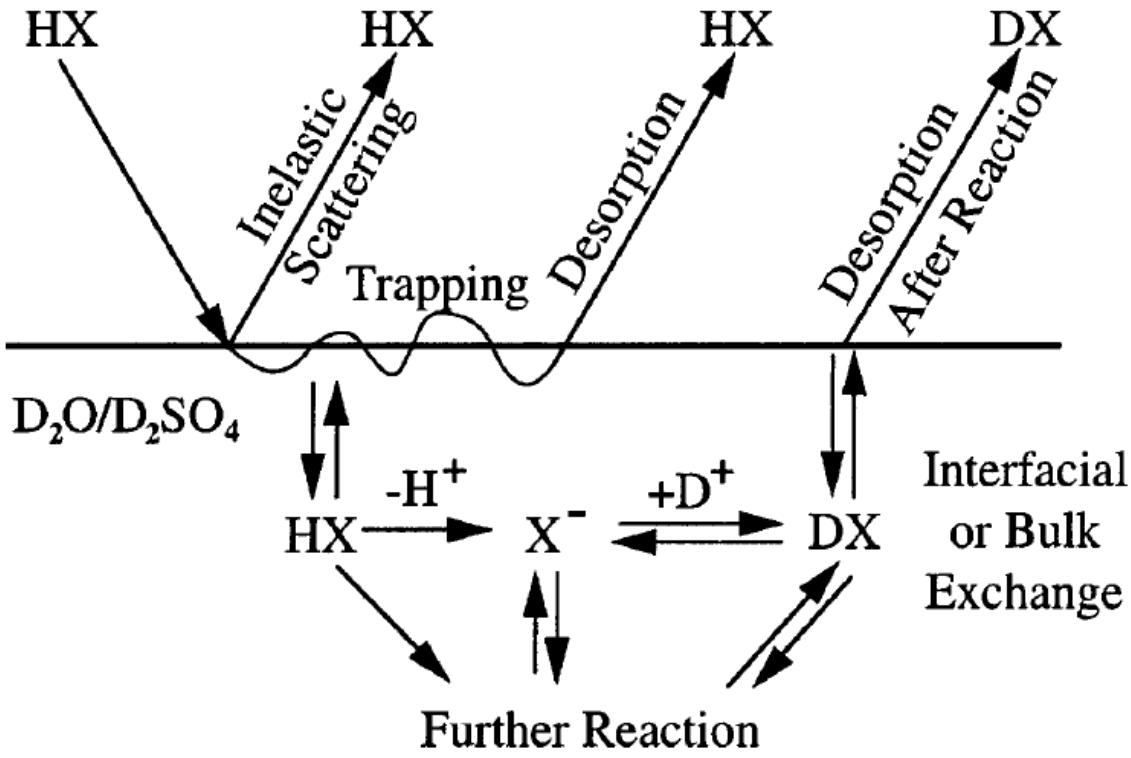

Figure 13. Observed pathways for an acidic molecule HX colliding into D_2O/D_2SO_4 [Nathanson, 2004].

The HX molecules are sent back to the gas phase, or some fraction are trapped and then desorb unchanged. The remaining molecules react in the acid interfacial region and/or in the acid bulk as intact HX or as H^+ and X^- after dissociation. These processes finally lead to the formation of DX molecules in the gas phase once desorbed from the liquid surface. If X is Cl, then the gas phase acid is HCl (see Figure 14). Further reactions cited in Figure 13 are unspecified.

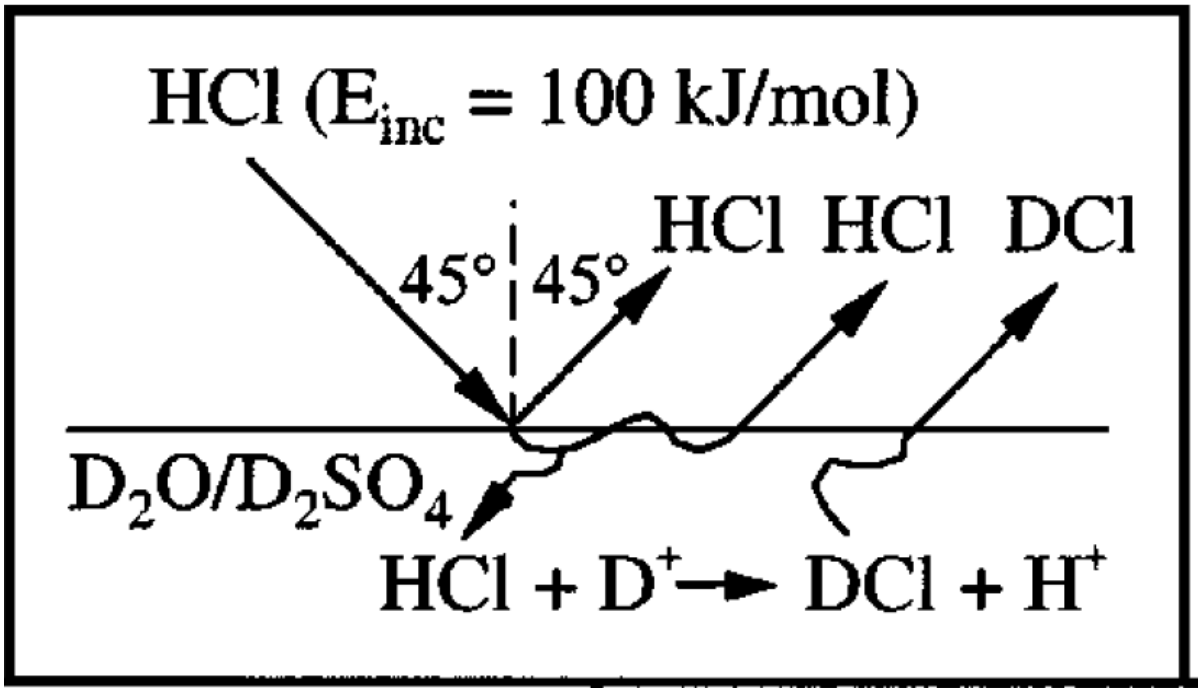

Figure 14. Observed pathways for HCl colliding into D_2O/D_2SO_4 [Nathanson, 2004].

HCl enters deuterated sulfuric acid solution in two steps: a fraction of the impinging molecules first thermalize upon collision with the surface and then a fraction of these trapped molecules enter the acid as intact HCl or as H^+ and Cl^-. Experiments show that at low incident energy, nearly all HCl molecules are trapped, but the amount of DCl formed indicates that only 1 in 9 HCl molecules dissociates in the interfacial or bulk regions of the acid and that the remaining 8 out of 9 trapped HCl molecules desorb from the acid before reacting. These results are particularly interesting for ILs/acid hypergolic systems if one considers that the impinging molecule is WFNA (a strong acid as is HCl) at the surface of an ionic liquid (as is the D_2O/D_2SO_4 solution). Most likely, HNO_3 will dissociate into H^+ and NO_3^- ions, which then react with the ions from the ionic liquid.

c. Collision of a gas phase strong acid with a neutral liquid surface

The interfacial and bulk reactions of a gas phase acid with a neutral liquid is also of interest for hypergolic ignition as is the case with the non-ionic liquid, MMH and HNO_3 system. Gas phase hydrogen chloride HCl and deuterated hydrogen chloride DCl have been studied with glycerol, a neutral liquid. Experiments show that most of the DCl molecules dissolve into glycerol. Of the DCl molecules that adsorb (or thermalize), 20% are found to desorb before dissolution and 7% of DCl are converted to HCl in the interfacial region and desorb before they can be dissolved into the bulk. It is presumed that the HCl molecules observed in the gas phase during DCl/liquid phase glycerol reaction are formed according to an ionic pathway described in Figure 15.

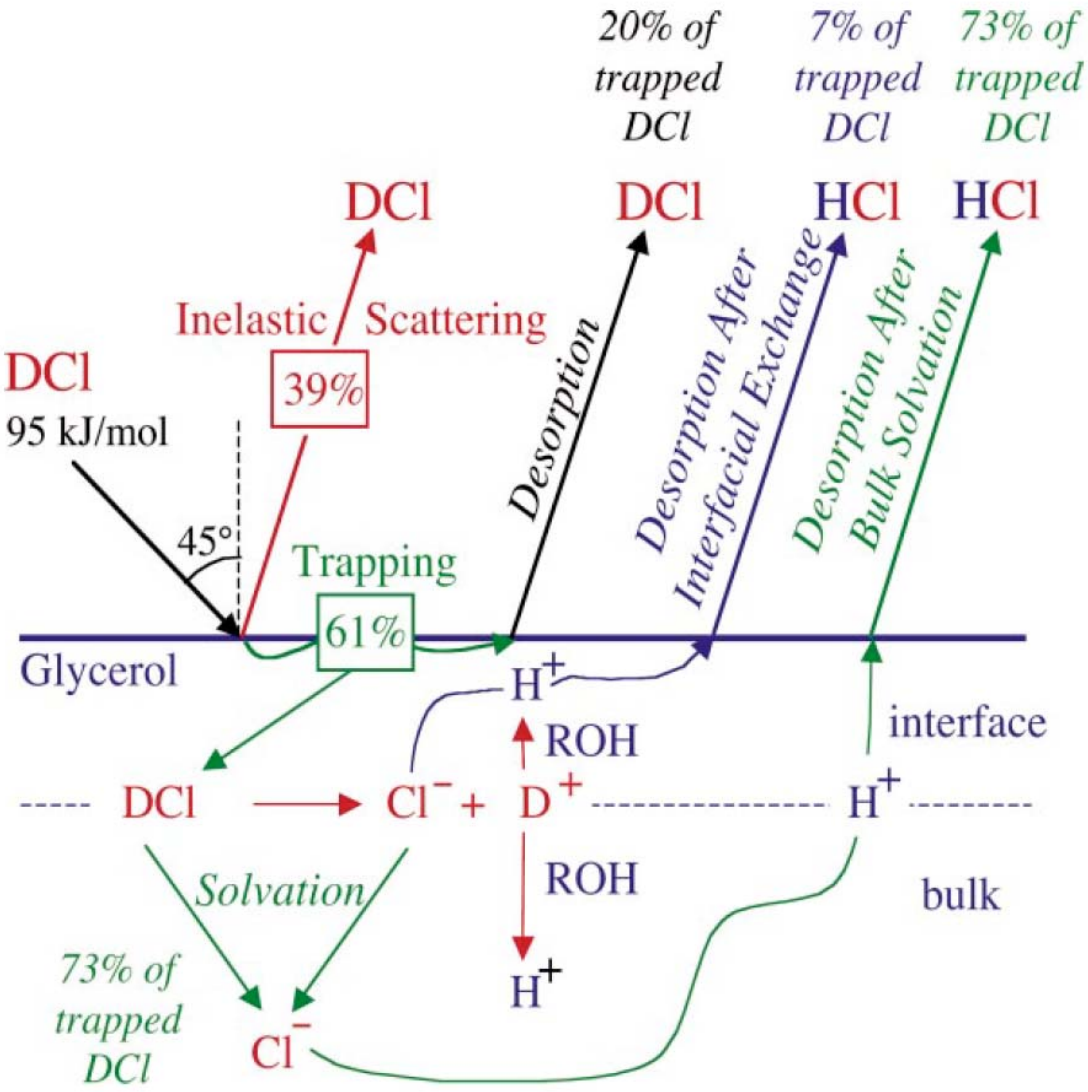

Figure 15. Scattering pathways for DCl collisions with glycerol. Only the partitioning between direct scattering and trapping depends on E_{inc} and t_{inc}. 7% of the trapped DCl undergoes rapid, near-interfacial exchange followed by immediate HCl desorption [Nathanson, 2004].

Another interesting feature is that HCl molecules dissolve exothermically in glycerol. Although this is neither surprising nor new (the same holds for the dissolution of HCl in water), it is however worthy to note because this will lead to an increase in the temperature of

the interfacial region, which can potentially play a beneficial role in the energy transfer process during ignition delay.

Molecular dynamics studies can provide information on the fate of the solvated solute at the water liquid-vapor interface. Figure 16 shows that the small Li^+ ion is able to keep its hydration shell intact when it is moved to the liquid-vapor interface. The ability of the larger I^- ion to do this is significantly diminished. In contrast with the case of charged particles, there is depletion in the number of water molecules in the first hydration shell for neutral atoms. The second hydration shell is significantly diminished as the solute is transferred to the interface [Benjamin, 2015]. Although not thoroughly discussed the transfer of ions from the liquid phase to the gas phase is probably possible.

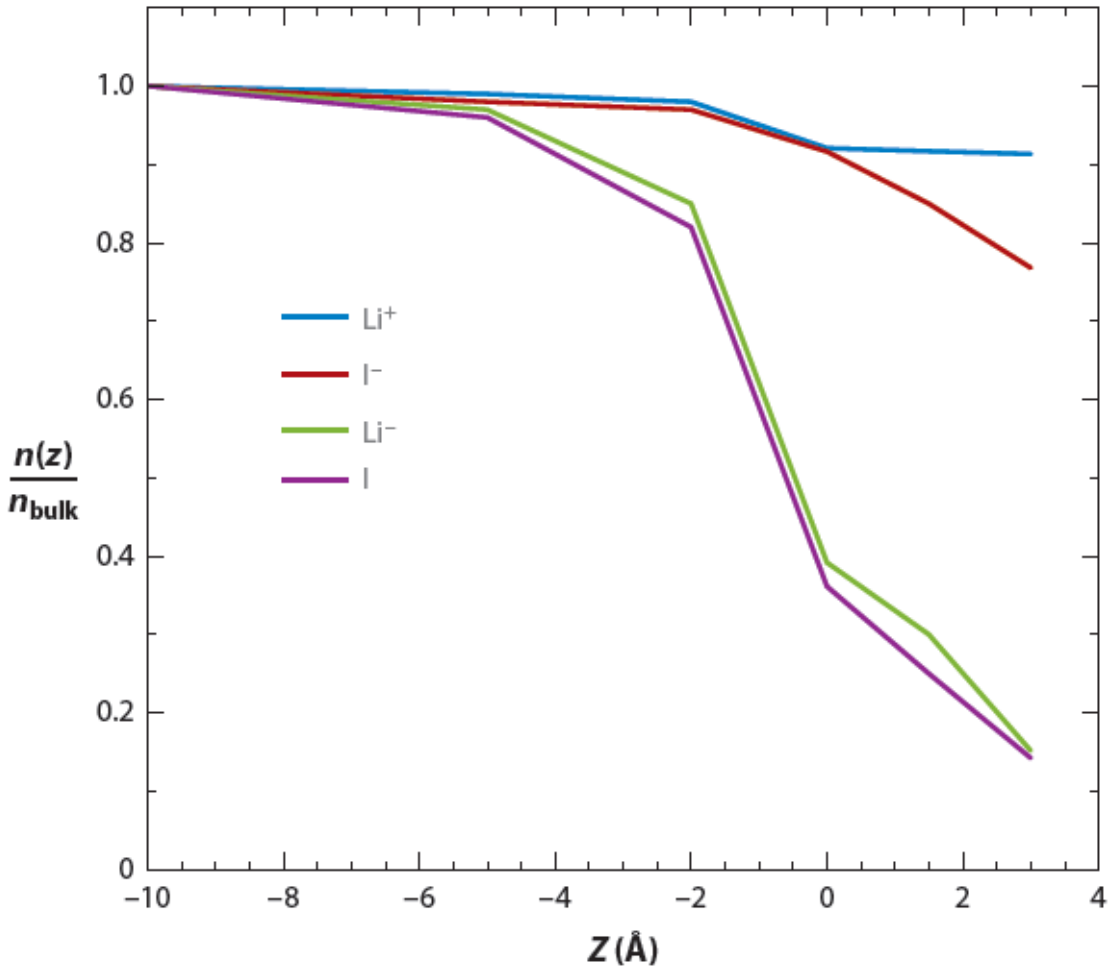

Figure 16. Relative (to the bulk) number of water molecules in the first solvation shell of different ions and neutral atoms as a function of the distance from the liquid-vapor interface. Z=0 is the location of the Gibbs dividing surface.

10. Reactions dynamics at liquid interfaces

The interface between a liquid and a second phase (vapor, another immiscible liquid, and solid) is a narrow and a few nanometer thick highly anisotropic region, where chemical reactions may take place. Benjamin presented a recent review on this topic [Benjamin, 2015], which was mostly devoted to the reactions in the interface of two immiscible electrolyte

solutions (IESs). For hypergolic ignition, which results from liquid-liquid contact, this interface exists even if the liquids are mixed in a turbulent manner. The characteristic molecular structure and dynamics of the liquid interfaces are expected to influence the rate of interfacial chemical reactions. This assumption is valid both for non-ionic/oxidant and ionic/oxidant hypergolic systems. In fact, the miscibility or immiscibility of the liquid reactants has not been thoroughly discussed in the frame of hypergolic systems. If both liquids are miscible, then the reactions will take place in the bulk. If they are immiscible, then reactions at the interface will be important. On the other hand, it could well be that these liquids are partially miscible depending on the nature of the reactants further increasing the complexity of the problem as discussed below.

a. Ion transfer (IT) reactions across a liquid-liquid interface between immiscible electrolyte solutions (IESs)

These transfers may be important because they could occur within ILs/oxidant systems when the oxidant is a strong acid such as nitric acid. The transfer of ions shares important characteristics with typical charge transfer reactions.

b. Electron transfer (ET) reactions at liquid-liquid interface

c. Interfacial S_N2 reactions

11. Interpretation of non-ionic/oxidant hypergolic ignition

This part is certainly of interest, but here the focused is on ILs/oxidant systems, and it will therefore be considered as future work.

12. Interpretation of IL/oxidant hypergolic ignition

In the case of nitric acid as the oxidant, the species that reacts either in the bulk IL or at the liquid-liquid interface or at the gas-liquid interface is either HNO_3 ($HONO_2$) or H^+ and NO_3^-. The IL reactant are presumably ions, which can be represented as $A^+ + B^-$. One task would be to ascertain what happens in the liquid phase and simultaneously in the gas phase by developing a detailed chemical kinetics.

13. Conclusions and future works

In part two, our literature investigation tends to show that reactions at gas-liquid and liquid-liquid interfaces may play an important role during hypergolic ignition (see Figure 17).

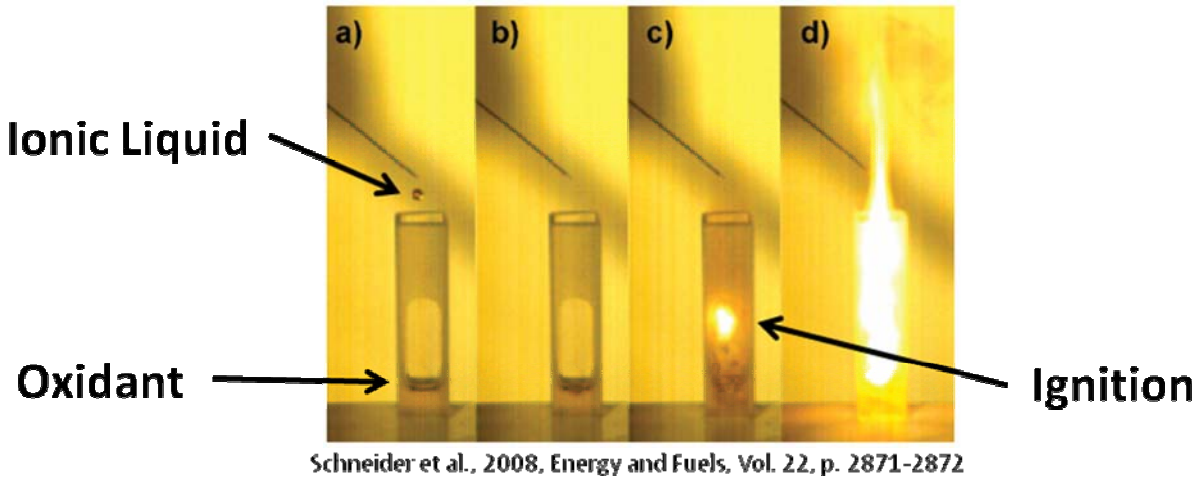

Figure 17. Visualization of IL/oxidant reactivity showing that the interface plays a major role in hypergolic ignition.

The effect of solvation on thermochemistry and on kinetics was examined. A detailed chemical kinetics model both in the liquid phase and in the gas phase to explain hypergolic ignition remains to be defined.

References

[Armstrong, 2007] J.P. Armstrong, Phys. Chem. Chem. Phys. 9 (2007) 982-990.

[Baranyai, 2004] K.J. Baranyai, Aus. J. Chem. 57 (2004) 145-147.

[Benjamin, 2015] I. Benjamin, Annual Review of Physical Chemistry 66 (2015) 165-188.

[Catoire, 2004] L. Catoire, J. Propulsion and Power 20 (2004) 87-92.

[Catoire, 2006] L. Catoire, Journal of Propulsion and Power 22 (2006) 120-126.

[Catoire, 2012] L. Catoire, Combustion and Flame 159 (2012) 1759-1768.

[Daimon, 1991] W. Daimon, Journal of propulsion 7 (1991) 946-952.

[Daimon, 2014] Y. Daimon, Journal of Propulsion and Power 30 (2014) 707-716.

[Emel'Yanenko, 2007] V.N. Emel'Yanenko, J. Am. Chem. Soc. 129 (2007) 3930-3937.

[Earle, 2006] M.J. Earle, Nature, 439 (2006) 831-834.

[Elles, 2006] C.G. Elles, Annual Review of Physical Chemistry 57 (2006) 273-302.

[Ferguson, 1975] E.E. Ferguson, Annual Review of Physical Chemistry 26 (1975) 17-38.

[Hynes, 1985] J.T. Hynes, Annual Review of Physical Chemistry 36 (1985) 573-597.

[Jalan, 2010] A. Jalan, Annual Reports Section "C" (Physical Chemistry) 106 (2010) 211-258.

[Jalan, 2013] A. Jalan, J. Phys. Chem. B 117 (2013) 2955-2970.

[Leal, 2007] J.P. Leal, J. Phys. Chem. A 111 (2007) 6176-6182.

[Livingston, 1955] R. Livingston, Annual Review of Physical Chemistry 6 (1955) 281-302.

[Masel, 2001] R.I. Masel, Chemical Kinetics and Catalysis, WILEY-INTERSCIENCE, city?, 2001.

[Nathanson, 2004] G.M. Nathanson, Annual Review of Physical Chemistry 55 (2004) 231-255.

[Olah, 1997] G. Olah, J. Am. Chem. Soc. 119 (1997) 8035-8042.

[Orozco, 2000] M. Orozco, Chemical Reviews 100 (2000) 4187-4226.

[Reichardt, 2011] C. Reichardt, Solvents and solvent effects in organic chemistry, Fourth edition, WILEY-VCH, Weinheim, 2011.

[Schmidt, 2005] M.W. Schmidt J. Phys. Chem. A 109 (2005) 7285-7295.

[Schneider, 2008] S. Schneider, Energy and Fuels 22 (2008) 2871-2872.

[Schroeder, 1987] J. Schroeder, Annual Review of Physical Chemistry 38 (1987) 163-190.

[Strasser, 2007] D. Strasser, J. Phys. Chem. A 111(2007) 3191-3195.

[Tanaka, 1985] M. Tanaka, Journal of propulsion 1 (1985) 314-316.

[Thomas, 1970] J.K. Thomas, Annual Review of Physical Chemistry 21 (1970) 17-38.

[Zhang, 2015] P. Zhang, Combustion and Flame 162 (2015) 237-248.

[Zorn, 2006] D.D. Zorn, J. Phys. Chem. B 110 (2006) 11110-11119.

Part three:

DETAILED CHEMICAL KINETIC MODELS FOR HYPERGOLIC IGNITION OF ILs BASED SYSTEMS

Table of Contents

List of Figures

1. Introduction

In the frame for searching new hypergolic (auto-igniting) propellant systems, it is necessary to discuss their reactions in both the liquid and gas phases. In practical hypergolic applications, propellant fuels and oxidants are liquids and upon contact, reactions occur in the liquid phase and also in the gas phase above the liquids. One point which seems clear is that ignition occurs in the gas phase even if the reactants come into contact as liquids. The issue of interest is related to the understanding of the qualitative and quantitative compositions of both phases when ignition occurs. In the frame of part two, it appears that the chemical reaction dynamics for liquid hydrazines/ liquid NTO (or liquid HNO3) hypergolic ignition is somehow elucidated, even if some points remain to be worked out or discussed.

Daimon et al. [Daimon, 1984], Tanaka et al. [Tanaka, 1985], and Daimon et al. [Daimon, 1991] observed a N_2H_4 droplet falling into a NTO pool (see Figure 1) and a NTO droplet falling into a N_2H_4 pool (see Figure 2). In both cases, they found that a layer of NTO was vaporized upon contact. Their interpretations of the visualizations given in Figures 1 and 2 are reported in Figures 3 and 4, respectively. In the first case, ignition is supposed to be due to gas-gas reactions at the interface of the two liquids whereas in the second case, NTO vapor

penetrates into the liquid hydrazine and, although not evoked explicitly by the authors, however, a gas-liquid interface is formed.

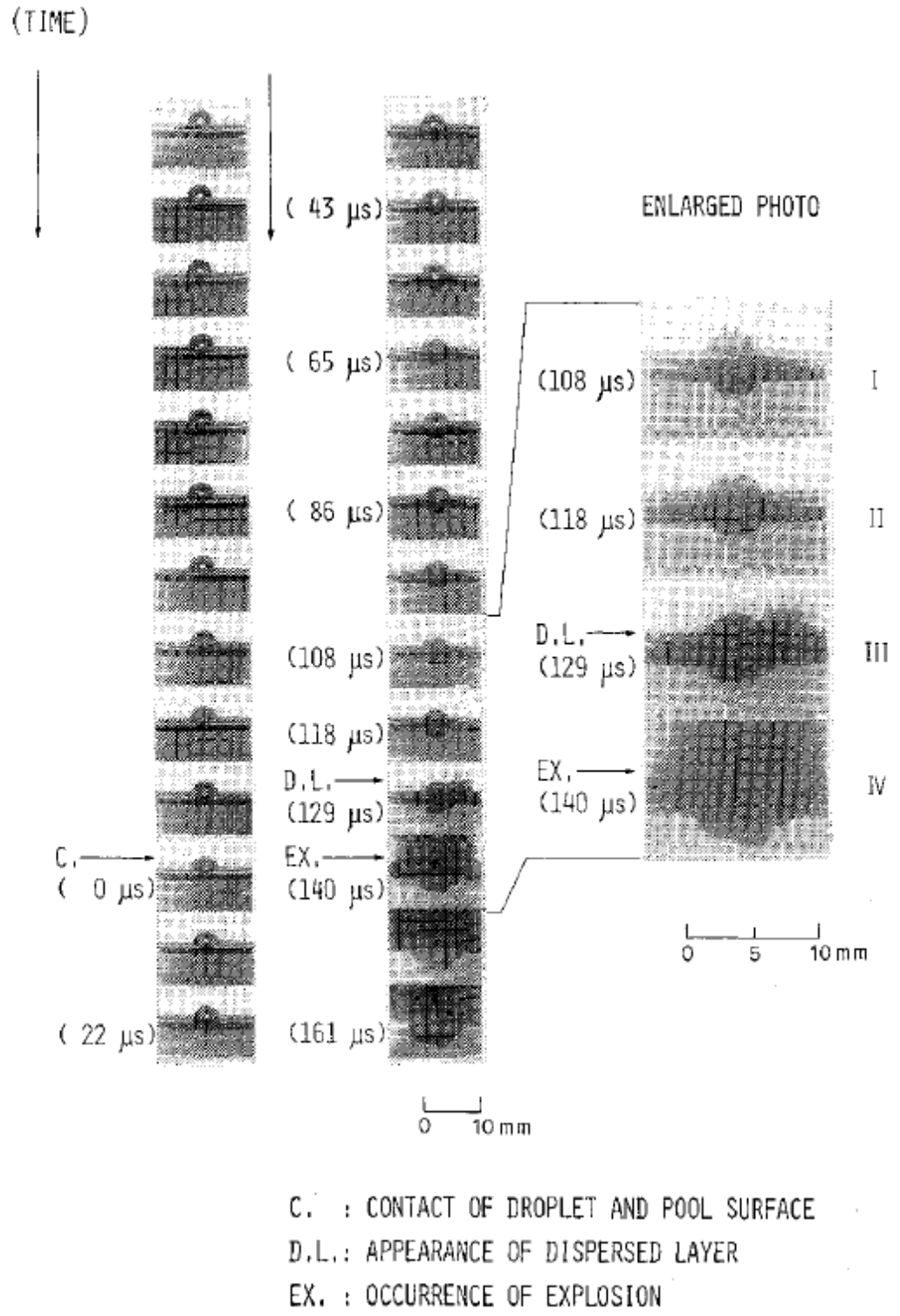

Figure 1. High speed motion pictures (92900 frames per second) of the contact of a N_2H_4 droplet falling into a NTO pool.

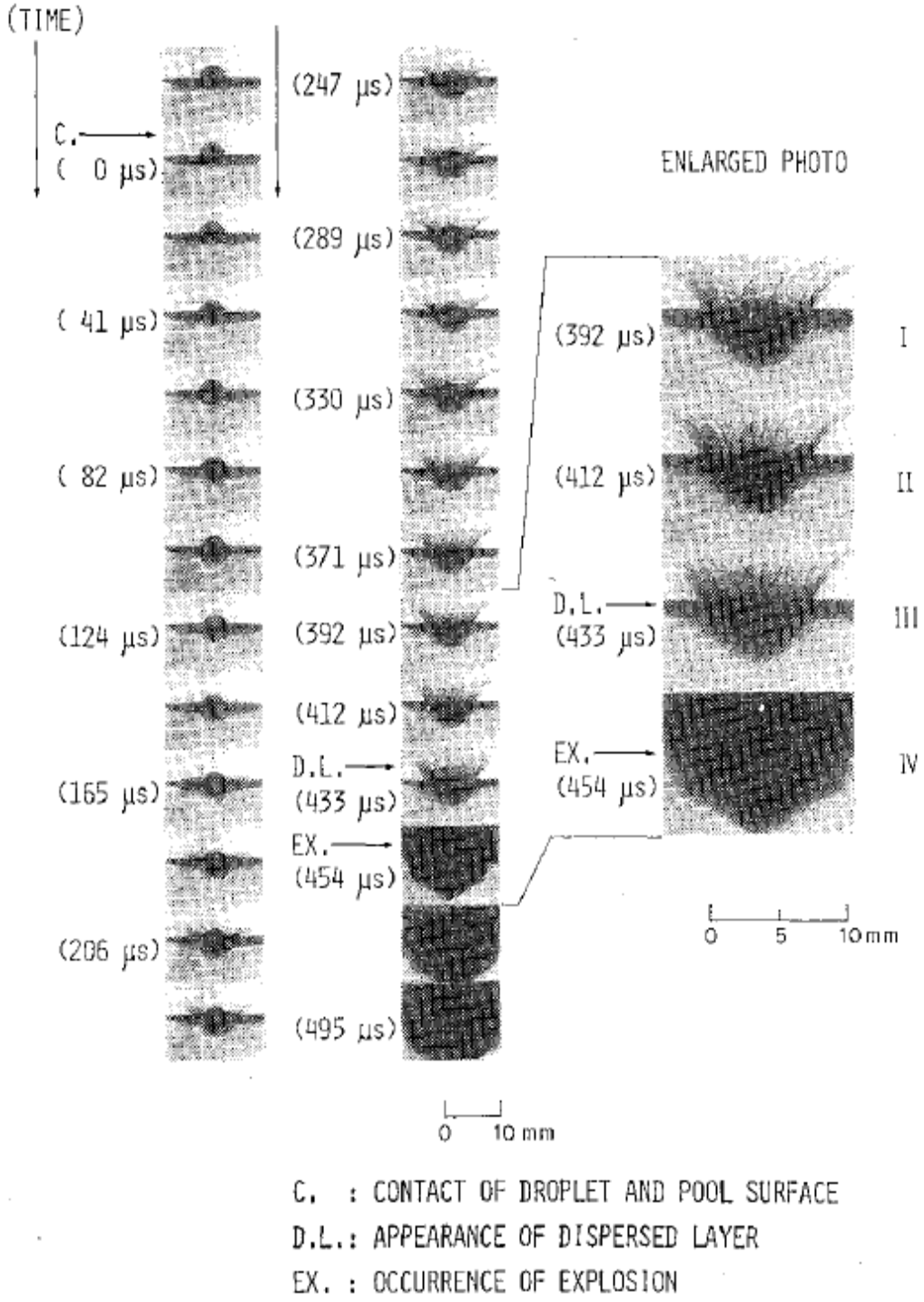

Figure 2. High speed motion pictures (48500 frames per second) of the contact of a NTO droplet falling into a hydrazine pool.

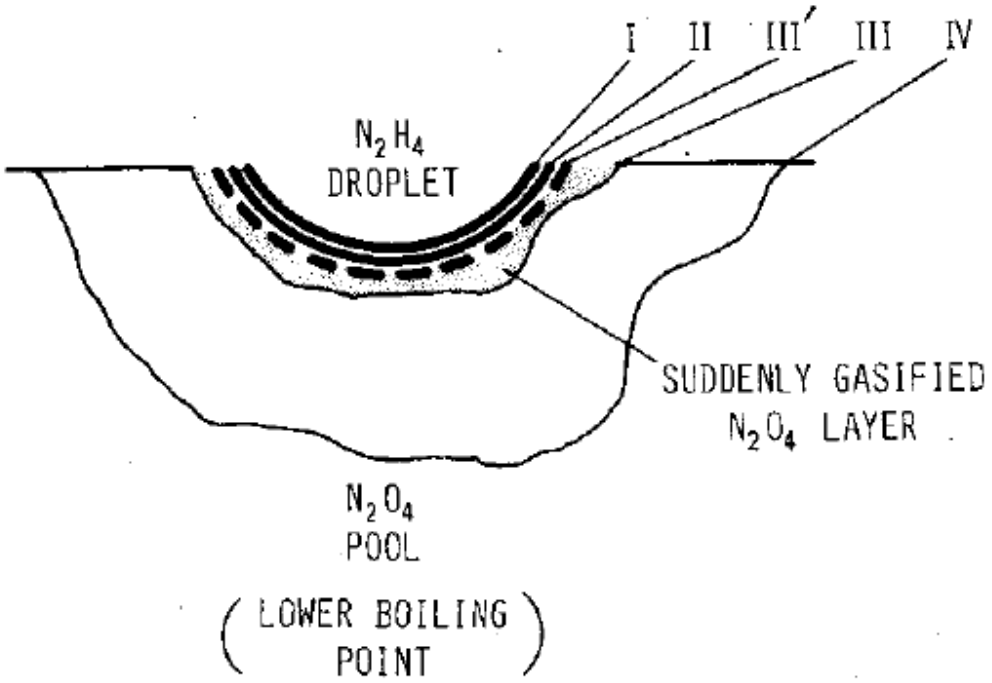

Figure 3. Interpretation of Tanaka et al. [Tanaka, 1985] to explain hypergolic ignition when a droplet of hydrazine is falling into a pool of liquid NTO.

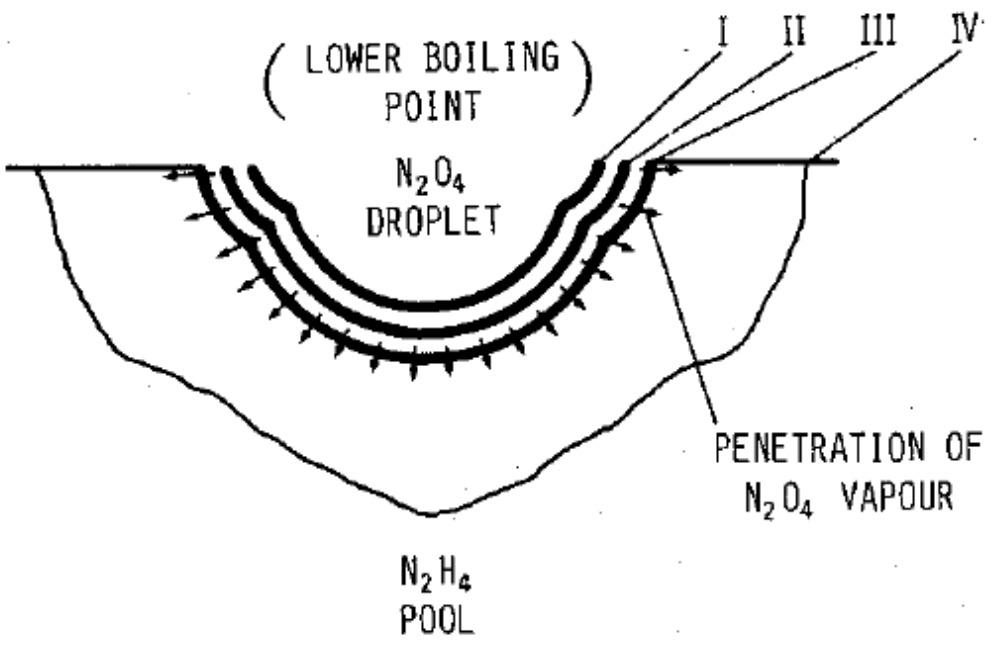

Figure 4. Interpretation of Tanaka et al. [Tanaka, 1985] to explain hypergolic ignition when a droplet of NTO is falling into a pool of liquid hydrazine.

For N_2H_4 and its methylated derivatives MMH and UDMH (unsymmetrical dimethyl hydrazine) and for two oxidizers NTO and FNA (fuming nitric acid) it is reported that the explosion phenomena observed can be classified into three categories [Daimon, 1991]:

- In the case of hydrazine/NTO, sudden gasification of a superheated liquid layer formed at the boundary of the two liquids occurs spontaneously and a detonation-like reaction proceeds in the reactive mixture produced.

- In the cases of MMH/NTO and UDMH/NTO, sudden gasification is caused by the shock from a local ignition source and a turbulent-combustion reaction proceeds in the reactive mixture produced.

- In the cases of hydrazine type fuels/FNA, sudden gasification occurs spontaneously as in the case of hydrazine/NTO, but it is not augmented by a chemical reaction and in these cases the observed explosion is weak.

In all these cases, the vapor layer, which is formed between the reactive fuel droplet and the liquid pool, plays an important role for the occurrence of the explosion. The composition of this layer (pure oxidant, pure fuel or mixture of both) is not clearly discussed and all these studies do not identify unambiguously the chemical cause of ignition or explosion. In the previous report item 2, the chemical dynamics and kinetics in the gas phase, in the liquid phase, at the gas-liquid interface, and at the liquid-liquid interface have been examined to get a deeper understanding of the hypergolic ignition phenomenon. The pure gas phase chemical dynamics and kinetics are not further examined here because this reactivity (or these reactivities) can be considered as sufficiently well known even if this statement is somehow contestable. More interesting, if one considers the above experimental evidences and interpretations, the chemical dynamics and kinetics at gas-liquid interface are certainly important. As underlined by Benjamin, [Benjamin, 2015] chemical reactions that take place at the interface between a liquid and a second phase (vapor, another immiscible liquid or a solid) are of major interest. Ordinarily, the gas-liquid interface is generally considered to play the role of a "gateway" into the liquid, and is believed not to play the role of a reaction medium. However, part two showed that the gas-liquid interface is a distinct region where often unique reactions can occur. Since Daimon et al. and Tanaka et al. have previously presented evidence that a gas-liquid interface exists just before ignition, it may therefore be possible that reactions taking place in this region are the cause of ignition.

Nathanson [Nathanson, 2004] has presented a review of experiments performed to clarify the role of the surface region during interfacial and bulk phase reactions. When a gas phase molecule collides with a liquid surface it can be sent back to the gas phase through

inelastic scattering or it can be trapped, i.e., its kinetic energy is absorbed and it is able to bind to the surface. The probability of the trapping event depends on many parameters: the kinetic energy of the impinging molecule, the mass of this molecule and the ones at the surface, the liquid temperature, its surface tension, etc. Experiments have demonstrated that gas-liquid reactions can occur as soon as the gas phase molecule enters the interfacial region and this region is therefore a reaction medium. The present work is devoted to the replacement of hydrazines by ionic liquids (ILs) and therefore the interaction of gas-phase molecule with a ionic liquid is of great interest. Part two emphasizes experimental results devoted to the interaction of a strong acidic molecule represented as HX with a ionic liquid in fact deuterated sulfuric acid D_2SO_4 diluted in deuterated water D_2O. This scenario can be representative of what happens when a liquid oxidant (such as NTO or nitric acid) droplet collides with a liquid pool or droplet of ILs. It is tenable that gaseous NTO or nitric acid is formed upon collision and enter the liquid according to reaction scheme described in Fig. 5 which illustrates the pathways observed after a gaseous acid, HX collides with the surface of a solution of deuterated sulfuric acid, D_2SO_4 in deuterated water, D_2O.

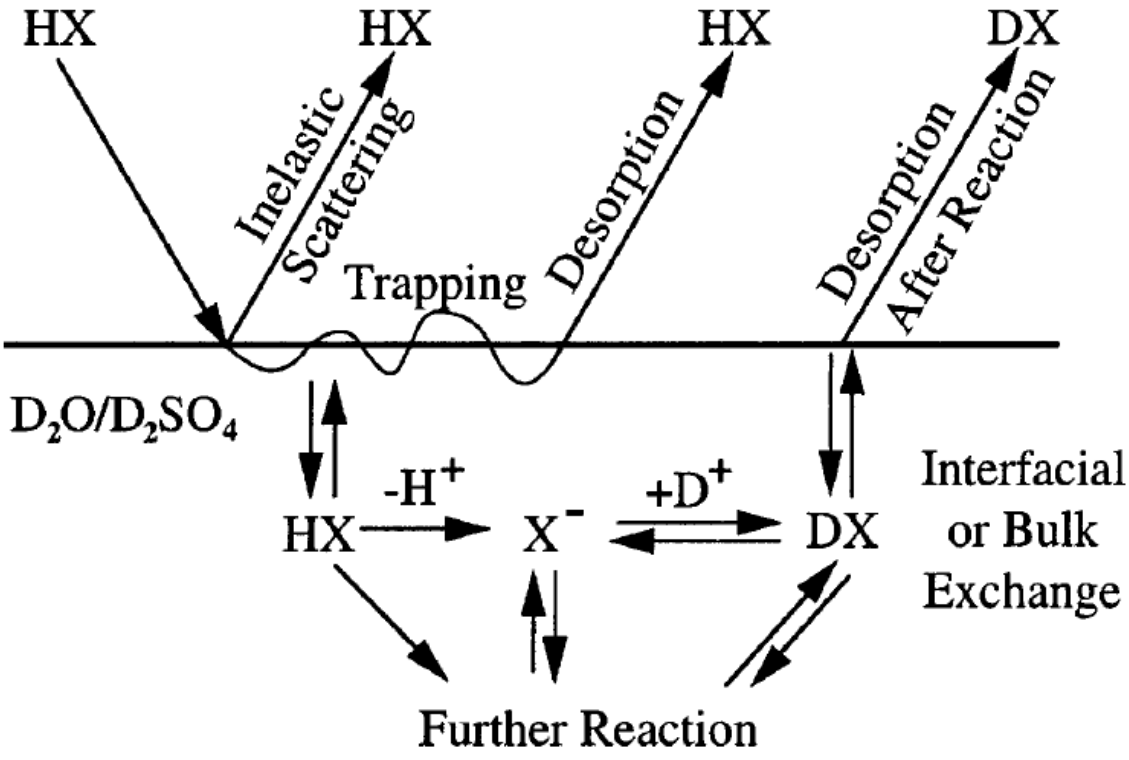

Figure 5. Observed pathways for an acidic molecule HX colliding into D_2O/D_2SO_4 [Nathanson, 2004].

The HX molecules are sent back to the gas phase, or some fraction are trapped and then desorb unchanged. The remaining molecules react in the acid interfacial region and/or in the acid bulk as intact HX or as H^+ and X^- after dissociation. These processes finally lead to the formation of DX molecules in the gas phase once desorbed from the liquid surface. If X is Cl, then the gas phase acid is HCl (see Figure 6). Further reactions cited in Figure 5 are unspecified.

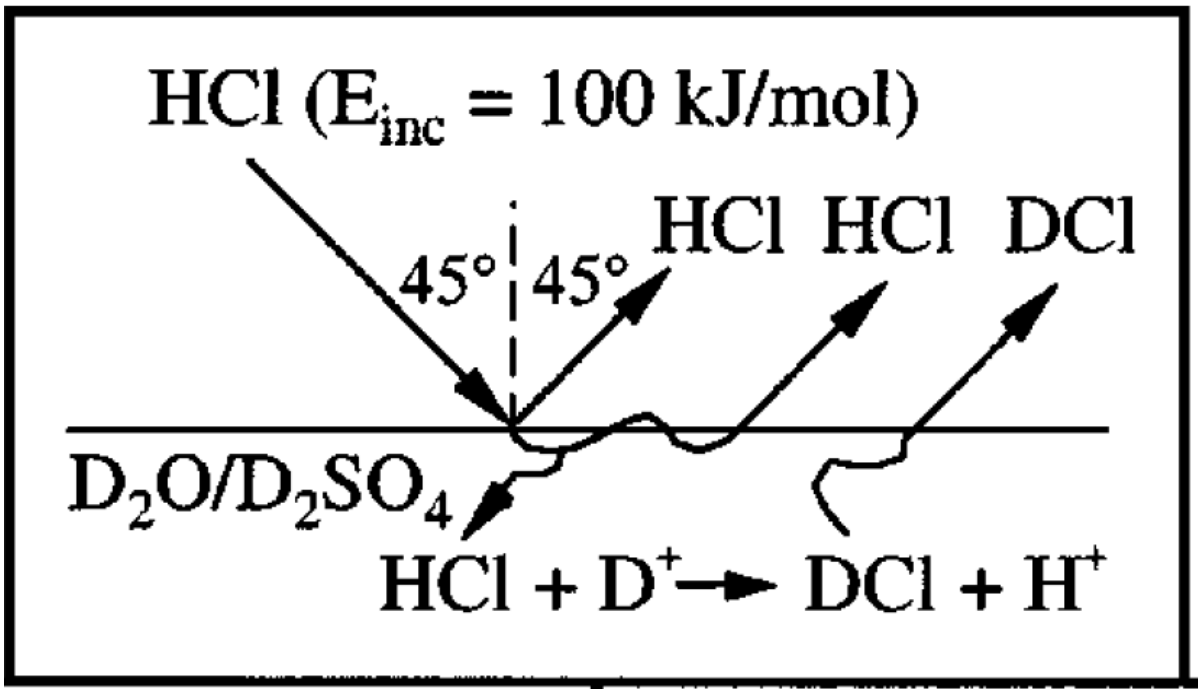

Figure 6. Observed pathways for HCl colliding into D_2O/D_2SO_4 [Nathanson, 2004].

HCl enters deuterated sulfuric acid solution in two steps: a fraction of the impinging molecules first thermalize upon collision with the surface and then a fraction of these trapped molecules enter the acid as intact HCl or as H^+ and Cl^-. Experiments show that at low incident energy, nearly all HCl molecules are trapped, but the amount of DCl formed indicates that only 1 in 9 HCl molecules dissociates in the interfacial or bulk regions of the acid and that the remaining 8 out of 9 trapped HCl molecules desorb from the acid without reacting. These results are particularly interesting for ILs/acid hypergolic systems if one considers that the impinging molecule is WFNA (a strong acid as is HCl) at the surface of an ionic liquid (as is the D_2O/D_2SO_4 solution). Most likely, HNO_3 will dissociate into H^+ and NO_3^- ions, which then react with the ions from the ionic liquid but HNO_3 can also react as $HONO_2$ molecule in its neutral form. In that case nitric acid will be present, in the liquid layer at the surface, as H+ and NO_3^- ions and as $HONO_2$ neutral molecule whereas the ionic liquid

itself is present in the layer as A^+ and B^- ions (without considering further separately protic and aprotic ILs). Therefore it is possible to propose a general chemical detailed kinetic scheme in this layer. For this purpose, it remains to examine existing reactions between ions in the liquid state and reactions between ions and neutrals in the liquid state.

2. Interpretation of IL/oxidant hypergolic ignition: detailed chemical kinetic model in liquid phase

Based on all the above features and interpretations or conclusions, in the case of nitric acid as the oxidant, the species that reacts either in the bulk IL or at the liquid-liquid Il/nitric acid interface or at the gas(nitric acid)/IL interface is either neutral HNO_3 ($HONO_2$) or H^+ and NO_3^-. The IL reactants are ions, which are abbreviated hereafter as A^+ and B^-. Therefore the reactants for all these systems, whatever their physical states, are $HONO_2$ (hereafter abbreviated as HNO_3), H^+, NO_3^-, A^+ and B^-. Reactions between $HONO_2$ and H^+ and reactions between $HONO_2$ and NO_3^- can be considered as marginal, even if they exist. For completeness, these reactions are considered here. This leads to the proposal of the following detailed chemical kinetic scheme.

Reactions between nitric acid and H^+

$HONO_2 + H^+ \rightarrow H_2 + NO_3^+$

$HONO_2 + H^+ \rightarrow H_2+ + NO_3^\bullet$

$HONO_2 + H^+ \rightarrow H_2O + NO_2^+$

$HONO_2 + H^+ \rightarrow H_2O^+ + NO_2^\bullet$

However, none of these reactions seem to be realistic. Species such as NO_3^+, for instance, have never been observed in the liquid phase as well as H_2^+ for instance.

Reactions between nitric acid and NO_3^-

$HONO_2 + NO_3^- \rightarrow HONO_2 + NO_3^-$

$HONO_2 + NO_3^- \rightarrow HOONO_2 + NO_2^-$

$HONO_2 + NO_3^- \rightarrow O_2NONO_2\ (N_2O_5?) + OH^-$

In this list, only the probable reactions are reported, i.e. reactions forming stable ions such as NO_3^-, OH^- and molecules. The first reaction will not be reported in the detailed chemical kinetic model because reactants and products are the same. Concerning the two remaining reactions, existence of N_2O_5 is assessed. Interestingly, the second reaction forms H-O-O-NO_2 a species belonging to the chemical family of peroxides containing O-O bond which is known to be very sensitive to heat and able to lead to the O-O bond breaking forming two radicals according to, here,

$HOONO_2 \rightarrow OH^\bullet + NO_3^\bullet$

and then to ignition, even if present at low level. It is also possible that this species formed in the liquid state is able to vaporize and decompose in the gas phase leading to ignition

Reactions between nitric acid and A^+

$HONO_2 + A^+ \rightarrow AH + NO_3^+$

$HONO_2 + A^+ \rightarrow AH^+ + NO_3^\bullet$

$HONO_2 + A^+ \rightarrow AOH + NO_2^+$

$HONO_2 + A^+ \rightarrow AOH^+ + NO_2^\bullet$

These reactions, as well as the ones with H^+ above, do not seem very significant.

Reactions between nitric acid and B^-

$HONO_2 + B^- \rightarrow BH + NO_3^-$

$HONO_2 + B^- \rightarrow BOH + NO_2^-$

$HONO_2 + B^- \rightarrow BNO_2 + OH^-$

All these reactions are particularly interesting and depending on the nature of B^- (to be defined) significant species can be formed to explain ignition.

Reactions between H^+ and B^-, NO_3^- and A^+ and between species formed in the previous reactions

$H^+ + B^- \rightarrow BH$ + other reactions depending on B^-

$A^+ + NO_3^- \rightarrow ANO_3$ + other reactions depending on A^+

$NO_3^\bullet + NO_3^\bullet \rightarrow N_2O_6$ (O_2NOONO_2)

$NO_3^\bullet + NO_2^\bullet \rightarrow N_2O_5$ (O_2NONO_2)

$NO_3^\bullet + OH^\bullet \rightarrow HO_2^\bullet + NO_2^\bullet$

$OH^\bullet + OH^\bullet \rightarrow H_2O_2$ (HOOH)

$NO_2^\bullet + NO_2^\bullet \rightarrow N_2O_4$ (O_2NNO_2)

$NO_2^- + NO_3^\bullet \rightarrow NO_3^- + NO_2^\bullet$

$OH^- + NO_3^\bullet \rightarrow OH^\bullet + NO_3^-$

$HO_2^\bullet + NO_2^\bullet \rightarrow HOONO_2$

Interestingly, the last reaction forms $HOONO_2$ again, the peroxide compound previously described.

$OH^\bullet + NO_2^\bullet \rightarrow HONO_2$

$OH^\bullet + NO_2^\bullet \rightarrow HO_2^\bullet + NO^\bullet$

etc.

An infinity of reactions may be written. Unfortunately, almost none of these reactions have been studied in the liquid phase and few data are reported in compilations

3. Conclusions and future works

In this part three, our literature investigation tends to show that reactions at gas-liquid and liquid-liquid interfaces may play an important role during hypergolic ignition (see Figure 17).

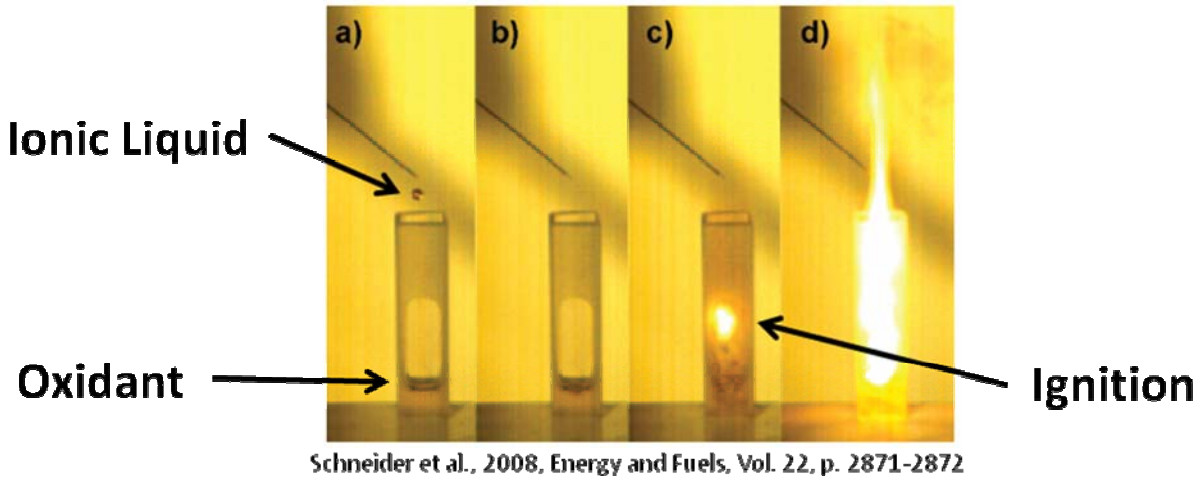

Figure 17. Visualization of IL/oxidant reactivity showing that the interface plays a major role in hypergolic ignition.

A detailed chemical kinetics model both in the liquid phase and in the gas phase to explain hypergolic ignition remains to be defined explicitly. Even if it is possible to write such a detailed chemical kinetic model and therefore to know what are the species formed in the liquid phase, it is certainly difficult to assess quantitatively their presence in the gas phase. According to this study it seems that some peroxy compounds may be formed in the liquid phase and that these species may be present in the gas phase where their thermal decompositions are able to induce ignition.

4. References

[Armstrong, 2007] J.P. Armstrong, Phys. Chem. Chem. Phys. 9 (2007) 982-990.

[Baranyai, 2004] K.J. Baranyai, Aus. J. Chem. 57 (2004) 145-147.

[Benjamin, 2015] I. Benjamin, Annual Review of Physical Chemistry 66 (2015) 165-188.

[Catoire, 2004] L. Catoire, J. Propulsion and Power 20 (2004) 87-92.

[Catoire, 2006] L. Catoire, Journal of Propulsion and Power 22 (2006) 120-126.

[Catoire, 2012] L. Catoire, Combustion and Flame 159 (2012) 1759-1768.

[Daimon, 1991] W. Daimon, Journal of propulsion 7 (1991) 946-952.

[Daimon, 2014] Y. Daimon, Journal of Propulsion and Power 30 (2014) 707-716.

[Emel'Yanenko, 2007] V.N. Emel'Yanenko, J. Am. Chem. Soc. 129 (2007) 3930-3937.

[Earle, 2006] M.J. Earle, Nature, 439 (2006) 831-834.

[Elles, 2006] C.G. Elles, Annual Review of Physical Chemistry 57 (2006) 273-302.

[Ferguson, 1975] E.E. Ferguson, Annual Review of Physical Chemistry 26 (1975) 17-38.

[Hynes, 1985] J.T. Hynes, Annual Review of Physical Chemistry 36 (1985) 573-597.

[Jalan, 2010] A. Jalan, Annual Reports Section "C" (Physical Chemistry) 106 (2010) 211-258.

[Jalan, 2013] A. Jalan, J. Phys. Chem. B 117 (2013) 2955-2970.

[Leal, 2007] J.P. Leal, J. Phys. Chem. A 111 (2007) 6176-6182.

[Livingston, 1955] R. Livingston, Annual Review of Physical Chemistry 6 (1955) 281-302.

[Masel, 2001] R.I. Masel, Chemical Kinetics and Catalysis, WILEY-INTERSCIENCE, city?, 2001.

[Nathanson, 2004] G.M. Nathanson, Annual Review of Physical Chemistry 55 (2004) 231-255.

[Olah, 1997] G. Olah, J. Am. Chem. Soc. 119 (1997) 8035-8042.

[Orozco, 2000] M. Orozco, Chemical Reviews 100 (2000) 4187-4226.

[Reichardt, 2011] C. Reichardt, Solvents and solvent effects in organic chemistry, Fourth edition, WILEY-VCH, Weinheim, 2011.

[Schmidt, 2005] M.W. Schmidt J. Phys. Chem. A 109 (2005) 7285-7295.

[Schneider, 2008] S. Schneider, Energy and Fuels 22 (2008) 2871-2872.

[Schroeder, 1987] J. Schroeder, Annual Review of Physical Chemistry 38 (1987) 163-190.

[Strasser, 2007] D. Strasser, J. Phys. Chem. A 111(2007) 3191-3195.

[Tanaka, 1985] M. Tanaka, Journal of propulsion 1 (1985) 314-316.

[Thomas, 1970] J.K. Thomas, Annual Review of Physical Chemistry 21 (1970) 17-38.

[Zhang, 2015] P. Zhang, Combustion and Flame 162 (2015) 237-248.

[Zorn, 2006] D.D. Zorn, J. Phys. Chem. B 110 (2006) 11110-11119.